Allele-selective transcriptional repression of mutant *HTT* for the treatment of Huntington's disease

Bryan Zeitler [1]*, Steven Froelich[1], Kimberly Marlen[1], David A Shivak[1], Qi Yu[1], Davis Li[1], Jocelynn R Pearl [1], Jeffrey C Miller[1], Lei Zhang[1], David E Paschon[1], Sarah J Hinkley[1], Irina Ankoudinova[1], Stephen Lam [1], Dmitry Guschin [1,8], Lexi Kopan[1], Jennifer M Cherone[1], Hoang-Oanh B Nguyen[1], Guijuan Qiao[1], Yasaman Ataei[1], Matthew C Mendel[1], Rainier Amora[1], Richard Surosky[1], Josee Laganiere[1,9], B Joseph Vu[1], Anand Narayanan[1], Yalda Sedaghat[2], Karsten Tillack[2], Christina Thiede[2], Annette Gärtner[2], Seung Kwak[3], Jonathan Bard[3], Ladislav Mrzljak[3], Larry Park[3], Taneli Heikkinen[4], Kimmo K Lehtimäki[4], Marie M Svedberg[5], Jenny Häggkvist[5], Lenke Tari[5], Miklós Tóth[5], Andrea Varrone[5], Christer Halldin[5], Andrea E Kudwa[6], Sylvie Ramboz[6], Michelle Day[7], Jyothisri Kondapalli[7], D James Surmeier[7], Fyodor D Urnov[1,10], Philip D Gregory[1], Edward J Rebar[1], Ignacio Muñoz-Sanjuán [3]* and H Steve Zhang[1,11]

Huntington's disease (HD) is a dominantly inherited neurodegenerative disorder caused by a CAG trinucleotide expansion in the *huntingtin* gene (*HTT*), which codes for the pathologic mutant HTT (mHTT) protein. Since normal HTT is thought to be important for brain function, we engineered zinc finger protein transcription factors (ZFP-TFs) to target the pathogenic CAG repeat and selectively lower mHTT as a therapeutic strategy. Using patient-derived fibroblasts and neurons, we demonstrate that ZFP-TFs selectively repress >99% of HD-causing alleles over a wide dose range while preserving expression of >86% of normal alleles. Other CAG-containing genes are minimally affected, and virally delivered ZFP-TFs are active and well tolerated in HD neurons beyond 100 days in culture and for at least nine months in the mouse brain. Using three HD mouse models, we demonstrate improvements in a range of molecular, histopathological, electrophysiological and functional endpoints. Our findings support the continued development of an allele-selective ZFP-TF for the treatment of HD.

HD is a fatal monogenic neurodegenerative disorder characterized by progressive motor, psychiatric and cognitive impairments[1,2]. In 1993, the causal mutation was mapped to an expansion of the CAG trinucleotide repeat in exon 1 of *HTT*[3]. There are currently no disease-modifying therapies for HD.

A variety of mechanisms for HD pathogenesis have been investigated, including toxicity from mHTT protein and loss of normal HTT[1,4]. Results from HD mouse models suggest that m*HTT* acts primarily through gain-of-function toxicity[2]. Inactivation of an inducible m*Htt* transgene can reverse disease progression[5], supporting HTT lowering as a potential therapeutic approach. RNA interference (RNAi) and antisense oligonucleotide (ASO) agents targeting *Htt* messenger RNA have shown efficacy in HD preclinical models[6–9], and a recent Phase 1/2a trial showed that multiple intrathecal ASO administrations reduced normal and mHTT protein levels in participants' cerebrospinal fluid (www.clinicaltrials.gov, identifier NCT02519036).

While partial reduction (~45%) of normal *HTT* expression is tolerated in the nonhuman primate striatum[10–12], the long-term ramifications of further reductions are unclear given its involvement in myriad biological functions[4]. In mice, *Htt* knockout is embryonic lethal[13,14] and perinatal loss leads to motor dysfunction and other neuropathology[15,16]. Although conditional neuronal *Htt* knockout in the adult mouse striatum and cortex appears to be tolerated[17], deleterious effects have been reported for other brain regions and cell types depending on the timing of *Htt* removal[18]. In humans, compound heterozygous (het) hypomorphic *HTT* variants have been linked to Rett syndrome-like disorders[19]. Because reduction of normal *HTT* below 50% concomitant with mHTT poses an unknown risk, the development of an allele-selective, m*HTT*-lowering approach suitable for clinical use has been a long-sought goal.

Several studies have investigated selective downregulation of m*HTT* transcripts by degradation or translational inhibition.

ASO- and RNAi-based strategies targeting single nucleotide polymorphisms (SNPs) linked to the mutant allele[20–22] can selectively lower m*HTT* in HD mouse models, although their clinical development has been limited because each SNP-specific therapy can treat only a subset of patients. Alternatively, direct targeting of the CAG repeat would in principle constitute a universal HD therapy. However, ASO- and RNAi-based reagents against the CAG repeat have yielded only modest levels of allelic discrimination with narrow effective dose ranges[20,23,24], possibly due to a common reliance on mass action to achieve selectivity.

A potentially more effective strategy would be to repress transcription via direct binding to the expanded CAG tract, which may provide greater allelic discrimination by leveraging functional synergies and cooperativities inherent to transcriptional regulation[25]. This approach would offer the added benefits of reducing m*HTT* RNA (a potentially pathogenic factor[26]) and requiring the recognition of just a single therapeutic target per cell. In a previous study, designed transcription factors targeted to poly-CAG were used to attempt allele-selective regulation via mass action[27]. Differential repression was demonstrated, but only in mouse cells bearing a nonpathogenic repeat that was too small (CAG4) to comprise a complete binding site for the examined reagents. Moreover the allele skew was exaggerated (four versus 111 CAGs; length ratio 28)[27,28] and over tenfold greater than the patient median (17 versus 43 CAGs; length ratio 2.5). Thus the feasibility of achieving highly allele-selective m*HTT* repression via poly-CAG targeting remains essentially unexplored.

A variety of engineerable DNA-binding modalities[29] could, in principle, be developed as *HTT* transcriptional regulators. Of these, designed ZFP-TFs offer several potential advantages. ZFPs can be targeted to virtually any DNA sequence, including poly-CAG and poly-CTG, whereas restrictions inherent to Cas9-related proteins prohibit standard CRISPR systems from recognizing poly-CAG. Relative to transcription activation-like effector proteins[30], ZFPs provide a more compact footprint for arrayed binding, enabling higher-order complex formation with potentially greater cooperativity and sharper discrimination of alleles. A further consideration is the extensive record of engineered ZFP-TFs in modulating a variety of pathological processes in disease models[31].

Here, we present a transcription-targeted approach that emphasizes the screening of a diverse panel of ZFP-TFs directly for allele-selective repression of endogenous m*HTT* in patient cells. We identify a new class of functionally synergistic ZFPs for which repression is highly dependent on poly-CAG tract length.

Results

Identification of ZFP-TFs that selectively repress m*HTT* across a wide dose range and diverse HD genotypes. We hypothesized that a ZFP-TF with appropriately tuned binding properties could exhibit synergistic function and therefore a steep dependence on repeat length (Fig. 1a). We assembled 41 distinct poly-CAG-targeted ZFPs bearing a diversity of architectures, target lengths and binding periodicities (Fig. 1b,c and Supplementary Table 1) and linked these to the KRAB transcriptional repression domain from human KOX1[32]. The ZFP-TFs were tested for allele-selective repression of endogenous *HTT* in CAG15/67 and CAG18/45 patient fibroblasts, which bracket a range of HD patient genotypes[33] (Fig. 1d). SNP-specific quantitative PCR with reverse transcription (RT–qPCR) assays were used to independently monitor expression levels of normal and mutant alleles (Fig. 1a and Extended Data Fig. 1a,b). This screen yielded a diverse range of *HTT* repression behaviors, including clear evidence of allele selectivity (Fig. 1e).

Three ZFP-TFs (ZFP-A, -B and -C; Fig. 1c,e and Supplementary Table 2) were chosen for further characterization. In CAG15/67 fibroblasts, ZFP-A and -B exhibited selective downregulation of the mHTT mRNA and protein levels, whereas ZFP-C strongly repressed both alleles (Fig. 1f,g). In titration studies, ZFP-A and ZFP-B repressed m*HTT* >90% with no or minimal repression of normal *HTT* over a dose range >100-fold (Fig. 1h). Companion analyses confirmed that relative ZFP protein levels mirrored the transfected mRNA doses (Extended Data Fig. 1c,d). In fibroblasts bearing repeat alleles more representative of the HD population (Fig. 1d),

Fig. 1 | Design, screening and characterization of allele-selective ZFPs targeting m*HTT*. a, Sketch of the structure and desired behavior of allele-selective repressors of *HTT*. A designed ZFP–KRAB fusion engineered to bind within the poly-CAG tract with appropriate affinity and target spacing should exhibit highly selective repression of the expanded disease allele. ZFP-TFs were screened for differential repression of normal (blue) and disease (red) alleles in patient cell lines bearing downstream SNPs, which enable independent quantitation of allele levels using SNP-specific RT–qPCR reagents targeting rs363099, rs362331 and rs362307. **b**, One- and two-finger units targeting sense and antisense frames within the poly-CAG sequence (top) and one- and two-base-spanning linkers used for assembling candidate ZFPs (bottom). Colors indicate alternative designs with distinct sets of DNA-contacting residues and binding properties (Supplementary Table 1). The target sequence of each one- and two-finger module is shown to the right. **c**, ZFP-TF sense- (left) and antisense-strand (right) targeted designs screened for selective repression of m*HTT*. One- and two-finger modules targeting either strand of the poly-CAG tract were linked to generate three-, four-, five- or six-finger ZFPs using alternative linkers to enable spanning of zero, one or two bases between adjacent fingers. Targeted sequences are indicated by the DNA sequence at left, middle and right. **d**, Frequency of CAG repeat lengths in the HD population. HD patient allele frequencies were calculated based on the third Enroll-HD periodic dataset obtained from www.enroll-hd.org[33]. All entries with CAG >35 (*n* = 6,602) were used for the analysis of mean and median m*HTT* allele length. Median alleles are indicated by boxes shaded blue (CAG17) and red (CAG43). Colored dots below CAG numbers denote normal (blue) and disease (red) allele lengths tested in our studies. **e**, Transcript levels for normal (blue) and disease (red) alleles of *HTT* were assessed 24 h after delivery of 100 ng ZFP-TF mRNA via nucleofection to patient fibroblasts (GM02151 or GM04723) bearing distinct poly-CAG tract lengths. Allele-selective repressors (ZFP-A, -B and -D) and one nonselective repressor (ZFP-C) were chosen for further study. *n* = 3 biologically independent samples; mean ± s.d. **f**, Allele-selective repression of three ZFPs chosen for further study and analyzed as in **e**. Studies were performed in patient GM04723 fibroblasts transfected with 100 ng ZFP-TF mRNA. Total (gray), normal (blue) and mutant (red) *HTT*. *n* = 3 biologically independent samples; mean ± s.d.; one-way analysis of variance (ANOVA) with Tukey's multiple comparison test; ** *P* < 0.01, **** *P* < 0.0001. **g**, Representative cropped images (top) and quantitation (bottom) of selective downregulation of mHTT (upper green band) protein by ZFP-A and ZFP-B in GM04723 fibroblasts as gauged by immunoblot 72 h after transient transfection. Similar results were obtained from at least two other independent experiments. Calnexin loading control (red bands). The uncropped scans are provided as source data. *n* = 3 biologically independent samples; mean ± s.d.; one-way ANOVA with Tukey's multiple comparison test; * *P* < 0.05; ** *P* < 0.01. **h–j**, Dose–response of allele-selective repression in patient GM04723 (**h**), GM02151 (**i**) or ND30259 (**j**) fibroblasts. RT–qPCR for total (gray), normal (blue) and mutant (red) *HTT* was performed on RNA isolated from patient fibroblasts transfected with ZFP-TF mRNA across a 100,000-fold dose range (1,000–0.01 ng at ~half-log dose steps). *n* = 3 biologically independent samples; mean ± s.d.; data were fitted using a nonlinear variable slope log(inhibitor) versus response curve. **h**, For CAG67, ZFP-A half-maximum effective concentration (EC50) = 7.5 ng; *R*² = 0.95; ZFP-B EC50 = 2.6 ng, *R*² = 0.96; ZFP-C EC50 = 0.18 ng, *R*² = 0.99. **i**, For CAG45, ZFP-A EC50 = 8.4 ng, *R*² = 0.98; ZFP-B EC50 = 3.3 ng, *R*² = 0.98; ZFP-C EC50 = 0.38 ng, *R*² = 0.90. **j**, For CAG38, ZFP-A EC50 = 9.8 ng, *R*² = 0.94; ZFP-B EC50 = 3.9 ng, *R*² = 0.94; ZFP-C EC50 = 0.29 ng, *R*² = 0.97. Source Data

both allele-selective ZFPs repressed CAG45 over a dose range ~100-fold with <15% repression of CAG18 at any dose (Fig. 1i). Moreover, in fibroblasts harboring an atypically narrow repeat length separation (CAG21/38), ZFP-A and -B selectively repressed CAG38 over a dose range 30- or 100-fold, respectively, albeit with some repression of CAG21 at higher doses (Fig. 1j). These studies highlight the ability of ZFP-A and -B to repress 100% of

fully-penetrant mutant alleles (CAG>39), while discriminating against at least 86% of normal *HTT* alleles[33] (Fig. 1d).

Our results contrasted with a previous study[27] in which repression was much less dependent on poly-CAG tract length, perhaps due to differences in our ZFP design strategy and screening systems. Consistent with this, evaluation of our designs in the HdhQ111/Q7 mouse striatal cells used in ref. [27], 25 ZFP-TFs exhibited >75%
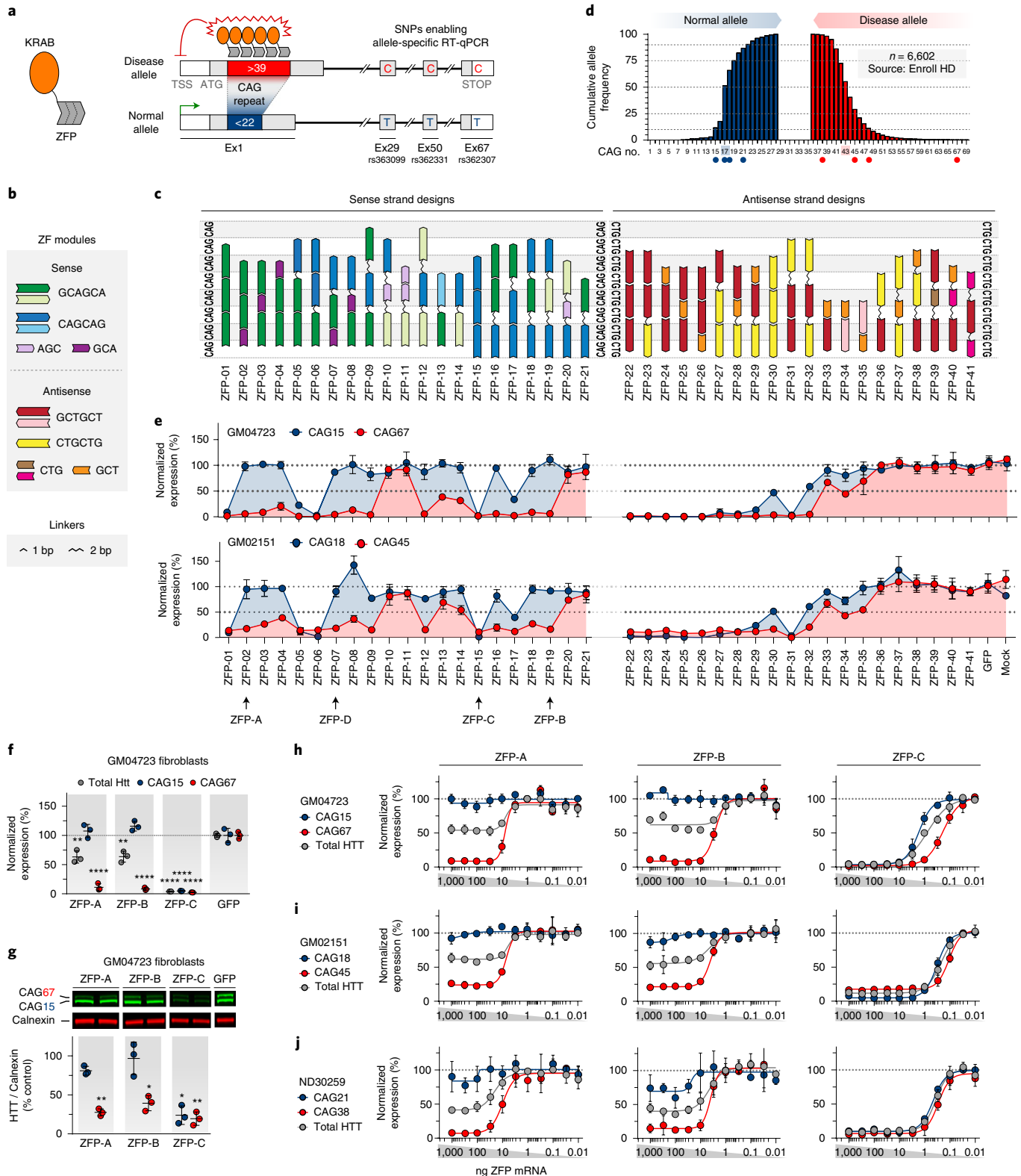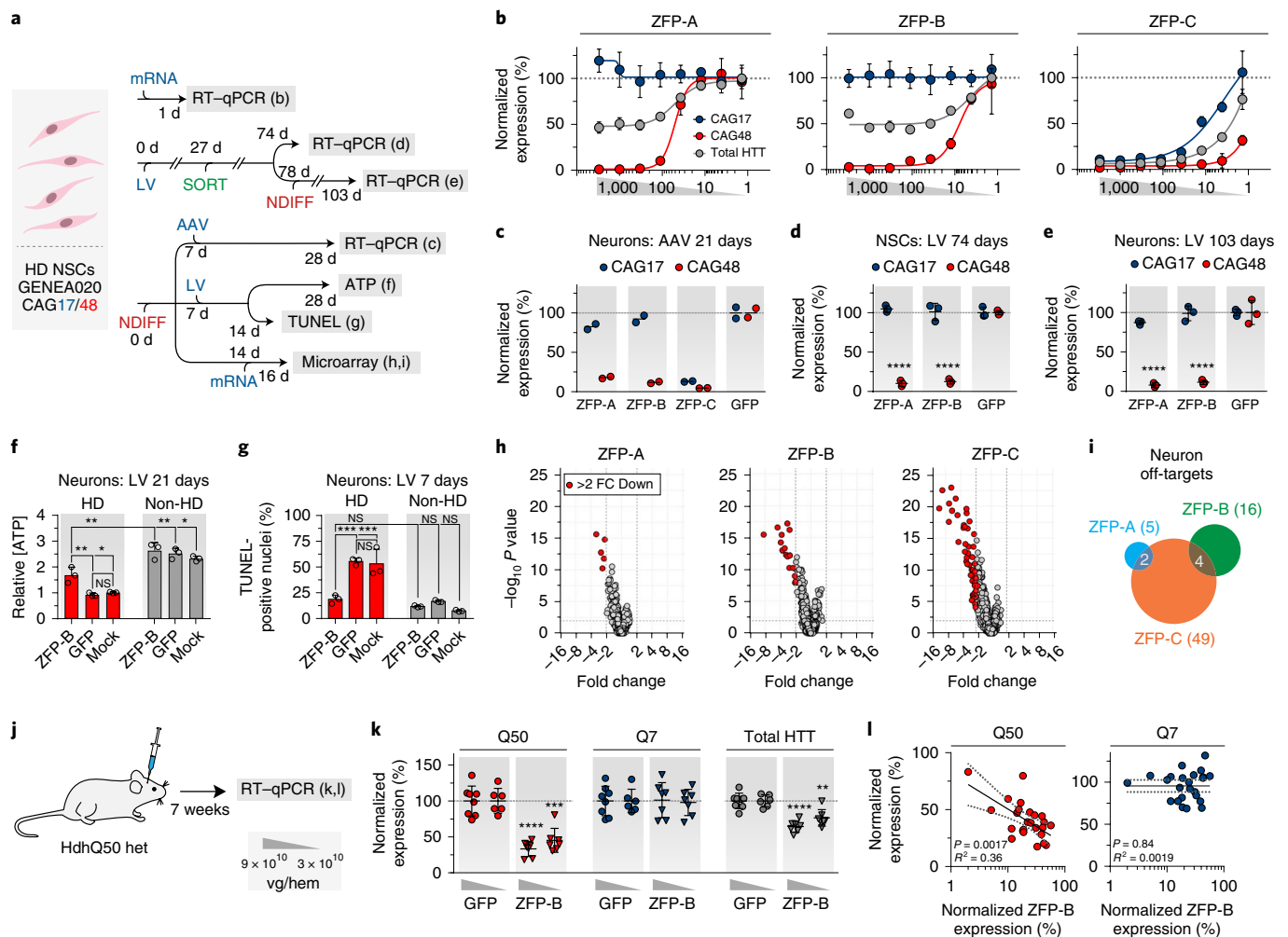
Fig. 2 | Allele-selective repression, specificity and phenotypic correction in HD neurons and m*HTT*-specific lowering in HdhQ50 mice. a, Overview timeline of studies performed using NSCs derived from GENEA020 hESCs. NDIFF, neural differentiation medium. **b**, ZFP-A, -B and -C were evaluated over a 3,000-fold dose range by transient transfection (3,000–1 ng ZFP-TF mRNA, ~half-log steps) in GENEA020 NSCs using a SNP-specific RT–qPCR assay for rs362307. Total (gray), normal (blue) and mutant (red) *HTT*. $n = 3$ biologically independent samples; mean ± s.d.; data were fitted using a nonlinear variable slope log(inhibitor) versus response curve. For CAG48, ZFP-A $EC_{50} = 50.3$ ng, $R^2 = 0.97$; ZFP-B $EC_{50} = 7.6$ ng, $R^2 = 0.92$; ZFP-C not determined. **c**, Normalized CAG17 (blue) and CAG48 (red) transcript levels in HD neurons 21 d post-transduction with AAV2/6 ZFP-A, -B or -C (1×10^5 vg/cell). $n = 2$ biologically independent samples; mean ± s.d. **d,e**, Normalized CAG17 (blue) and CAG48 (red) transcript levels in NSCs infected with ZFP.T2A. GFP or GFP LV 47 d after fluorescent activated cell sorter enrichment at 27 d (**d**) followed by neuronal differentiation and testing at 103 d post-infection (**e**). Representative gating images are provided in Supplementary Data Fig. 1. $n = 3$ biologically independent samples; mean ± s.d; one-way ANOVA with Tukey's multiple comparison test; **** $P < 0.0001$. **f,g**, Intracellular ATP levels (**f**) or apoptosis (TUNEL) 48 h after growth factor withdrawal (**g**) in HD (red) or non-HD (gray) neurons treated with ZFP-B or GFP LV 21 (**f**) or 7 d (**g**) after infection. $n = 3$ biologically independent samples; mean ± s.d.; two-way ANOVA with Tukey's multiple comparison test; * $P < 0.05$, ** $P < 0.01$, *** $P < 0.001$. **h**, Microarray assessment of HD neurons (CAG17/48) transfected with ZFP-A, -B or -C (1,500 ng mRNA). Each dot represents the mean fold change compared to control-treated cells for a given gene (*x* value) and the associated *P* value (*y* value) determined by eBayes ANOVA analysis. Genes with ≥ 2 fold change (FC) and $P < 0.01$ are colored red (downregulated). ZFP-A, -B and -C: $n = 4$ biologically independent samples; control: $n = 12$ biologically independent samples. **i**, Venn diagram of regulated genes in **h**. No genes were commonly regulated (≥ 2 FC change; $P < 0.01$) by ZFP-A ($n = 5$) and ZFP-B ($n = 16$); there was partial overlap with genes regulated by ZFP-C ($n = 49$). **j**, Overview of het HdhQ50 mouse study. **k**, Normalized Q50 (red), Q7 (blue) and total (gray) *Htt* mRNA levels in Q50 het mice injected with AAV2/6 ZFP-B or GFP 7 weeks after treatment. $n = 7$ (ZFP-B, high and low dose), $n = 8$ (GFP, high dose) and $n = 6$ (GFP, low dose) hemispheres (hem) per group; mean ± s.d.; two-tailed *t*-test with Welch's correction; ** $P < 0.01$, *** $P < 0.001$, **** $P < 0.0001$. The striatal section with the highest ZFP expression from each hemisphere is presented. **l**, Regression analysis of all striatal sections for mRNA levels of ZFP-B and either Q50 (left; $P = 0.0017$, $R^2 = 0.36$) or Q7 (right; $P = 0.84$, $R^2 = 0.0019$). Dotted lines indicate the 95% confidence range. Source Data

reduction in m*HTT* and <10% reduction in normal *HTT*, while only ZFP-A, -B and -D yielded quantitatively comparable behavior in CAG18/45 patient fibroblasts (Extended Data Fig. 2a,b). Moreover ZFP-C showed apparent allele selectivity in HdhQ111/Q7 cells but potently repressed normal *HTT* in patient fibroblasts (Extended Data Fig. 2a,b and Fig. 1e–j). Finally, neither lead ZFP from ref. [27] was allele selective in CAG18/45 fibroblasts (Extended Data Fig. 2c).

Long-term allele-selective *mHTT* repression and improvement in HD-related phenotypes in human neurons. We tested our ZFPs in neural stem cells (NSCs) and neurons differentiated from CAG17/48 embryonic stem cells (ESCs) (Fig. 2a and Extended Data Fig. 3). In transfected NSCs, ZFP-B exhibited >90% repression of the disease allele over a 100-fold dose range with no repression of normal *HTT* (Fig. 2b). In neurons, delivery of ZFP-A and -B via
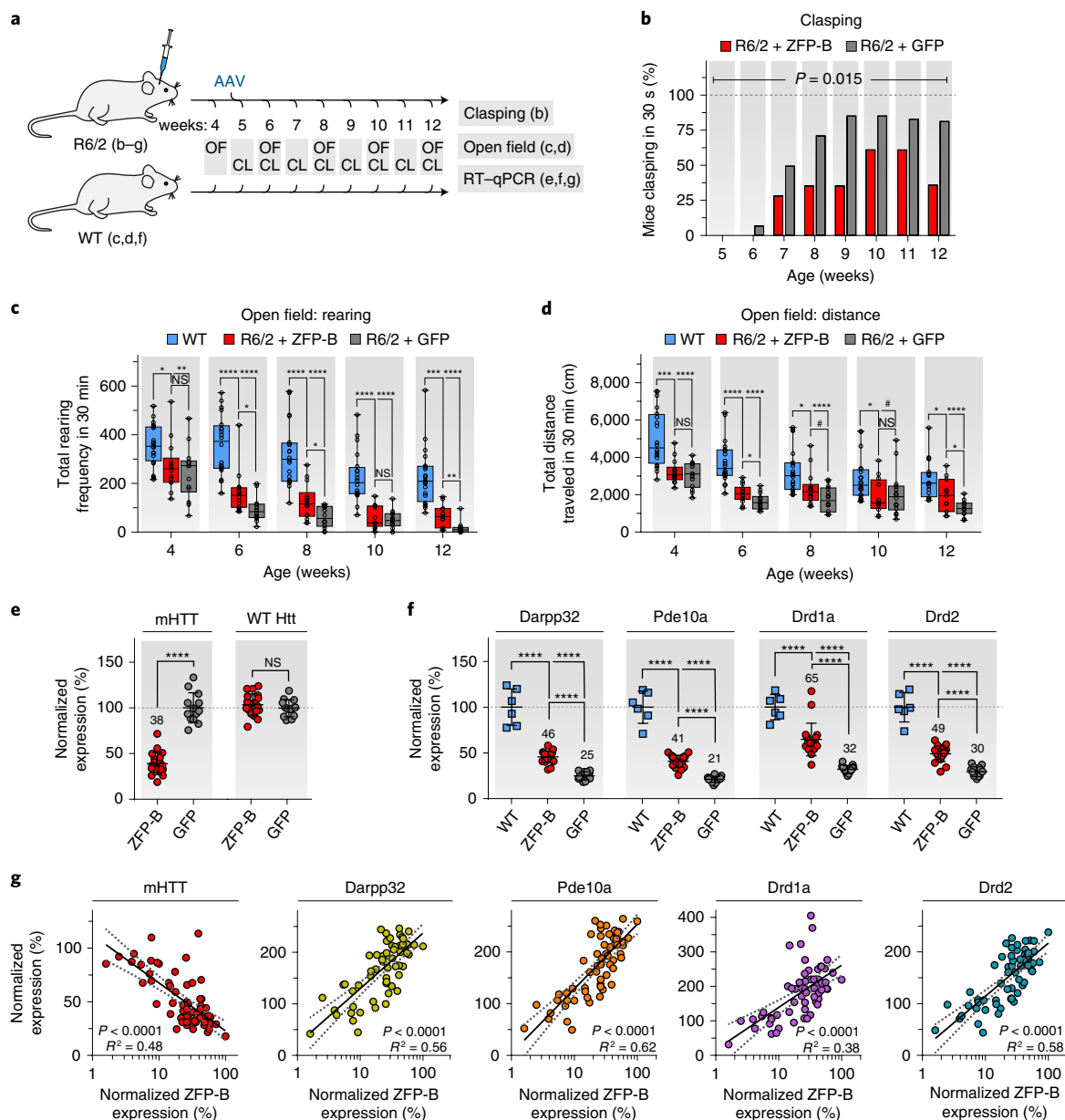
Fig. 3 | Improvement in behavioral deficits and striatal biomarkers in R6/2 mice. a, Timeline overview of behavioral and molecular endpoints assessed in WT and AAV2/6-treated R6/2 mice. **b,** Percentage of mice displaying clasping behavior assessed weekly following ZFP-B (red) or GFP (gray) treatment. $n = 14$ per group; $P = 0.015$, odds ratio, 2.4, generalized estimating equation. **c,d,** Open field testing for rearing frequency (**c**) or total distance traveled (**d**) was performed at 4 (baseline), 6, 8, 10 and 12 weeks of age on untreated WT (blue, $n = 20$), ZFP-B-treated R6/2 (red, $n = 14$) or GFP-treated R6/2 mice (gray, $n = 14$). Center line, median; limits, 25–75th percentiles; whiskers, min–max; all points shown. Repeated measures with mixed-effects models; genotype main effect $P < 0.0001$ (**c,d**), treatment effect $P = 0.030$ (**c**) and $P = 0.038$ (**d**). Unpaired two-tailed t-test results are also shown for each timepoint: # $P < 0.10$, * $P < 0.05$, ** $P < 0.01$, *** $P < 0.001$, **** $P < 0.0001$. **e,** Normalized striatal m*Htt* (R6/2) or WT *Htt* expression 7 weeks after delivery. $n = 13$ (GFP) and $n = 19$ (ZFP-B) hemispheres; mean ± s.d.; two-tailed t-test with Welch's correction; **** $P < 0.0001$. The striatal section with the highest ZFP expression is presented. **f,** Striatal neuron marker levels of *Darpp32*, *Pde10a*, *Drd1a* and *Drd2* as in **e**. $n = 6$ (WT), $n = 13$ (GFP) and $n = 19$ (ZFP-B) hemispheres per group; mean ± s.d.; one-way ANOVA with Tukey's multiple comparison test; **** $P < 0.0001$. **g,** Regression analysis of all striatal sections for normalized mRNA levels of ZFP-B and either m*Htt* ($R^2 = 0.48$; $P < 0.0001$), *Darpp32* ($R^2 = 0.56$; $P < 0.0001$), *Pde10a* ($R^2 = 0.62$; $P < 0.0001$), *Drd1a* ($R^2 = 0.38$; $P < 0.0001$) or *Drd2* ($R^2 = 0.58$; $P < 0.0001$) levels. Dotted lines indicate the 95% confidence range.

adeno-associated virus (AAV; Supplementary Table 3) yielded highly allele-selective repression, albeit with modest reductions in CAG17 (Fig. 2c). To test ZFPs in a setting of persistent expression, NSCs were infected with ZFP-encoding lentivirus (LV) and differentiated into neurons (Fig. 2a). Sustained, undiminished repression was observed on days 74 (NSCs; Fig. 2d) and 103 (neurons; Fig. 2e). In agreement with previous studies[34,35], untreated CAG17/48 neurons

showed a substantial decrease in intracellular ATP levels and increased susceptibility to apoptosis compared to non-HD neurons (Fig. 2f,g). Following ZFP-B treatment, ATP levels in CAG17/48 neurons increased by ~70% compared to control-treated neurons (Fig. 2f), and levels of apoptosis were restored to baseline (Fig. 2g).

Consistent with these results, microarray analysis ($n = 18,149$ genes queried) revealed limited levels of off-target gene

repression by ZFP-A and -B in CAG17/48 neurons (Fig. 2h and Supplementary Table 4) and CAG18/45 fibroblasts (Extended Data Fig. 4a and Supplementary Table 5) under conditions of robust on-target allele-selective m*HTT* regulation (Extended Data Fig. 4b,c). Microarray performance was broadly confirmed via RT–qPCR of a control transcript set (Extended Data Fig. 4d,e). A substantially greater number of genes were repressed by the non-allele-selective ZFP-C, and most contained CAG arrays within 1 kb of the transcription start site (TSS; Supplementary Tables 4–7). In contrast, the few genes regulated by ZFP-A and -B showed no strict correspondence with the presence, length or location of a CAG repeat (Supplementary Tables 4–7). Membership analyses revealed no overlap between the genes regulated by ZFP-A and -B (Fig. 2i, Extended Data Fig. 4f and Supplementary Tables 6 and 7). Finally, using a ranking-based enrichment analysis with statistical thresholding (false discovery rate ≤ 0.05), we found no overlapping biological processes dysregulated by ZFP-A and -B, suggesting that even sub-critical effects were distinct (data not shown). Together these findings reduced the possibility that a CAG-targeted approach might unavoidably perturb a common set of human genes, and imply that optimization of our designs could yield ZFPs with even greater specificity.

In vivo reduction of m*Htt* bearing a CAG allele length relevant to human disease. We initially tested ZFP-B for in vivo m*Htt* reduction using het Q50 (HdhQ50/Hdh⁺) mice. Although phenotypically normal, this model harbors a m*Htt* allele (CAG48) that is typical of patients with HD and equivalent in length to that tested in human neurons (Figs. 1d and 2a). AAV ZFP-B or GFP was bilaterally administered by intrastriatal injection to 11-week-old Q50 het mice at two doses (Fig. 2j). Seven weeks after delivery, Q50 transcripts were reduced by 55% (low dose) and 67% (high dose) whereas endogenous mouse *Htt* was unchanged (Fig. 2k). ZFP-B expression was inversely correlated with the levels of Q50, but not Q7 (Fig. 2l). Variability in ZFP expression and Q50 repression among striatal sections was consistent with the incomplete AAV striatal coverage (typically 30–70%) obtained in all of our stereotaxic injection studies.

ZFP-driven neuroprotection and impact on locomotor deficits in R6/2 mice. Having established selective mHTT repression in several contexts, we evaluated ZFP-B in transgenic R6/2 mice (~120 CAG), which exhibit early and progressive changes in neuronal physiology,

body weight loss, motor deficits, cognitive alterations and medium spiny neuron (MSN) biomarker loss[36,37]. Five-week-old R6/2 mice received bilateral intrastriatal injections of AAV encoding ZFP-B or GFP and were compared to non-transgenic, age-matched controls (Fig. 3a). Over the seven-week study, the ZFP-treated group was 2.4-fold less likely to clasp than the GFP group (Fig. 3b). In biweekly open field assessments, ZFP treatment conferred significant longitudinal improvements in rearing frequency (Fig. 3c) and total distance traveled (Fig. 3d). Moreover ZFP-treated mice performed better than controls at several timepoints after ZFP administration, and the largest effects were observed at the final assessment. Notably, there was no significant treatment effect on body weight, grip strength or rotarod performance (Extended Data Fig. 5a–d).

Following the 12-week behavioral evaluation, striatal tissue was subjected to RT–qPCR analysis. ZFP treatment resulted in 62% reduction of m*HTT*, whereas the expression of normal mouse *Htt* was unchanged (Fig. 3e). Companion immunohistochemistry (IHC) analyses showed AAV coverage of ~50–70% of the striatum (data not shown), suggesting near-complete repression of m*HTT* in the delivered area. The levels of the MSN marker genes *Darpp32* and phosphodiesterase 10a (*Pde10a*) and dopamine receptors D1 (*Drd1a*) and D2 (*Drd2*) in ZFP-treated mice were 1.6–2.0-fold higher than in GFP-treated mice (Fig. 3f). These levels remained 1.5–2.3-fold lower than non-transgenic controls, possibly due to incomplete vector coverage and extensive pathology at the time of intervention. Regression analysis revealed a significant negative relationship between ZFP and m*HTT* transcript levels, and a positive relationship between ZFP expression and the levels of all MSN markers tested (Fig. 3g), suggesting a potential neuroprotective benefit conferred by ZFP treatment.

Correction of histopathology and electrophysiology deficits in zQ175 mice. We next examined whether ZFP-mediated m*HTT* repression could improve neuropathological deficits in the slower-progressing zQ175 knock-in model (~188 CAG repeats). Het zQ175 mice develop hallmark mHTT-containing inclusions accumulating from three to 12 months, molecular and electrophysiological disease signatures between four and six months and relatively mild locomotor deficits at 10–12 months[37–40], thereby permitting an assessment of ZFP efficacy and tolerability at different stages of disease progression. We confirmed that AAV delivery of ZFP-B and -D (another allele-selective ZFP used in our zQ175 studies; Fig. 1e)

Fig. 4 | Molecular, histopathological and electrophysiological improvements in zQ175 het mice. a,b, mRNA (**a**) or soluble protein (**b**) levels of WT and m*HTT* in zQ175 het neurons 10 d after infection with AAV2/1 + 2 ZFP-B or ΔDBD assessed by RT–qPCR (**a**), Singulex (mouse HTT) or Meso Scale Discovery (MSD) (mHTT) (**b**). LOD, limit of detection; Bkg, background limit. *n* = 3 biologically independent samples; mean ± s.d.; one-way ANOVA with Tukey's multiple comparison test; mean ± s.d.; **P < 0.01; ***P < 0.01; ****P < 0.0001. **c,** Timeline overview and endpoints in zQ175 het mouse studies. **d,h,** Representative striatal immunostaining images from 2–4- (**d**) or 6–10-month (**h**) zQ175 het cohorts injected with AAV2/1 + 2 ZFP-B.T2A. GFP; scale bar, 200 µm. HTT inclusions (mEM48), yellow; GFP, green; DARPP32, red; DAPI, blue. Expanded GFP⁺ and GFP⁻ regions are shown at right; scale bar, 20 µm. Similar results were replicated in one additional independent experiment. **e–g,i–k,** Quantitation of nuclear inclusions (**e,i**), perinuclear inclusions (**f,j**) and total mEM48 intensity (**g,k**) in GFP⁺ DARPP32⁺ MSNs for 2–4- (**e–g**) or 6–10-month (**i–k**) cohorts treated with ZFP-B.T2A.GFP, GFP (**e–g,i–k**) and ΔDBD.T2A.GFP (**i–k**). *n* = 5 mice; mean ± s.d.; two-tailed unpaired *t*-test with Welch's correction; * *P* < 0.05, ** *P* < 0.01, *** *P* < 0.001, **** *P* < 0.0001. **l,m,** DARPP32 levels in untreated WT and het zQ175 striata at 10 months of age (**l**), or ZFP-B.T2A.GFP-, ΔDBD.T2A.GFP- or GFP-treated 6–10-month cohorts (**m**). hem, hemispere. *n* = 5 mice; mean ± s.d.; two-tailed unpaired *t*-test with Welch's correction; ** *P* < 0.01. **n,** Representative line scans of bAP-evoked Ca²⁺ imaging depicting proximal and distal locations within the same dendrite used to calculate dendritic index. Scale bars, 40 µm (left), 5 µm (right). **o,** Ca²⁺ transients from 4–6-month-old cohort mice injected with AAV2/9 ZFP-D.T2A.tdTomato (zQ175, left), ΔDBD.T2A.tdTomato (zQ175, middle) or ZFP-D.T2A.tdTomato (WT littermate, right). ΔF, change in fluorescence; F₀, initial fluorescence. **n,o,** Similar results were replicated in at least one additional independent experiment. **p,q,** Rescue of the dendritic index in 2–6-month (**p**) or 4–6-month (**q**) cohorts treated with ZFP-D. T2A.tdTomato (zQ175 2–6 months, *n* = 17 dendrites; 4–6 months, *n* = 19 dendrites), ΔDBD.T2A.tdTomato (zQ175 2–6 months, *n* = 10 dendrites; 4–6 months, *n* = 17 dendrites) and ZFP-D.T2A.tdTomato (WT 2–6 months, *n* = 15 dendrites; 4–6 months, *n* = 17 dendrites). Center line, median; limits, 25–75th percentiles; whiskers, min–max; all points shown. One-tailed Mann–Whitney *U*-test; * *P* < 0.05, ** *P* < 0.01. **r,** Representative striatal GFAP and IBA1 immunostaining images from 6–10-month zQ175 cohorts injected with ZFP-B.T2A.GFP; scale bar, 200 µm. GFP, green; DAPI, blue; GFAP, red; IBA1, yellow. Expanded GFP⁺ and GFP⁻ regions are shown at right; scale bar, 50 µm. Similar results were replicated in one additional independent experiment. **s,t,** Quantitation of GFAP⁺ (**s**) and IBA⁺ (**t**) cells in zQ175 striata injected with ZFP-B.T2A.GFP, GFP or ΔDBD.T2A.GFP from the 6–10-month cohort. *n* = 5 mice; mean ± s.d.; two-tailed unpaired *t*-test with Welch's correction.

reduced mHTT mRNA and protein by ≥98% in cultured primary zQ175 het striatal neurons (Fig. 4a,b and Extended Data Fig. 6a,b). No change in mouse *Htt* was observed, and controls lacking the ZFP DNA-binding domain (ΔDBD) did not substantially reduce mHTT.

We monitored mHTT inclusions by EM48 immunoreactivity in cohorts treated before (early) or after (late) neuropathological onset (Fig. 4c). For the early cohort, AAV ZFP-B or GFP was injected into the 2-month-old dorsal striatum and aggregation was assessed at 4 months. A self-cleaving T2A-GFP tag was used to visualize ZFP-expressing cells. In transduced MSNs, ZFP-B reduced nuclear HTT aggregates by 99.6% (Fig. 4d,e), perinuclear HTT inclusions by 88% (Fig. 4f) and total EM48 immunofluorescence by 48% (Fig. 4g).

For the late cohort, intrastriatal AAV injections of ZFP-B.T2A. GFP, ΔDBD.T2A.GFP or GFP were administered to 6-month-old zQ175 het mice bearing substantial pre-existing inclusions[38], with aggregates evaluated at 10 months. Relative to GFP treatment, ZFP-B reduced the number of nuclear EM48^{+} inclusions by 19% (Fig. 4h,i), perinuclear inclusions by 87% (Fig. 4j) and EM48 intensity by 24% (Fig. 4k). Similar results were obtained for ZFP-D (Extended Data Fig. 6c,d). Compared to age-matched wild-type (WT) mice, 10-month-old zQ175 hets exhibited a 17% striatal reduction in DARPP32 immunoreactivity (Fig. 4l). Consistent with our findings in R6/2 mice, ZFP-B increased DARPP32 levels by 20% in the late-treatment cohort (Fig. 4m). There was no significant
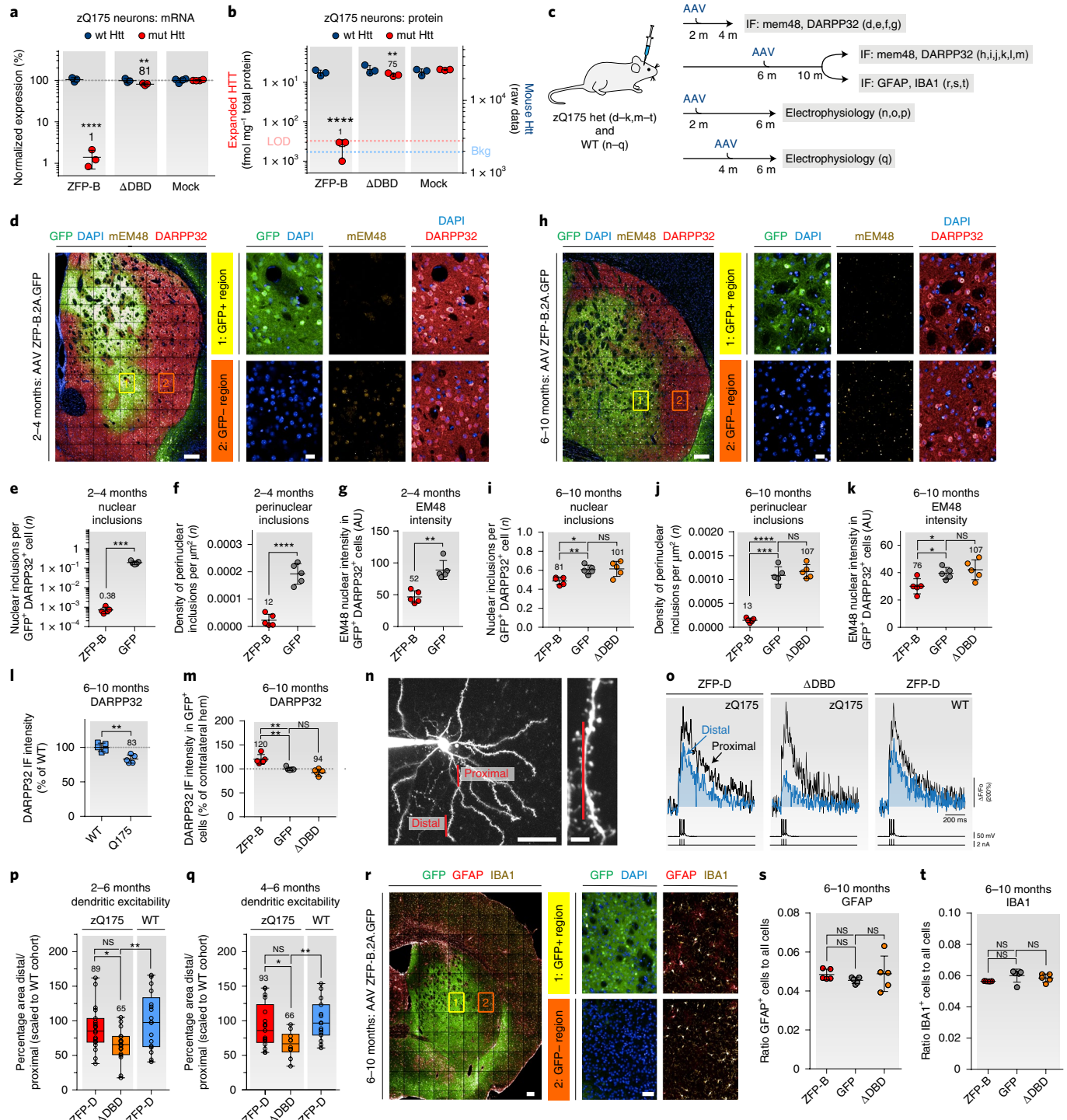
difference between ΔDBD- and GFP-treated mice for any endpoint (Fig. 4i–k,m and Extended Data Fig. 6e–g).

Electrophysiological deficits affecting zQ175 indirect pathway projection neurons (iSPNs) manifest by four months of age[40]. We therefore injected 2- and 4-month-old mice intrastriatally with AAV ZFP-D.T2A.tdTomato or ΔDBD.T2A.tdTomato and assessed iSPN dendritic excitability at 6 months (Fig. 4c,n) using a simplified back-propagating action potential (bAP) burst protocol (Fig. 4o). Relative to control-treated zQ175 iSPNs, which displayed an average 35% suppression of dendritic excitability, ZFP-D-treated zQ175 iSPNs were restored to near WT levels in both the 2- (Fig. 4p) and 4-month cohorts (Fig. 4q). Thus, iSPN electrophysiology deficits in zQ175 mice are both preventable and reversible by a m*Htt*-targeted ZFP. Moreover, since mHTT repression was restricted to the striatum, our findings are consistent with a regionally autonomous model for the development of dendritic hypoexcitability, rather than a secondary consequence of dysfunctional innervating neurons.

Tolerability and specificity of chronic ZFP-TF expression in vivo.
To assess whether striatal ZFP expression provokes a neuroinflammatory response, we monitored markers of astrogliosis (GFAP), microgliosis (IBA1) and general neuronal viability (NEUN) in both early- and late-treatment groups. Apart from the transient effects of the injection (localized to the needle track), we observed no changes in marker intensity or the number of GFAP+ or IBA1+ cells (Fig. 4r–t and Extended Data Fig. 6h–n) for any treatment. Moreover there was no reduction in NEUN+ cells or NEUN staining intensity in ZFP-treated WT or zQ175 het mice (Extended Data Fig. 7a–h), suggesting that long-term striatal expression is generally well tolerated.

To understand the potential for in vivo off-target regulation, we first mapped the location of the closest perfect and imperfect CAG array to every annotated TSS in the mouse and human genomes (see Methods and Supplementary Tables 8–15). Although the mouse genome has a substantially greater total CAG content than the human genome (3,472 versus 1,053 perfect and 32,328 versus 21,456 imperfect CAG repeats; Extended Data Fig. 8a,b), both genomes have a similar number of TSS-adjacent (within 1 kb) CAG arrays (150 versus 176 perfect and 1,720 versus 1,872 imperfect CAG repeats; Extended Data Fig. 8c,d). We then performed bidirectional ortholog analyses whereby each protein-coding mouse gene was mapped to the corresponding human ortholog (if present), and vice versa (Supplementary Tables 16–19). CAG conservation between species was notably low, with just 12 of the top 100 CAG human genes having an ortholog with a TSS-adjacent CAG array of any length, and 15 of the top 100 mouse genes for the converse comparison (Extended Data Fig. 8e–f). Twelve genes containing large TSS-adjacent CAG arrays in the mouse ortholog were selected for in vivo assessment (Extended Data Fig. 8g). Six-month-old WT and zQ175 het mice were unilaterally injected with AAV ZFP-B, ZFP-D or ΔDBD, and striatal tissue was collected one month later for RT–qPCR analysis (Extended Data Fig. 9a). m*Htt* mRNA levels were reduced by >70% with no repression of mouse *Htt* (Extended Data Fig. 9b–d). Overall, no regulation was detected for genes with arrays ≤19 CAG (*Mtus2*, *Rsl24d1*, *Akt3*, *Kcna6*, *Itga7*; Extended Data Fig. 9e–i), the exception being *Dnajc12*, which lacks a CAG repeat in the human ortholog (Extended Data Fig. 8g and 9j). Examination of the mouse *Dnajc12* promoter revealed 12 CAA repeats directly adjacent to the CAG array, which may explain why it was regulated whereas other similar-length CAG candidates were not. For the six mouse candidates with arrays ≥24 CAG (Extended Data Fig. 9k–p), regulation ranged from 38% reduction by ZFP-D (*Runx2*; CAG28, TSS 100 bp) to 79% by ZFP-B (*Nap1l3*; CAG28, TSS 511 bp). In all but two cases, ZFP-D resulted in significantly less off-target repression than ZFP-B despite equivalent m*Htt* reduction. Consistent with our previous long-term analyses, we found no significant

reduction in the levels of *Drd1*a, *Drd2*, *Darpp32*, *Pde10A* and *Rbfox3*/*Neun* (Extended Data Fig. 9q–u).

Tolerability was further investigated in two behavioral studies using large cohorts of mice over extended treatment durations. We first evaluated ZFP-B and ZFP-D in both early (2–6 months of age) and late (6–12 months of age) treatment cohorts of WT and zQ175 het mice following unilateral intrastriatal AAV injections. We observed no loss of body weight for the duration of the study (Extended Data Fig. 7i,j) and no changes in general activity, spontaneous behavior, grooming, nest building, food and fluid uptake or body temperature (data not shown). Histological analysis showed no evidence of brain volumetric changes, no loss of NEUN expression and no elevation in astroglial markers compared to the contralateral hemisphere (data not shown). In the second study, 6-month-old zQ175 het mice were injected bilaterally with vehicle, AAV ZFP-D or AAV eGFP and monitored for open field, rotarod, clasping, neurological index, brain magnetic resonance imaging (MRI) and body weight over 9 months (Extended Data Fig. 10a). Uninjected age-matched littermates were also included. At these ages, zQ175 het mice did not show any obvious clasping phenotype (data not shown), alterations in spontaneous open field locomotion or neurological index deficits (Extended Data Fig. 10b–f). Importantly, ZFP-treated and control zQ175 groups were equivalent in each of these measures. Striatal ZFP treatment did not alter the minor zQ175 het rotarod performance deficit observed at 15 months, nor did it affect changes in body weight observed during aging (Extended Data Fig. 10g,h). Moreover ZFP treatment had no impact on zQ175 whole-brain, striatal and cortical volume as assessed by MRI (Extended Data Fig. 10i).

Restoration of translational biomarkers in zQ175 mice. In patients with HD, *PDE10A*, *DRD1A* and *DRD2* undergo early, progressive and profound changes, beginning many years before clinical diagnosis[41,42]. Similar alterations are recapitulated in zQ175 mice[43]. We therefore explored whether ZFP-driven restoration of these markers could be detected using two approaches: in vitro autoradiography (ARG) of striatal brain sections and longitudinal micro-positron emission tomography (microPET) imaging in live animals[41–43].

For the ARG studies, zQ175 het mice received unilateral intrastriatal injections of AAV ZFP-D or GFP in both early- (2–6 months of age) and late- (4–10 months of age) treatment cohorts (Fig. 5a). Expression was evaluated using tritiated ligands for D1-like receptors ([³H]NNC112), D2-like receptors ([³H]raclopride) or PDE10A ([³H]MNI-659). Binding was measured within a striatal region-of-interest (ROI) delineated by the area showing decreased accumulation of mHTT (assessed by EM48 staining of an adjacent section). In ZFP-treated mice, [³H]NNC112, [³H]raclopride and [³H]MNI-659 binding in the injected striatum ROI were all significantly higher than in the contralateral striatum ROI in both the early (34, 26 and 31%, respectively) and late (24, 7 and 11%, respectively) cohorts (Fig. 5b–d). Thus ZFP treatment can both prevent and restore specific binding in mice with established disease, with the greatest benefit occurring before symptom onset.

In a translational paradigm, the impacts of ZFP treatment on [¹¹C]raclopride and [¹⁸F]MNI-659 binding were evaluated by microPET in live animals. Raclopride and MNI-659 binding in zQ175 striata decrease from 60 to 56% and from 52 to 41%, respectively, between 6 and 9 months of age[43]. We therefore injected 4-month-old mice unilaterally with AAV ZFP-D or GFP and monitored ligand binding from 6.5 to 10 months (Fig. 5a and Supplementary Table 20). [¹⁸F]MNI-659 binding potential (BP$_{ND}$) for the ZFP-injected versus untreated striatum was significantly increased, by 12.8 and 16.5% at 6.5 and 10 months of age, respectively (Fig. 5e,f and Supplementary Table 21). There was no statistically significant change for the GFP cohort at either timepoint. Moreover, when the percentage difference in BP$_{ND}$ between hemispheres
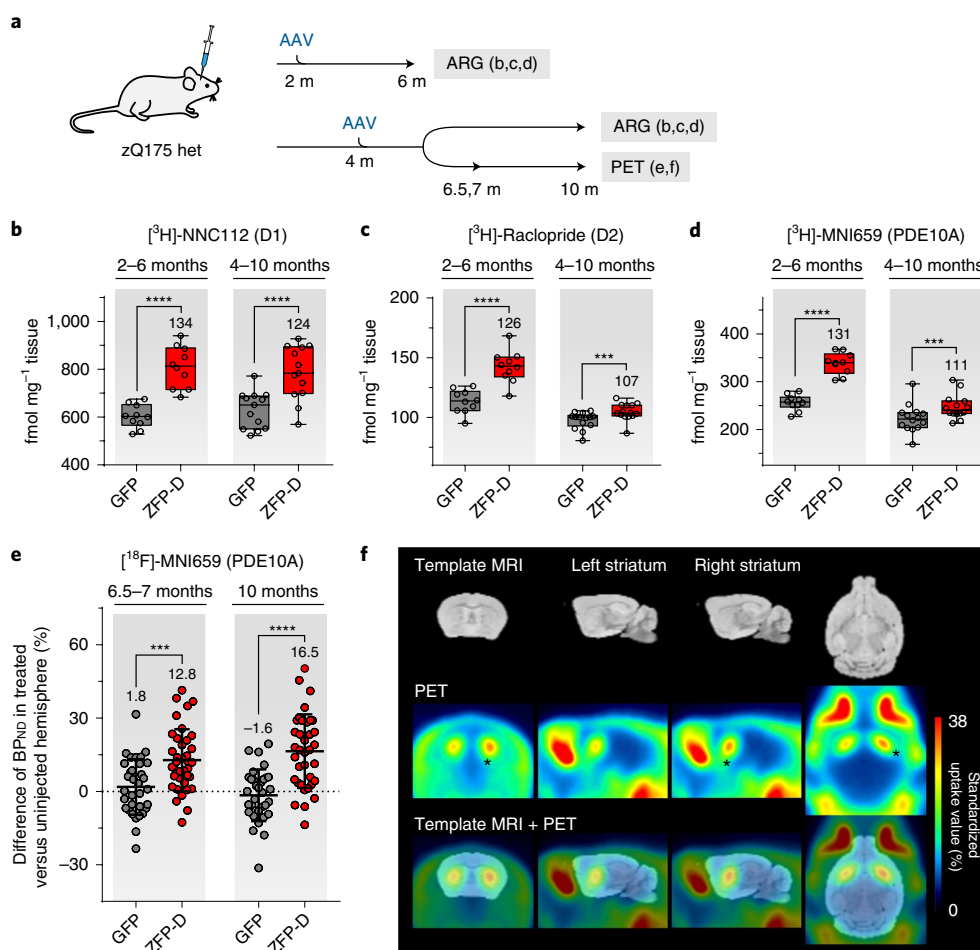
Fig. 5 | Restoration of imaging markers by ZFP expression in the striatum of zQ175 het mice. a, Timeline overview and endpoints in zQ175 ARG and microPET imaging studies. **b–d**, ARG analysis for D1-like (**b**), D2-like (**c**) and PDE10A (**d**) specific binding for mice injected unilaterally with either AAV2/1+2 ZFP-D (red) or GFP (gray). Mice were injected at 2 months and analyzed at 6 months (left panel; $n = 10$ mice per treatment) or injected at 4 months and analyzed at 10 months (right panels; $n = 13$ mice per treatment for the D1 group, $n = 14$ mice per treatment for the D2 and PDE10A groups). Center line, median; limits, 25–75th percentiles; whiskers, min–max; all points shown. Two-tailed paired t-test; *** $P < 0.001$, **** $P < 0.0001$. **e**, Percentage difference for [¹⁸F]MNI-659 BP_ND in ZFP-D or GFP injected versus uninjected zQ175 het striata imaged at 6.5/7.0 months (left panel; $n = 33$ GFP, $n = 37$ ZFP-D) and 10 months (right panel; $n = 33$ GFP, $n = 35$ ZFP-D) of age. Unpaired two-tailed t-test with Welch's correction; *** $P < 0.001$, **** $P < 0.0001$. **f**, Mean [¹⁸F]MNI-659 percentage standardized uptake value images of 10-month-old zQ175 het mice treated with ZFP-D, averaged from 15 to 63 min. Template MRI (upper row) and PET (middle row) are shown co-registered (bottom row). Both the left (untreated) and right (treated) striatum are shown in the sagittal plane. A black asterisk (*) indicates the PDE10A binding increase obtained in the ZFP-D-treated striatal hemisphere.

was compared across treatments, the ZFP-D cohort showed significantly elevated BP_ND compared to GFP mice in both early (+11.0%) and late (+18.1%) measurements (Fig. 5e). Despite seeing a 7% increase in raclopride binding in the 4–10-month ARG cohort, we did not detect a significant increase in [¹¹C]raclopride BP_ND for ZFP-D (Supplementary Table 21). Collectively, our findings demonstrate that allele-selective ZFP-TFs can prevent and reverse the loss of a translational marker of HD progression.

Discussion

Our study presents the first direct demonstration of allele-selective transcriptional repression at the native *HTT* locus. We describe CAG-targeted ZFPs exhibiting a combination of high selectivity, genome-wide specificity and long-term tolerability that—to our knowledge—establish new benchmarks for synthetic transcription factors. A key aspect of our work was the recognition that it might be possible to identify ZFPs with a steep functional dependence on repeat length by screening a sufficiently large and diverse panel of ZFP architectures at the endogenous *HTT* locus. Of note, a previous

attempt to engineer CAG-targeted ZFPs employed a single reiterated finger and screened far fewer candidates for allelic discrimination (four) using artificial contexts[27]. The resultant designs did not achieve disease-relevant allele selectivity and were poorly tolerated in vivo[28]. In contrast, the ZFPs described here selectively repress 100% of fully-penetrant m*HTT* alleles while preserving normal *HTT* expression for >86% of patients with HD. Moreover, under conditions of chronic ZFP expression in human neurons and in the mouse striatum using multiple promoters and AAV serotypes, we observed no evidence of neurodegeneration, neuroinflammation or toxicity up to at least 15 months of age.

It has long been recognized[44] that macromolecular systems can offer the capacity for highly cooperative behavior, in which initial binding events facilitate subsequent ones resulting in a concerted all-or-none response. The chief requirement for such behavior is a means for communication between substrate-bound ligands. ZFP-TF binding to a chromosomal repeat array offers myriad possibilities for such communication, including noncovalent contacts between adjacent DNA-bound fingers[45], binding-dependent DNA

distortion[46], nucleosome ejection[47] and the potential for avidity effects given the interaction of the KRAB repression domain with large corepressor complexes, components of which form multimers and higher-level oligomers[48–50]. Our finding that allele selectivity is ZFP design-dependent disfavors an indirect communication mechanism, and a lack of binding cooperativity in gel shift studies (data not shown) is inconsistent with direct contacts between adjacent bound ZFPs. These observations, along with the requirement for the KRAB repression domain, are consistent with avidity effects potentially mediated by higher-order complexes, which will be investigated in future studies.

While no other human gene has a TSS-adjacent CAG tract as large as the minimum, fully-penetrant m*HTT* allele (CAG40), the potential for off-target regulation poses a challenge for any CAG-targeted strategy. The human genome contains 1,053 perfect CAG arrays, a subset of which are adjacent to the promoters of 176 genes. Discontiguous imperfect arrays are more abundant, with a subset of the 21,456 total sites proximal to 1,872 genes. Because of the unknown influence of promoter context, distal regulatory elements, epigenetic modifications and the potential of our ZFP-TFs to synergize with other factors, we pursued an unbiased approach to interrogate specificity. The allele-selective ZFPs identified in our initial screen exhibited a high degree of genome-wide specificity in HD neurons and fibroblasts. Interestingly, ZFP-A and -B had distinct off-target profiles, despite exhibiting similar on-target behavior for all examined m*HTT* alleles. For example, *MBD5*, which harbors a discontiguous CAG19 array (TSS 0 bp), was repressed by ZFP-B but not by ZFP-A (Extended Data Fig. 4d,e). ZFP-A and -B target different frames of the CAG tract, are comprised of different ZF modules and employ different linker architectures, suggesting that their off-target properties may be design-dependent and therefore amenable to optimization. Recent advances in the engineering of ZF modules, as well as the modulation of non-specific interactions between the ZF and DNA backbone (Miller et al., in press), provide potential complementary paths to optimize specificity.

We anticipated that our proteins could manifest some off-target activity in mice, albeit at different loci given the substantial lack of CAG repeat conservation between orthologs. Remarkably, 85 of the top 100 mouse genes with the largest TSS-adjacent CAG arrays have no corresponding repeat in the human genome. Of the mouse genes significantly regulated in vivo, all had substantially larger CAG repeats in the mouse ortholog. For example, *DNAJC12*—a gene with a CAG19/CAA12 tract present in the mouse promoter but absent in the human ortholog—was regulated in the mouse striatum but not in human fibroblasts or neurons. Among orthologs, only *NAP1L3* was regulated in human neurons and fibroblasts, and only by ZFP-A (3.1- to 5.8-fold repression) but not by ZFP-B (no change detected), further confirming our observations that off-target regulation is influenced by ZFP design. Nevertheless, although the allele-selective ZFPs were well tolerated in our extensive intrastriatal delivery studies, the potential for some off-target regulation in mice should be a consideration when using the current reagents outside of our experimental systems.

While the CAG expansion in the *HTT* gene is causal for HD, the resultant molecular species that potentially drive neurodegeneration continue to be elucidated. For example, a mis-spliced *Htt* isoform containing intron 1 is present in several HD rodent models as well as postmortem HD brains, and may contribute to the formation of pathogenic polyQ-containing N-terminal protein species[51]. Additionally, a growing number of disease-implicated microsatellite expansions—including the m*HTT* CAG repeat—undergo antisense transcription and repeat-associated non-ATG translation, yielding neurotoxic dipeptides that accumulate in patient brains[52]. These *HTT* isoforms may be resistant to ASO- and RNAi-based strategies that target sequences downstream of exon 1. In contrast, allele-selective ZFP-TFs are expected to reduce all CAG-containing sense

and antisense m*HTT* products, potentially providing an important therapeutic advantage.

ZFP-treated R6/2 mice exhibited improvements on certain behavioral endpoints (clasping and open field tests); however, we did not observe significant treatment effects for other standard HD model phenotypes (for example, accelerating rotarod). An important consideration in this regard is the limited AAV coverage achievable for stereotaxic administration to the mouse brain. In our studies, intraparenchymal injections yielded 30–70% coverage of the mouse striatum, thereby limiting the ability to evaluate the impact of ZFP treatment on certain measures of disease progression, most importantly at the level of behavior. Moreover, in contrast to adult-onset HD in humans where motor deficits manifest as hyperkinetic symptoms, most mouse models of HD develop disease quickly and become hypokinetic. While the involvement of the striatum is critical for motor control, whether striatal selective suppression of mHTT is sufficient to ameliorate these symptoms is unclear given the role of the broader cortico-striatal-thalamocortical loops in motor pattern learning and execution. Additionally, it is unknown whether changes in locomotor behavior in HD mice are driven exclusively by striatal mHTT expression. Other brain regions contribute to spontaneous locomotor control in mice, including the motor-relevant cortical areas, cerebellum and brainstem nuclei[53], and there is clear evidence of extra-striatal alterations in HD mouse models[54,55]. Widespread suppression of mHTT might be necessary to rescue some behavioral phenotypes, as has been reported for alternative agents (for example, ASOs) shown to distribute more broadly throughout the murine brain, albeit with effects that are typically mild or partially restorative[8,9,56].

The ARG studies in zQ175 mice demonstrated a more pronounced effect for reducing mHTT before the decline of dopamine D1- and D2-like receptors and PDE10A enzyme levels. Nonetheless, significant improvements were observed when mice were treated after downregulation of these markers[43], suggesting that ZFP administration can partially restore pre-existing loss of these proteins. The PDE10A ARG results were confirmed using [18F]MNI-659 microPET, where a significant elevation in binding potential was observed after symptom initiation using a clinically relevant translational endpoint[57,58]. In contrast, raclopride binding was unchanged in the microPET study, which may reflect methodological differences between in vitro and in vivo detection of D2-like receptor levels, as well as insufficient viral vector distribution necessary to observe a small effect on this marker. Collectively, our findings provide encouraging support for the use of imaging ligands as early readouts for striatal mHTT lowering in human trials.

MRI-guided delivery of AAV directly to the human striatum is clinically feasible and can be monitored in real time to achieve precise administration[59]. Our results in HD mouse models indicate that a one-time striatal AAV-ZFP infusion can correct histopathological, electrophysiological and biomarker deficits that are characteristic of human HD pathology. Given that the striatum is one of the most vulnerable brain regions in HD[60], these efficacy data may be directly relevant to the ultimate goal of modifying disease progression and support the continued development of an allele-selective ZFP-TF for the treatment of HD.

Online content

Any methods, additional references, Nature Research reporting summaries, source data, statements of code and data availability and associated accession codes are available at https://doi.org/10.1038/s41591-019-0478-3.

References

1. Ross, C. A. & Tabrizi, S. J. Huntington's disease: from molecular pathogenesis to clinical treatment. *Lancet Neurol.* **10**, 83–98 (2011).
2. Bates, G. P. et al. Huntington disease. *Nat. Rev. Dis. Prim.* **1**, 15005 (2015).
3. The Huntington's Disease Collaborative Research Group. A novel gene containing a trinucleotide repeat that is expanded and unstable on Huntington's disease chromosomes. *Cell* **72**, 971–983 (1993).
4. Zuccato, C., Valenza, M. & Cattaneo, E. Molecular mechanisms and potential therapeutical targets in Huntington's disease. *Physiol. Rev.* **90**, 905–981 (2010).
5. Yamamoto, A., Lucas, J. J. & Hen, R. Reversal of neuropathology and motor dysfunction in a conditional model of Huntington's disease. *Cell* **101**, 57–66 (2000).
6. Boudreau, R. L. et al. Nonallele-specific silencing of mutant and wild-type huntingtin demonstrates therapeutic efficacy in Huntington's disease mice. *Mol. Ther.* **17**, 1053–1063 (2009).
7. Harper, S. Q. et al. RNA interference improves motor and neuropathological abnormalities in a Huntington's disease mouse model. *Proc. Natl Acad. Sci. USA* **102**, 5820–5825 (2005).
8. Kordasiewicz, HollyB. et al. Sustained therapeutic reversal of Huntington's disease by transient repression of huntingtin synthesis. *Neuron* **74**, 1031–1044 (2012).
9. Stanek, L. M. et al. Silencing mutant huntingtin by AAV-mediated RNAi ameliorates disease manifestations in the YAC128 mouse model of Huntington's disease. *Hum. Gene Ther.* **25**, 461–74 (2014).
10. Grondin, R. et al. Six-month partial suppression of huntingtin is well tolerated in the adult rhesus striatum. *Brain* **135**, 1197–1209 (2012).
11. McBride, J. L. Preclinical safety of RNAi-mediated HTT suppression in the rhesus macaque as apotential therapy for Huntington's disease. *Mol. Ther.* **19**, 2152–2162 (2011).
12. Stiles, D. K. et al. Widespread suppression of huntingtin with convection-enhanced delivery of siRNA. *Exp. Neurol.* **233**, 463–471 (2012).
13. Duyao, M. P. et al. Inactivation of the mouse Huntington's disease gene homolog Hdh. *Science* **269**, 407–410 (1995).
14. Nasir, J. et al. Targeted disruption of the Huntington's disease gene results in embryonic lethality and behavioral and morphological changes in heterozygotes. *Cell* **81**, 811–823 (1995).
15. Dragatsis, I., Levine, M. S. & Zeitlin, S. Inactivation of Hdh in the brain and testis results in progressive neurodegeneration and sterility in mice. *Nat. Genet.* **26**, 300–306 (2000).
16. Arteaga-Bracho, E. E. et al. Postnatal and adult consequences of loss of huntingtin during development:implications for Huntington's disease. *Neurobiol. Dis.* **96**, 144–155 (2016).
17. Wang, G., Liu, X., Gaertig, M. A., Li, S. & Li, X. J. Ablation of huntingtin in adult neurons is nondeleterious but its depletion in young mice causes acute pancreatitis. *Proc. Natl Acad. Sci. USA* **113**, 3359–3364 (2016).
18. Dietrich, P., Johnson, I. M., Alli, S. & Dragatsis, I. Elimination of huntingtin in the adult mouse leads to progressive behavioral deficits, bilateral thalamic calcification, and altered brain iron homeostasis. *PLoS Genet.* **13**, e1006846 (2017).
19. Lopes, F. et al. Identification of novel genetic causes of Rett syndrome-like phenotypes. *J. Med. Genet.* **53**, 190–199 (2016).
20. Monteys, A. M., Wilson, M. J., Boudreau, R. L., Spengler, R. M. & Davidson, B. L. Artificial miRNAs targeting mutant huntingtin show preferential silencing in vitro and in vivo. *Mol. Ther. Nucleic Acids* **4**, e234 (2015).
21. Pfister, E. L. et al. Five siRNAs targeting three SNPs in huntingtin may provide therapy for three-quarters of Huntington's disease patients. *Curr. Biol.* **19**, 774–778 (2009).
22. Southwell, A. L. et al. In vivo evaluation of candidate allele-specific mutant huntingtin gene silencing antisense oligonucleotides. *Mol. Ther.* **22**, 2093–2106 (2014).
23. Gagnon, K. T. et al. Allele-selective inhibition of mutant huntingtin expression with antisense oligonucleotides targeting the expanded CAG repeat. *Biochemistry* **49**, 10166–10178 (2010).
24. Yu, D. et al. Single-stranded RNAs use RNAi to potently and allele-selectively inhibit mutant huntingtin expression. *Cell* **150**, 895–908 (2012).
25. Reiter, F., Wienerroither, S. & Stark, A. Combinatorial function of transcription factors and cofactors. *Curr. Opin. Genet. Dev.* **43**, 73–81 (2017).
26. Marti, E. RNA toxicity induced by expanded CAG repeats in Huntington's disease. *Brain Pathol.* **26**, 779–786 (2016).
27. Garriga-Canut, M. et al. Synthetic zinc finger repressors reduce mutant huntingtin expression in the brain of R6/2 mice. *Proc. Natl Acad. Sci. USA* **109**, 3136–3145 (2012).
28. Agustin-Pavon, C., Mielcarek, M., Garriga-Canut, M. & Isalan, M. Deimmunization for gene therapy: host matching of synthetic zinc finger constructs enables long-term mutant Huntingtin repression in mice. *Mol. Neurodegener.* **11**, 64 (2016).
29. Gersbach, C. A. & Perez-Pinera, P. Activating human genes with zinc finger proteins, transcription activator-like effectors and CRISPR/Cas9 for gene therapy and regenerative medicine. *Expert Opin. Ther. Targets* **18**, 835–839 (2014).
30. Boch, J. et al. Breaking the code of DNA binding specificity of TAL-type III effectors. *Science* **326**, 1509–1512 (2009).
31. Thakore, P. I., Black, J. B., Hilton, I. B. & Gersbach, C. A. Editing the epigenome: technologies for programmable transcription and epigenetic modulation. *Nat. Methods* **13**, 127–137 (2016).
32. Margolin, J. F. et al. Kruppel-associated boxes are potent transcriptional repression domains. *Proc. Natl Acad. Sci. USA* **91**, 4509–4513 (1994).
33. Landwehrmeyer, G. B. et al. Data analytics from Enroll-HD, a global clinical research platform for Huntington's disease. *Mov. Disord. Clin. Pract.* **4**, 212–224 (2017).
34. Consortium, H. Di Developmental alterations in Huntington's disease neural cells and pharmacological rescue in cells and mice. *Nat. Neurosci.* **20**, 648–660 (2017).
35. Mattis, V. B. et al. HD iPSC-derived neural progenitors accumulate in culture and are susceptible to BDNF withdrawal due to glutamate toxicity. *Hum. Mol. Genet.* **24**, 3257–3271 (2015).
36. Menalled, L. et al. Systematic behavioral evaluation of Huntington's disease transgenic and knock-in mouse models. *Neurobiol. Dis.* **35**, 319–336 (2009).
37. Heikkinen, T. et al. Characterization of neurophysiological and behavioral changes, MRI brain volumetry and 1H MRS in zQ175 knock-in mouse model of Huntington's disease. *PLoS ONE* **7**, e50717 (2012).
38. Carty, N. et al. Characterization of HTT inclusion size, location, and timing in the zQ175 mouse model of Huntington's disease: an in vivo high-content imaging study. *PLoS ONE* **10**, e0123527 (2015).
39. Menalled, L. B. et al. Comprehensive behavioral and molecular characterization of a new knock-in mousemodel of Huntington's Disease: zQ175. *PLoS ONE* **7**, e49838 (2012).
40. Plotkin, J. L. & Surmeier, D. J. Corticostriatal synaptic adaptations in Huntington's disease. *Curr. Opin. Neurobiol.* **33**, 53–62 (2015).
41. Russell, D. S. et al. Change in PDE10 across early Huntington disease assessed by [18F]MNI-659 and PET imaging. *Neurology* **86**, 748–754 (2016).
42. Niccolini, F. et al. Striatal molecular alterations in HD gene carriers: a systematic review and meta-analysis of PET studies. *J. Neurol. Neurosurg. Psychiatry* **89**, 185–196 (2018).
43. Haggkvist, J. et al. Longitudinal small-animal PET imaging of the zQ175 mouse model of Huntington disease shows in vivo changes of molecular targets in the striatum and cerebral cortex. *J. Nucl. Med.* **58**, 617–622 (2017).
44. Monod, J., Wyman, J. & Changeux, J. P. On the nature of allosteric transitions: a plausible model. *J. Mol. Biol.* **12**, 88–118 (1965).
45. Pavletich, N. P. & Pabo, C. O. Zinc finger-DNA recognition: crystal structure of a Zif268-DNA complex at 2.1 A. *Science* **252**, 809–817 (1991).
46. Nekludova, L. & Pabo, C. O. Distinctive DNA conformation with enlarged major groove is found in Zn-finger-DNA and other protein-DNA complexes. *Proc. Natl Acad. Sci. USA* **91**, 6948–6952 (1994).
47. Mirny, L. A. Nucleosome-mediated cooperativity between transcription factors. *Proc. Natl Acad. Sci. USA* **107**, 22534–22539 (2010).
48. Iyengar, S. & Farnham, P. J. KAP1 protein: an enigmatic master regulator of the genome. *J. Biol. Chem.* **286**, 26267–26276 (2011).
49. Lupo, A. et al. KRAB-zinc finger proteins: a repressor family displaying multiple biological functions. *Curr. Genom.* **14**, 268–278 (2013).
50. Hinde, E., Cardarelli, F. & Gratton, E. Spatiotemporal regulation of oligomerization and dynamics in live cells. *Sci. Rep.* **5**, 12001 (2015).
51. Sathasivam, K. et al. Aberrant splicing of HTT generates the pathogenic exon 1 protein in Huntington disease. *Proc. Natl Acad. Sci. USA* **110**, 2366–2370 (2013).
52. Banez-Coronel, M. et al. RAN translation in Huntington disease. *Neuron* **88**, 667–677 (2015).
53. Capelli, P., Pivetta, C., Soledad Esposito, M. & Arber, S. Locomotor speed control circuits in the caudal brainstem. *Nature* **551**, 373–377 (2017).
54. Wang, N. et al. Neuronal targets for reducing mutant huntingtin expression to ameliorate disease in a mouse model of Huntington's disease. *Nat. Med.* **20**, 536–541 (2014).
55. Indersmitten, T., Tran, C. H., Cepeda, C. & Levine, M. S. Altered excitatory and inhibitory inputs to striatal medium-sized spiny neurons and cortical pyramidal neurons in the Q175 mouse model of Huntington's disease. *J. Neurophysiol.* **113**, 2953–2966 (2015).
56. Datson, N. A. et al. The expanded CAG repeat in the huntingtin gene as target for therapeutic RNA modulation throughout the HD mouse brain. *PLoS ONE* **12**, e0171127 (2017).
57. Russell, D. S. et al. The phosphodiesterase 10 positron emission tomography tracer, [18F]MNI-659, as a novel biomarker for early Huntington disease. *JAMA Neurol.* **71**, 1520–1528 (2014).
58. Wilson, H. et al. Loss of extra-striatal phosphodiesterase 10A expression in early premanifest Huntington's disease gene carriers. *J. Neurol. Sci.* **368**, 243–248 (2016).

59. Bankiewicz, K. S. et al. AAV viral vector delivery to the brain by shape-conforming MR-guided infusions. *J. Control Release* **240**, 434–442 (2016).
60. Waldvogel, H. J., Kim, E. H., Tippett, L. J., Vonsattel, J. P. & Faull, R. L. The neuropathology of Huntington's disease. *Curr. Top. Behav. Neurosci.* **22**, 33–80 (2015).

Acknowledgements

Author contributions

B.Z., E.J.R., I.M.-S. and H.S.Z. developed the conceptual framework for these studies. J.C.M., L.Z., D.E.P. and E.J.R. contributed to ZFP design. S.J.H., S.L. and R.A. contributed to ZFP assembly. B.Z., K.M., Q.Y., J.R.P., J.M.C., G.Q., M.C.M., R.A., J.L., B.J.V. and A.N. contributed to ZFP testing in Q111/Q7 mouse cells and patient-derived fibroblasts. B.Z. and D.A.S. performed bioinformatics. B.Z., D.A.S., I.A. and D.G. performed microarray analysis. S.F., D.L., L.K., Y.A. and R.S. contributed to ZFP testing in HD NSCs and neurons. B.Z., H.-O.B.N., Y.S., K.T., C.T., A.G., S.K., J.B., L.M, L.P. T.H., K.K.L. and I.M.-S. contributed to zQ175 studies. M.D., J.K. and D.J.S. conducted the electrophysiology studies. J.B., L.M., M.M.S., J.H., L.T., M.T., A.V. and C.H. contributed to the autoradiography and imaging studies. B.Z., Q.Y., A.E.K. and S.R. contributed to the Q50 and R6/2 studies. B.Z., S.F., S.K., J.B., L.M., L.P., I.M.-S. and H.S.Z. designed the experiments. B.Z., F.D.U., P.D.G., E.J.R., I.M.-S. and H.S.Z. supervised the experiments. B.Z. prepared the Figures. B.Z., E.J.R., I.M.-S. and H.S.Z. wrote the manuscript.

Competing interests

Additional information

Methods

Design and assembly of ZFP-TFs. Zinc finger protein for the CAG array were assembled using an archive of pre-validated one- and two-finger modules as previously described[61]. The resulting ZFPs were cloned into a mammalian expression vector (pVAX) to produce a fusion to the KRAB repression domain of KOX1. See Supplementary Tables 1 and 2 for ZF modules, linkers and full ZFP–KRAB sequence information.

Messenger RNA production for transient transfection. Templates for in vitro transcription were generated from pVAX-ZFP or pVAX-GFP plasmids using PCR (forward primer GCAGAGCTCTCTGGCTAACTAGAG; reverse primer $T_{(180)}$CTGGCAACTAGAAGGCACAG). mRNA was synthesized using a mMESSAGE mMACHINE T7 ULTRA Transcription Kit (Thermo Fisher Scientific) as per the manufacturer's instructions and purified using RNeasy96 columns (Qiagen). For testing of previously described CAG-targeted ZFPs[27], the published sequences ZF6xHunt–Kox-1 and ZF11xHunt–Kox-1 were cloned into the same pVAX cassettes used for the current study and mRNA was prepared in the same manner as above.

Production of lentiviral vectors. The coding sequence for ZFP-2A-GFP was cloned into the LV transfer vector pRRL[62] downstream of the CMV promoter. HEK293T cells cultured in 15-cm tissue culture dishes were transfected with the following plasmids: pRRL-CMV-ZFP-2A-GFP (37.5 µg), the VSVG envelope plasmid (18.75 µg) and the packaging plasmids pMDL and pREV (18.75 µg each)[62], using Lipofectamine 2000 (Thermo Fisher Scientific). The viral supernatants (30 ml) were harvested 48 and 72 h post-transfection and filtered through a 0.45-µm filter before being concentrated 300-fold by ultracentrifugation at 4 °C (Optima L-80K preparative ultracentrifuge, Beckman Coulter) at 50,000g for 90 min. The pellets were then suspended in an appropriate volume of Hank's buffered salt solution (Lonza). To determine infectious titer, 2×10^4 HEK293T cells were transduced in triplicate with 100 µl of serially diluted vector preparations overnight, then incubated for an additional 48 h at 37 °C with 5% CO_2. The infectious titer was determined using dilutions that gave a linear dose–response for GFP expression.

Production of AAV vectors. AAV6-CMV-GFP and AAV6-CMV-ZFP (A, B and C) used in the R6/2, HdhQ50 and in vitro neuron studies were generated by Virovek Inc. using baculovirus-based AAV production. All AAV6 vectors were purified by double-CsCl ultracentrifugation, buffer-exchanged to PBS with 0.001% Pluronic F-68. AAV titers were determined using qPCR.

Cell culture and mRNA transfection. Immortalized mouse striatal cell line STHdhQ111/HdhQ7 (Q111/Q7)[63] was a gift from CHDI. The Q111/Q7 cells were maintained in DMEM with 10% fetal bovine serum, penicillin/streptomycin and G418 (0.4 mg ml⁻¹) at 33 °C. mRNA transfection was performed using a 96-well Shuttle Nucleofector (Lonza); 100 ng ZFP mRNA per 1×10^5 cells was transfected using P3 solution and program EN-132. Twenty-four hours after transfection, cells were harvested for gene expression analysis by RT–qPCR.

Huntington's disease fibroblast lines GM04723 (CAG15/67), GM02151 (CAG18/45) and ND30259 (CAG21/38) were obtained from Coriell Cell Repository and maintained in complete minimal essential medium with 20% fetal bovine serum. CAG repeat lengths were confirmed by sequencing. mRNA transfection was performed using a 96-well Shuttle nucleofector (Lonza). We transfected 0.01–1,000 ng ZFP mRNA per 1.5×10^5 cells using Amaxa solution P2 (Lonza) and program CA-137; for doses <100 ng ZFP mRNA, GFP mRNA was added to bring the total amount of mRNA transfected to 100 ng. Twenty-four hours after transfection, cells were harvested for gene expression analysis by RT–qPCR.

Huntington's disease ESC line GENEA020 (CAG17/48)[64] was a gift from CHDI. CAG repeat lengths were confirmed by sequencing. HD ESCs were passaged with accutase and cultured on matrigel-coated plates in E8 media (Thermo Fisher Scientific). Neural stem cells were derived using StemPro Neural Induction Medium (Thermo Fisher Scientific). Briefly, ESCs were seeded in geltrex-coated six-well dishes with 2×10^5 cells per well and, when 10–20% confluent, the medium was changed to StemPro Neural Induction Medium (Thermo Fisher Scientific). Medium was changed every 2 d and NSCs were harvested and expanded on day 7. StemPro NSC SFM medium (Life Technologies) was used to culture HD NSCs and non-HD NSCs (HIP Neural Stem Cells, Globalstem). NSCs were passaged with accutase on geltrex-coated plates. mRNA transfection was performed using a 96-well Shuttle nucleofector (Lonza). NSCs were prepared in accordance with the NSC subculture protocol (StemPro NSC, Life Technologies), and 2×10^5 cells were transfected using 20 µl Amaxa solution SF (Lonza) and program CM-130. Immediately afterwards, 80 µl of media was added to the well before transfer to a 96-well plate containing 50 µl of warm medium.

Neuronal differentiation from NSC was induced by changing to neural differentiation medium (NDIFF) consisting of Neurobasal medium with B-27 Serum-Free Supplement and GlutaMAX (Thermo Fisher Scientific). Medium was changed every 3–4 d. After 7 d in NDIFF, cells adopt neuronal morphology.

To confirm NSC and neuron differentiation, HD NSC or neurons were cultured on chamber slides (Lab-Tek, Thermo Fisher) for immunohistochemistry

analysis of neuronal marker genes. Briefly, cells were fixed and permeabilized using the BD Cytofix/Cytoperm Kit (No. 554714, BD Biosciences). Slides were blocked with 4% normal goat serum and stained with primary antibodies anti-PAX6 (Merck-Millipore, No. AB2237, 1/1,000), anti-Nestin-488 (Merck-Millipore, No. NMAB5326A4, 1/250) or anti-β-III-tubulin (R&D Systems, No. MAB1195, 1/500) overnight at 4 °C. Anti-Mouse IgG (H + L) Alexa 488 (Molecular Probes, No. A11001, 1/500) and anti-Rabbit IgG (H + L) Alexa 555 (Molecular Probes, No. A21428, 1/500) were used for secondary staining.

Generation of stable NSC lines expressing ZFPs. Lentiviral vectors encoding CMV.ZFP.T2A.eGFP were used to create GENE020A NSCs expressing ZFP-A or -B. Concentrated vectors were inoculated with 1×10^6 cells in a six-well plate. After several passages, the resulting cells were subjected to cell sorting to enrich GFP-positive cells. Sorted cells were further expanded and differentiated into neurons as described above.

Immunoblot analysis of primary human fibroblasts. GMO4723 (CAG15/67) human fibroblasts were transfected with 100 ng ZFP mRNA at 1.5×10^5 cells per transfection using Lonza program CA-137 in P2 solution. To obtain sufficient Htt protein for knockdown analysis, each biological replicate consisted of quadruplicate transfections pooled in complete media, followed by separation into four wells of a 24-well plate and incubated at 37 °C, 5% CO_2 for 72 h. For ZFP detection, single transfections were sufficient. Cells were trypsinized, washed, pelleted and lysed in hot 95 °C Laemmli sample buffer and incubated at 95 °C for 5 min. Samples were loaded onto a Bio-Rad 4–15% TGX gel at 5 µl per lane and run at 150 V for 3.5 h at room temperature in tris/glycine/SDS running buffer. Wet transfer onto polyvinylidenedifluoride membrane was performed at 4 °C for 2.5 h at 90 V in transfer buffer containing MeOH (10%). Membranes were blocked at 4 °C in Odyssey blocking buffer, then incubated with primary antibodies for 3 h at room temperature: mouse anti-Htt (1/500; Millipore, No. MAB2166) and rabbit anti-calnexin (1/5,000; Sigma, No. C4731) in 0.2% Tween-20 Odyssey blocking buffer. Blots were washed 3×10 min in PBS-T (PBS + 0.1% Tween-20). Blots were incubated with secondary antibodies for 1 h at room temperature with protection from light: goat anti-Mouse IgG1 (1/5,000; Li-Cor IRDye 800CW, No. 926–32350) and goat anti-Rabbit (1/10,000; Li-Cor IRDye 680RD, No. 926–68071) in Odyssey blocking buffer containing 0.2% Tween-20 and 0.01% SDS. With light protection, blots were washed 3×10 min in PBS-T, dried between Whatman paper and scanned on a Li-Cor Odyssey near-infrared fluorescence imaging system.

Alternatively, for detection of ZFP protein levels, human fibroblasts were transfected with ZFPs (10–1,000 ng) at 2×10^5 cells per transfection in duplicate. Duplicate transfections were pooled post-transfection and incubated for 5 h in 24-well plates at 37 °C, 5% CO_2. Lysates were prepared from cell cultures as previously described above and similarly electrophoresed using 10 µl sample per lane at 120 V for 1 h, followed by wet transfer at room temperature for 1.5 h at 80 V. Membranes were blocked for 3 h at room temperature in Odyssey blocking buffer, then incubated with primary antibodies overnight at 4 °C: mouse anti-M2 IgG1 (1/250; Sigma, No. F1804) and mouse anti-GAPDH IgM (1/5,000; Sigma, No. G8795) in 0.2% Tween-20 Odyssey blocking buffer. Blots were washed 4×15 min in PBS-T, then incubated with the following secondary antibodies in Odyssey blocking buffer containing 0.2% Tween-20 and 0.01% SDS for 1 h at room temperature with protection from light: anti-Mouse IgG1 (1/5,000; Li-Cor IRDye 800CW, No. 926–32350) and goat anti-mouse IgM (1/15,000; Li-Cor IRDye 680RD, No. 926–68180). Blots were washed, scanned and analyzed as above.

Gene expression analysis using RT–qPCR. Total RNA was extracted from cultured cells and mouse striata using the HighPure RNA isolation kit (Roche) and Purelink RNA mini Kit (Ambion), respectively. Complementary DNA was generated using High capacity cDNA reverse transcription kits (Thermo Fisher Scientific). RT–qPCR was performed using SsoAdvanced Universal probes supermix (Bio-Rad) and the CFX real-time PCR instrument (Bio-Rad). Each biological replicate was assessed by RT–qPCR in technical triplicate or quadruplicate.

The following pre-designed RT–qPCR primer/probe assays for gene expression analysis were ordered from Integrated DNA Technologies (IDT):

Mouse assays: total *HTT* (Mm.PT.58.6953479), *Akt3* (Mm.PT.58.679551), *Arpp21* (Mm.PT.58.33472235), *Atp5b* (Mm.PT.53a.17279462), *Darpp32* (Mm.PT.53a.9253526.gs), *Dnajc12* (Mm.PT.53a.12381720), *Drd1a* (Mm.PT.56a.43576955.g), *Drd2* (Mm.PT.56a.7811767), *Eif4a2* (Mm.PT.53a.9498195.g), *Fam155a* (Mm.PT.58.13863189), *Itga7* (Mm.PT.58.32174757), *Kcna6* (Mm.PT.58.9401005), *Mtus2* (Mm.PT.58.16516017), *Nap1l3* (Mm.PT.58.41884267.g), *Nrg2* (Mm.PT.58.29171122), *Pde10a* (Mm.PT.56a.16919824), *Rbfox3/Neun* (Mm.PT.58.11738514), *Rpl38* (Mm.PT.58.42993403.g), *Rsl24d1* (Mm.PT.58.28622487), *Runx2* (Mm.PT.58.41866893), *Stk32c* (Mm.PT.58.10492155).

Human assays: total *HTT* (Hs.PT.49a.14676852.g), *ATXN2* (Hs.PT.58.40126607), B2M (Hs.PT.20234084), *DNM1* (Hs.PT.58.25262501), *ENO2* (Hs.PT.53a.25227282), *FBXO11* (Hs.PT.58.2665601), *FOXG1* (Hs.PT.56a.26906112.g), *FOXP2* (Hs.PT.58.15357735), *GAD1* (Hs.PT.56a.21283000), GLS (Hs.PT.53a.20624732), *MAP2* (Hs.PT.53a.40791337.g), *NANOG* (Hs.PT.53a.21480849), NAPL3 (Hs.PT.56a.24655549.g), *NES* (Hs.PT.53a.20758620), *OCT4* (Hs.

PT.58.14494169.g), ORC4 (Hs.PT.56a.24527823.g), *PAX6* (Hs.PT.53a.814314), *REX1* (Hs.PT.53a.23001209), SOX1 (Hs.PT.53a.28041414.g), *STC1* (Hs. PT.51.14992722), *TBP* (Hs.PT.56a.20792004), THAP11 (Hs.PT.49a.15404553.g), *TOP1* (Hs.PT.53a.19541381).

The following custom assays were also ordered from IDT at a primer/probe ratio of 2/1:

Human/mouse *GAPDH*
Probe: CCCATCACCATCTTCCAGGAGCGAGA
Primers: AGATGATGACCCTTTTGGCTC, CCCTTCATTGACCTCAACTACAT

Human *ATP5B*
Probe: TGCTCCCATTCATGCTGAGGCT
Primers: CCTGAGACTTTGGGCAGAATC, ACCAGTCACCAGAATTTCCTG

Human *EIF4A2*
Probe: AGCAGATGAAATGTTGAGCCGTGGT
Primers: GCAGAAAGCAACACAACCTG, GTTAAACAGAAGATACCTTTCTCCA

MCS (detects the 5′ UTR of the ZFP or GFP transcripts expressed from the AAV6-CMV vectors)
Probe: AGCACGTTGCCCAGGAGGTCA
Primers: GGAACGGTGCATTGGAACG, GTTCGAATCCCAATTCTTTGCC

Unless otherwise indicated, all data were analyzed using Bio-Rad CFX Manager Software v.3.1. Target genes of interest were normalized to the geometric mean of multiple housekeeping genes. Fibroblast and in vivo mouse expression experiments used *EIF4A2*, *ATP5B* and *GAPDH*. For HD NSC and neuron experiments, *ENO2*, *TOP1* and *GAPDH* were used.

Mutant *Htt* mRNA in R6/2 mice was detected using the following primer/probe set:

Forward primer: CGCAGGCTGCAGGGTTAC
Reverse primer: GCTGCACCGACCGTGAGT
Probe: CAGCTCCCTGTCCCGGCGG

Allele-specific detection of mouse *Htt* expression in STHdhQ111/HdhQ7 cells and in Q50 mice was performed with custom-designed primer/probe sets:

m*Htt*_WT_e 5′ (forward primer for the WT *Htt* allele):
CAGGTCCGGCAGAGGAACC
m*Htt*_Q175_l 5′ (forward primer for knock-in *mHtt* allele):
GCCCGGCTGTGGCCTGA
m*Htt*_WT_e 3′ (reverse primer for both WT and KI *Htt* alleles):
TTCACACGGTCTTTCTTGGTGG
Q-PR1 (probe for both WT and KI *Htt* alleles):
TGCACCGACCAAAGAAGGAACTCT

For each sample, 10-μl qPCR reactions were set up for the WT and KI allele as follows: 5 μl SsoFast Probes Supermix (Bio-Rad), 0.5 μl of 20× WT or KI primer/probe Mastermix (final concentration 0.5 μM for each primer and 0.25 μM for the probe), 2.5 μl H_2O and 2 μl of cDNA sample. Thermal cycling conditions were as follows: (1) 95 °C for 2 min; (2) 95 °C for 10 s; (3) 66.8 °C for 30 s; (4) 72 °C for 30 s; (5) plate read, repeat steps 2–5, 45 times; (6) end.

Allele-specific detection of *Htt* expression in CAG17/48 NSC and neurons was performed using a SNP (rs362307 C/T) genotyping assay (C___2229302_10, Thermo Fisher Scientific). For each sample, 10-μl qPCR reactions were set up as follows: 5 μl SsoFast Probes Supermix (Bio-Rad), 0.25 μl of 40× TaqMan SNP Genotyping Assay, 2.75 μl H_2O and 2 μl of cDNA sample. Thermal cycling conditions were as follows: (1) 95 °C for 30 s; (2) 95 °C for 5 s; (3) 60 °C for 25 s; (4) plate read; repeat steps 2–4, 36 times; (5) end.

Allele-specific detection of human *HTT* expression in HD fibroblasts GM04723 (CAG15/67) and GM02151 (CAG18/45) was performed with custom-designed primers based on SNP rs363099-C/T (Exon 29):

363099C-F (099-C forward primer): AGTTTGGAGGGTTTCTC
363099T-F (099-T forward primer): AGTTTGGAGGGTTTCTT
363099T-BL (099-T blocker): AGGGTTTCTCCGCTCAGC/phos/
363099-R (reverse primer, used with both 099-C and 099-T forward primers): TCGACTAAAGCAGGATTTCAGG

The 099-T blocker oligo was designed to anneal to the 'C/G' allele and was phosphorylated at the 3′-end base to suppress amplification of the mutant allele[65]; it was added at a 2/1 molar ratio relative to the 099-T forward primer. For each sample, 10-μl qPCR reactions were set up for 099-T and 099-C as follows: 5 μl SsoFast Evagreen Supermix (Bio-Rad), 0.5 μl of 20× 099-C or 099-T mastermix (final concentration 0.5 μM for each primer and 1 μM of blocker oligo in 099-T assays), 2.5 μl H_2O and 2 μl of cDNA sample. Thermal cycling conditions were as follows: (1) 98 °C for 2 min; (2) 98 °C for 5 s; (3) 58.3 °C for 9 s for the 099-C assay or 55.6 °C for 9 s for the 099-T assay; (4) plate read; (5) repeat steps 2–4, 45 times; (6) end.

Allele-specific detection of human *HTT* expression in HD fibroblasts ND30259 (CAG21/38) was performed with custom-designed primers based on SNP rs362331C/T (Exon 50):

362331-F (331 forward primer): TCTCCTCCACAGAGTTTGTGA
362331-R (331 reverse primer): CCTTCTTTCTGGACTAAGAAGCTG
362331-C probe: TCC CTC ATC +C +AC TGT GT
362331-T probe: CTC +A +T +C +T +A +C TGT GT

For each assay, allele-specific Taqman probes to detect 331-C or 331-T, which contained locked nucleic acid (LNA) bases (indicated by '+N'), were added. The LNA probes were utilized to improve allele discrimination, as compared to unmodified DNA probes[66,67]. For each sample, 10 μl qPCR reactions were set up for 331-T and 331-C as follows: 5 μl SsoFast Probes Supermix (Bio-Rad), 1 μl of 10× 331-C mastermix (final concentration in assay, 0.5 μM each of F and R primers and 0.25 μM of 331-C probe) or 331-T mastermix (final concentration in assay, 0.5 μM each of F and R primers and 0.25 μM of 331-T probe), 2 μl H_2O and 2 μl of cDNA sample. Thermal cycling conditions were as follows: (1) 95 °C for 45 s; (2) 95 °C for 5 s; (3) 62 °C for 1 min for the 331-C assay or 62.7 °C for 1 min for the 331-T assay; (4) plate read; (5) repeat steps 2–4, 45 times; (6) end.

Measuring ATP levels in cultured neurons. In vitro-differentiated CAG17/48 neurons and normal neurons (~1.5 × 10^5 cells) were infected in triplicate with Lenti-CMV-ZFP-2A-GFP or Lenti-CMV-GFP at multiplicity of infection (MOI) 500. Twenty-one d after infection, intracellular ATP levels were measured using the CellTiter-Glo Luminhscent Assay (Promega) and cell numbers in each sample were determined using the ApoLive-Glo assay (Promega). ATP levels per cell from different cells/treatment were then normalized to those of mock-infected HD neurons.

Measuring apoptosis induced by growth factor withdrawal in cultured neurons. In vitro-differentiated CAG17/48 neurons and normal neurons (~1.5 × 10^5 cells) were infected in triplicate with Lenti-CMV-ZFP-2A-GFP or Lenti-CMV-GFP at MOI 500. Five days after infection, medium was changed to fresh neurobasal medium without growth factors. After 48 h of growth factor withdrawal, levels of cell death were measured using a terminal deoxynucleotidyl transferase dUTP nick end labeling (TUNEL) assay kit following the manufacturer's protocol (ApoBrdU Red DNA fragmentation kit, BioVision). The percenage of apoptotic cells (positive for anti-BrdU staining) among lenti-transduced (GFP-positive) cells was measured.

Microarray studies. In vitro-transcribed mRNA encoding the ZFP-TFs was transfected into 1.5 × 10^5 GM02151 HD fibroblasts (100 ng ZFP mRNA, Amaxa shuttle setting CA-137, solution P2, Lonza) or GENEA020 human ESCs (hESC)-derived accutase-detached neurons (1,500 ng ZFP mRNA, Amaxa shuttle setting CA-138, solution P4, Lonza). After 24 h, cells were washed once with PBS then processed for total RNA extraction (High Pure, Roche). Each replicate (50 ng total RNA) was processed according to the manufacturer's protocol for sample preparation, hybridization, fluidics and scanning (Human Primeview GeneChip arrays, Affymetrix). Robust multi-array average (RMA) was used to normalize the raw signal from each probe set. Fold-change analysis was performed using Transcriptome Analysis Console 4.0 (Applied Biosystems) with 'Analysis Type – Expression (Gene)' and 'Summarization – RMA' options selected. Fibroblast samples transfected with ZFP-A, -B and -C were compared to samples treated with a non-CAG-targeted ZFP-TF that has two known targets in fibroblasts (*PAPPA* and *LMCD1*, both repressed by <2 fold change). Neuron samples transfected with ZFP-A, -B and -C were compared to samples treated with GFP, which is known to specifically upregulate *RAP1A* message by several hundred-fold and was therefore excluded from our gene expression analyses[68]. Change calls are reported for transcripts (probe sets) with a difference greater than twofold in mean signal relative to control, and a *P* value < 0.05 (one-way ANOVA analysis, unpaired *t*-test for each probe set). For any gene with more than one probe set, the probe set with the largest absolute fold change is reported.

Human and mouse genome CAG searches and transcription start site mapping. Human chromosomes 1–22, X and Y (version GRCh38) and mouse chromosomes 1–19, X and Y (version GRCm38) were scanned for hexameric CAG motifs with moods_dna.py from the MOODS package (v.1.9.3, https://github.com/jhkorhonen/MOODS/blob/master/python/scripts/moods_dna.py), with mismatch thresholds set to detect either zero or up to three mismatches in the motif. Regions found with this approach were converted to BED format (https://genome.ucsc.edu/FAQ/FAQformat#format1) using a custom python script (moods2bed.py, v.0.1.0). BED CAG motif regions that were adjacent or overlapping (0 bp distance) were fused into single regions using bedtools[12] (v.2.25.0) 'merge' function independent of strandedness.

ENSEMBL human transcripts and their transcription start site coordinates (Ensembl release 92) were obtained from ENSEMBL Biomart (http://www.ensembl.org/biomart/martview) and filtered for only those with a GENCODE BASIC annotation and biotype of 'protein_coding'. TSSs with the same EnsEMBL gene ID were fused if their distance was within 100 bp of each other. Distance of a CAG motif from a given TSS region was determined via the bedtools command 'bedtools closest -D'. For genes with multiple TSS regions, the closest CAG region was used to annotate the gene distances. Affymetrix Primeview annotations (v.36) for EnsEMBL ENSG were used to map probe set ID to ENSG IDs.

Ortholog mapping from human (GRCh38) to mouse (mm10) was queried from EnsEMBL biomart using a custom script (get_biomart_orthologs.py v.0.1.0), which uses pybiomart v.0.2.0 (https://github.com/jrderuiter/pybiomart). Only

genes with an annotation of biotype = 'protein_coding' were considered for mapping tables.

HdhQ50 mouse study. The HdhQ50 and R6/2 mouse studies were performed at Psychogenics Inc. in accordance with the United States Public Health Service Policy on Humane Care and Use of Laboratory Animals, and procedures were approved by the Institutional Animal and Use Committee at PsychoGenics.

HdhQ50/Hdh[+] (Q50)[69] C57BL/6 J mice were provided by CHDI. At 11 weeks of age, AAV6-CMV-ZFP or AAV6-CMV-GFP (1 × 10^{13} viral genomes (vg) ml^{−1}) was bilaterally delivered to the striatum of Q50 mice using stereotaxic injection (n = 4 per group, two males and two females, group size determined by pilot studies). To increase vector coverage of the striatum, two injection sites were used in each striatum: 5 μl was delivered into the anterior site (coordinates: A/P +1.4 mm, M/L ±1.7 mm, D/V −3.5 mm) and 4 μl was delivered into the posterior site (coordinates: A/P +0.2 mm, M/L ±2.3 mm, D/V −3.2 mm) at a rate of 0.5 μl min^{−1} using a stepped cannula design. Body weight was monitored twice per week through the course of the study. At 7 weeks post-injection, mice were decapitated and the brain was rapidly removed from the skull and rinsed in ice-cold saline to remove any surface blood. The striatum was dissected on a chilled surface and subdivided into three equal-sized pieces representing the rostral, middle and caudal portions of the striatum; striatal tissues were treated in RNALater (Qiagen) at 4 °C overnight then stored at −80 °C until RNA extraction. Because AAV injection does not lead to complete and uniform coverage of the striatum (data not shown), each striatum was dissected into three sections to reduce the likelihood that baseline *Htt* levels in poorly transduced regions would interfere with detection of *Htt* regulation in well-transduced regions. For each striatal section, expression of both *Htt* and ZFP was quantified by RT–qPCR. Fig. 2k shows the analysis that includes the highest ZFP-expressing section from each treated striatum.

R6/2 mouse study. R6/2 transgenic mice[70] were bred at PsychoGenics by crossing ovarian-transplanted females on a CBA × C57BL/6 background (Jackson Laboratories) with C57BL/6 WT males. CAG repeat length was confirmed in transgenic mice to be 123 ± 0.6. All experimenters were blinded to group treatments. At 5 weeks of age, AAV6-CMV-ZFP or AAV6-CMV-GFP (1 × 10^{13} vg ml^{−1}) was bilaterally delivered to the striatum of R6/2 mice using stereotaxic injection (n = 14 per group, 7 males and 7 females; group size was chosen based on historical studies testing other agents in the same model); the same injection volume and coordinates were used as in the Q50 mouse study. Mice were monitored for survival twice per day. Body weights were measured once per week until 12 weeks of age, when mice were euthanized.

Clasping behavior was recorded during each body weight session. In brief, each mouse was removed from its home cage, the cage lid was turned upside down and the mouse was placed onto this surface. The animal was then gently pulled backward and upward by the observer in a smooth motion until the animal was suspended above the surface by about 30 cm. The animal was observed for 30 s. A full clasp, defined by simultaneous hindlimb and forelimb clasp pulled tightly into the core, was recorded and used for analysis.

Mice were also subjected to open field testing at 4 (baseline), 6, 8, 10 and 12 weeks of age. Animals were placed in square, plexiglass chambers (27.3 × 27.3 × 20.3 cm³; Med Associates Inc.) surrounded by infrared photobeam sources for 30 min. Total horizontal activity (distance traveled) and vertical activity (rearing) were measured from consecutive beam breaks.

Mice were tested for rotarod performance over three consecutive days at 4 (baseline), 6, 8, 10 and 12 weeks of age. Each daily session included a training trial of 5 min at 4 r.p.m. on the rotarod apparatus (Rotamex). One hour later, the animals were tested for three consecutive accelerating trials per day of 5 min each, with the speed increasing from 0 to 40 r.p.m. over 300 s. The inter-trial interval was at least 30 min. The latency to fall from the rod was recorded. Mice remaining on the rod for more than 300 s were removed and their time scored as 300 s.

The grip strength assay was used to assess muscular strength in limb muscles at 4 (baseline), 6, 8, 10 and 12 weeks of age. Mice were scruffed by the lower back and tail and lowered towards the mesh grip piece on the gauge (Chatillon Force Gauge, San Diego Instruments) until the animal grabbed with both front paws. The animal was then lowered toward the platform and gently pulled straight back with consistent force until it released its grip. The forelimb grip force was recorded on the strain gauge. After testing, animals were placed back into their home cage.

Three mice in the AAV-CMV-ZFP group and five in the AAV-CMV-GFP group died during the course of the study. After mice were euthanized at 12 weeks of age, striata were dissected out (n = 7 and 10 mice for the GFP and ZFP groups, respectively) for gene expression analysis as described for the Q50 mouse study. Tissue from two GFP-treated mice and one ZFP-treated mouse was collected for IHC to confirm vector spread and coverage by IHC.

Repeated measures analysis (age as repeated factor) was carried out with SAS/STAT (SAS Institute, Inc.) using mixed-effect models. An alpha level of 0.05 was selected for all inferential statistics. The models were fitted using the procedure PROC MIXED. Because the WT group was untreated, one analysis was completed to evaluate the genotype effect using genotype, gender and age at testing as factors. For the assessment of treatment effects in the R6/2 groups, data were compared in a second analysis using treatment, gender and age as factors.

Histology, tolerability and specificity studies in ZFP-treated zQ175 and WT mice. *Animal studies.* Male and female zQ175 C57B/L6J knock-in mice were obtained from the Jackson Laboratory. The zQ175 line was derived from a spontaneous expansion of the CAG copy number in the CAG 140 knock-in mice, and generated at Psychogenics. Transgenic mice were back-crossed to C57BL/6J to generate het zQ175 mice and WT littermates. Animals were housed in Eurostandard Type II long cages and given access to food and water ad libitum. Environmental conditions were as follows: 21 ± 1 °C ambient temperature, 55 ± 10% humidity and 12 h/12 h light/dark cycle, with lights on from 07:00 to 19:00. Animals were checked for health status daily. All animal handling was carried out in accordance with the regulations of the German Animal Welfare Act and EU legislation (EU directive No. 2010/63/EU). The study protocol was approved by the local Ethics committee of the Authority for Health and Consumer Protection of the city and state of Hamburg (Behörde für Gesundheit und Verbraucherschutz BGV, Hamburg) under file No. V11307/591 00.33.

AAV vector construction and production. For expression of ZFPs, plasmids were modified from the AAV vector pAAV-6P-SWB[71]. ZFP-B and ZFP-D (FLAG-tagged) were cloned after the human synapsin 1 promoter (hSyn1) to generate pAAV-SWB-ZFP-B and pAAV-SWB-ZFP-D. In addition, the ZFP control construct ΔDBD was generated by deleting the ZFP DNA-binding domain from ZFP-B. Pseudotyped recombinant AAV (rAAV)2/1 + 2 particles were produced and purified as previously described[38,72]. In brief, HEK293 cells were co-transfected with AAV vector carrying the transcription units of interest and plasmids containing rep and cap genes (pDP1rs and pDP2rs, Plasmid Factory) in equimolar ratios by polyethylenimine-mediated plasmid transfection. Cells were lysed 48 h after transfection by three freeze–thaw cycles, and cellular debris removed by centrifugation. The supernatant containing viral particles was treated with benzonase and subjected to iodixanol density centrifugation (S6, S7) at 60,000 r.p.m. Iodixanol was removed and viral particles were concentrated in PBS 300 MK (300 mM NaCl, 1 mM MgCl₂, 2.5 mM KCl) by filter centrifugation. The remaining rAAV solution was filtered through a Millex GV, 0.22-μm pore size. Sterile rAAV particles were stored at 4 °C and diluted 1/1 with sterile PBS buffer to obtain PBS MK (150 mM NaCl, 0.5 mM MgCl₂, 1.25 mM KCl) for in vivo application. AAV titers were determined using qPCR. Before in vivo application, ZFP-expressing rAAV particles were tested in vitro for downregulation of WT or mutant *Htt* in primary striatal neurons from zQ175 het mice. In brief, striatal cultures were prepared in 24-well plates at a cell density of 2 × 10⁵ cells well⁻¹. rAAV particles (3 × 10⁸ genome-containing copies) were added at 3 days in vitro and cells harvested at 14 days in vitro. WT and mutant *Htt* knockdown was assessed by RT-qPCR using the following primers: forward CAG GTC CGG CAG AGG AAC C and reverse TTC ACA CGG TCT TTC TTG TGT G for WT, and forward GCC CGG CTG TGG CTG A and reverse TTC ACA CGG TCT TTC TTG TGT G for mutant *Htt*, respectively.

AAV ZFP in vivo application. zQ175 het mice (mixed gender) received bilateral intrastriatal injections of rAAV constructs encoding ZFP-ΔDBD control at either 2 or 6 months of age. Mice were individually anaesthetized with 3% isoflurane at a flow rate of 1 l min⁻¹ and placed in a stereotaxic instrument (Kopf, No. 940). Anesthesia was maintained throughout the surgical procedure via gas nose cone delivery of 2% isoflurane at a flow rate of 0.5 l min⁻¹. A longitudinal mid-sagittal incision of length 1 cm was made in the scalp, after sterilization with 70% ethanol and iodine solution and lidocaine application. Following skin incision, a small hole corresponding to the striatal injection site was made in the skull using an electrical drill (Foredom, No. H.30). The coordinates measured according to the mouse bregma were 0.8 mm anterior, 1.8 mm lateral (right) and 3.8 mm deep with flat skull nosebar setting. A total volume of 4 μl (4 × 10¹⁰ genome copies) ZFP viral vectors were administered using a Hamilton gas-tight syringe (model 1801 RN, No. 7659–0, customized 26-gauge needle) connected to an automated micro-injection pump at a constant flow rate of 200 nl min⁻¹. After injection, the surgical wound was sealed and the animal was kept on a heating pad until fully recovered.

Histology and immunohistochemistry. Mice were euthanized at 6, 10 or 12 months by transcardial perfusion. For perfusions, mice were deeply anesthetized by intraperitoneal injection of ketamine/xylazine (120/15 mg⁻¹ kg⁻¹ at 15 μl g⁻¹ body weight) using a 27-gauge needle. Before perfusion, animals were assessed for loss of toe pinch reflex and corneal reflex to ensure that the correct level of anesthesia was achieved. Mice were transcardially perfused with 30 ml of ice-cold PBS followed by 50 ml of 4% paraformaldehyde using a peristaltic pump. Brain samples were removed from the skull and post-fixed overnight in the same fixative at 4 °C, and cryoprotected by incubation in 30% sucrose solution until saturated. Whole brains were embedded in TissueTek and stored at −80 °C. Coronal sections of 25 μm were cut using a cryostat, collected as free-floating in 24-well plates and directly used for staining or stored in a cryoprotection solution (25 mM NaPO₄ buffer, pH 7.4, 30% ethylene glycol, 20% glycerol) at −20 °C until time of use. The following primary antibodies were used for immunostaining: monoclonal mouse anti-mutant huntingtin (1/100; EM48, Millipore, No. MAB5374, lot No. 2135055), monoclonal rabbit anti-DARPP32 (1/250; clone 19A3, Cell Signaling, No. 2306, lot No. 2), polyclonal rabbit anti-NEUN (1/500; Millipore, No. ABN78, lot No. 2140086),

monoclonal mouse anti-GFAP (1/500, Millipore, No. MAB3402, lot No. 1990686), polyclonal rabbit anti-IBA1 (1/500, Wako, No. 019–19741, lot No. SAE6921), polyclonal rabbit anti-ZNF-10 (1/100, Novus Biologicals, No. NBP1–81348, lot No. A95371). All staining was performed with floating sections. Sections were permeabilized in 0.3% Triton X-100/PBS, blocked in 10% normal goat serum/PBS and incubated with the primary antibody diluted in 1% normal goat serum and 0.1% Triton X-100 in PBS at 4 °C overnight. Sections were washed three times in PBS for 15 min and incubated in secondary antibody for 2 h at room temperature: anti-mouse IgG (1/1,000, CF-568, Sigma-Aldrich, No. SAB4600082), anti-rabbit IgG (H + L) (1/1,000, CF-647, Sigma-Aldrich, No. SAB4600184), anti-rabbit IgG (H + L) (1/1,000, CF-488, Sigma-Aldrich, No. SAB4600042). Sections were washed in PBS as described above and mounted using aqueous mounting medium containing DAPI (Fluoroshield, Sigma, No. F6057), in 24-well glass-bottom plates (Sensoplate, Greiner, No. 662892) suitable for imaging with the Opera High Content Screening system (PerkinElmer Inc.).

Image acquisition and automated image analysis. Image acquisition and analysis were performed as previously described[38]. In brief, automated image acquisition was conducted using the Opera High Content Screening system and Opera software v.2.0.1 (PerkinElmer Inc.) using a ×40/1.15 numerical aperture water immersion objective (Olympus, pixel size 0.32 μm) for imaging of mHTT inclusions, or ×20/0.7 water immersion objective (Olympus, pixel size 0.64 μm) for analysis of glial cells in tissue. Image analysis scripts for characterization and quantification of mHTT inclusions were developed using Acapella Studio v.3.1 (PerkinElmer Inc.), and the integrated Acapella batch analysis as part of the Columbus system. To identify astroglia and microglia cells, the algorithm searched for neurite-like cell extensions in the GFAP and Iba1 channels. Extensions that connected to the previously determined nucleus border in a rim of width four pixels around the nucleus were considered valid. A cell was considered GFAP- or Iba1-positive only if extensions could be detected. Subsequently, a 'local' background signal intensity was determined within an extranuclear rim region of 3 pixel width and 2 pixel distance from the previously determined nuclear border. Finally, only cells with a nuclear GFAP or Iba1 intensity higher than the mean local background intensity were considered astroglia or microglia, respectively. Image data from six sections were averaged per animal, and five animals per treatment group were used for statistical evaluation. Quantitative analyses (n = 5 animals with six sections per animal per treatment group) were performed using an unpaired two-tailed *t*-test with Welch's correction.

Tissue homogenization for Meso Scale Discovery (MSD) and Singulex analysis. Whole striata dissected from brain hemispheres were lysed in 80 μl of tissue lysis buffer (20 mM Tris (pH 7.5), 150 mM NaCl, 1 mM EDTA, 1 mM EGTA, 1% Triton X-100, 10 mM NaF, 1 mM PMSF, Phosphatase Inhibitor Cocktail II (Sigma), Phosphatase Inhibitor Cocktail III (Sigma), Protease Inhibitors (Roche Diagnostics)) using a FastPrep24 homogenizer (MP Biomedicals). Crude lysates were centrifuged three consecutive times for 10 min at 16,000 relative centrifugal force and 4 °C, and the supernatant collected after each centrifugation step. Total protein concentration was determined using the bicinchoninic acid assay (BCA, Thermo Scientific) and adjusted to 1 mg ml^{-1} using lysis buffer. Homogenates were aliquoted, snap-frozen, and stored at −80 °C until analysis.

MSD analysis. Meso Scale Discovery plates (384-well) were coated overnight at 4 °C with 10 μl coating antibody in carbonate-bicarbonate coating buffer (15 mM Na$_2$CO$_3$/35 mM NaHCO$_3$, pH 9.6) per well. Plates were then washed three times with 35 μl wash buffer (0.2% Tween-20 in PBS) per well and blocked with 35 μl blocking buffer (2% probumin/0.2% Tween-20 in PBS) per well for 1 h at room temperature with rotational shaking. Striatal extracts were diluted to 0.5 mg ml^{-1} in a mixture of 50% tissue lysis buffer and 50% blocking buffer. After an additional washing step, 10 μl per sample were transferred to each well of the antibody-coated MSD plate and incubated with shaking for 1 h at room temperature. After disposal of samples and four wash cycles with 35 μl of wash buffer each, 10 μl of the detection antibody was added to each well and incubated with shaking for 1 h at room temperature. After three washes with wash buffer, 35 μl of read buffer T with surfactant (MSD) was added to each well and the plate was imaged on a Sector Imager 6000 (MSD) according to the manufacturer's instructions. The following antibody combinations were used: 4 μg l^{-1} 2B7/0.1 μg ml^{-1} 4C9-ST; 4 μg ml^{-1} MW8/1 mg ml^{-1} 4C9-ST (SULFO-tag (ST)). Samples were quantified against human HTT-Q73, aa 1–573 (for assay 2B7/4C9-ST) or aggregated exon1-Q46 (for MW8/4C9-ST) standard curves. ST labeling of antibodies was performed using the MSD SULFO-TAG NHS-Ester reagent (MSD) according to the manufacturer's instructions.

Singulex detection assay for mouse huntingtin. The Erenna Singulex platform (Merck-Millipore, No. 95–0001–03) was utilized to measure mouse huntingtin protein in cellular and tissue lysates according to the manufacturer´s procedures. Labeled antibodies were prepared according to the Erenna Kit manufacturer's instructions (No. 03–0076–02). Specific detection of mouse soluble huntingtin was performed by immunoreaction with capture antibody CHDI-90000147 (625 ng ml^{-1}) and detection antibody MAB2166–4C8 (125 ng ml^{-1}).

Electrophysiology experiments. *AAV construction, manufacture and delivery.* Plasmids containing ZFP-D cDNA and ΔDBD.KRAB cDNA were subcloned and packaged into AAV9 by Virovek. The expression of N-term NLS- and C-term FLAG-tagged human mutant Htt-repressor ZFP and tdTomato was bridged by viral 2 A cleavage peptide. Stereotaxic injections of AAV carrying ZFP.T2A.tdTomato or ΔDBD.T2A.tdTomato genes were made in the striatum (ML = −1.7, AP = −0.98, DV = −3.6) of isoflurane-anesthetized, 4-month-old A2a-EGFP and A2a-EGFP/Q175 het mice. Mice were allowed to recover for at least 2 months post-injection.

Brain slice preparation. Parasagittal mouse brain slices (275 μm) were obtained following procedures approved by the Northwestern University Animal Care and Use Committee and guidelines of the National Institutes of Health (NIH). Mice were acutely anesthetized with a mixture of ketamine (50 mg kg^{-1}) and xylazine (4.5 mg kg^{-1}) and perfused transcardially with oxygenated ice-cold saline (4 °C) containing (in mM): 125 NaCl, 3 KCl, 1 MgCl$_2$, 2 CaCl$_2$, 25 NaHCO$_3$, 1.25 NaH2PO$_4$ and 11 glucose (saturated with 95% O$_2$/5% CO$_2$, pH 7.4, 298 mOsm l^{-1}). After perfusion, mice were decapitated and brains rapidly removed. The slices were transferred to a holding chamber where they were incubated in artificial cerebrospinal fluid (ACSF) at 35 °C for ~30 min, after which they were stored at room temperature until whole-cell recording experiments (1–5 h). The external ACSF solutions were bubbled with 95% O$_2$/5% CO$_2$ at all times to maintain oxygenation and pH ≈ 7.4. The solutions were periodically checked and adjusted to maintain physiological osmolality (300 mOsm l^{-1}).

Electrophysiological recordings. For electrophysiological recordings, slices were transferred to a submersion-style recording chamber mounted on an Olympus BX51 upright microscope (×60/0.9 numerical aperture objective) equipped with infrared differential interference contrast. Whole-cell patch clamp electrophysiological recordings were performed with a Multiclamp 700B amplifier. Signals were filtered at 1 KHz and converted to digital format with Digidata 1400. Stimulation and display of electrophysiological recordings were obtained with the custom-written software WinFluor (John Dempster, Strathclyde University, Glasgow, UK) that synchronizes two-photon imaging and electrophysiology. Targeted electrophysiological recordings were obtained from either iSPNs or direct SPNs. Patch pipettes (4–6 MΩ) were prepared with a Sutter Instruments horizontal puller using borosilicate glass with filament, and filled with (in mM): 135 KMeSO$_4$, 5 KCl, 5 HEPES, 0.05 EGTA, 2 ATP-Mg$_2$, 0.5 GTP-Na, 10 phosphocreatine-di (Tris); pH was adjusted to 7.25 with KOH and osmolarity to 270–280 mOsm. To record Ca^{2+} transients in dendritic spines and shafts, cells were filled with 100 μM Fluo-4 pentapotassium salt and 25 μM Alexa Fluor 568 hydrazide Na salt (Invitrogen). All recordings were made 30 min after whole-cell configuration was established. Electrophysiological characterization of neurons was made in current clamp configuration. The amplifier bridge circuit was adjusted to compensate for electrode resistance. Access resistances were continuously monitored and experiments were discarded if changes > 20% were observed. Only stable recorded neurons were considered for analysis. Thirty per cent of our recordings were discarded because of changes in access resistance. Membrane potential was maintained at −80 mV. Digitized data were imported for analysis with commercial software (IGOR Pro 6.0, WaveMetrics).

Two-photon Ca^{2+} imaging. Calcium transients were evoked by bAPs (five bAP triplets, each 50 Hz intra-train and 5 Hz inter-train; in the ZFP experiments, bAPs were generated with a single 50-Hz triplet). Calcium transients were recorded at proximal (~50–60 μm) and distal dendritic spines (>100 μm) from co-planar sections of the same dendrite using the Ultima Laser Scanning Microscope system (Bruker Technologies, formerly Prairie) attached to a tunable laser (Chameleon, Coherent Laser Group) with 820-nm excitation wavelength (80-MHz pulse frequency, 250-femtosecond (fs) pulse duration). Red signals from Alexa Fluor 568 (580–630 nm) were used to visualize dendrites, whereas green signals from Fluo-4 (490–560 nm) were used to record Ca^{2+} transients. The red channel was used to normalize the signals obtained from proximal and distal sections. Thus, Ca^{2+} transients were expressed as the ratio between green and red fluorescence. Only proximal and distal dendrites lying in the same focal plane and whose red fluorescence differed by <10% were considered for further analysis, thus avoiding dye diffusion artifacts. Line scan signals were acquired at a resolution of 512 pixels per line and 10 μs per pixel dwell time. For ZFP experiments using the triplet bAP, IGOR Pro v.6.32 (WaveMetrics) was used for data smoothing and statistics. Mean fluorescence as a function of time, $F(t)$, was the spatial average of five adjacent pixels while basal fluorescence, F_o, was an average of the first 30 timepoints within a line scan. The normalized difference in Ca^{2+} signal ($\Delta F/F_o$) due to current injection was defined as the maximum fluorescence change normalized by basal fluorescence.

Two-photon laser uncaging. Simultaneous two-photon Ca^{2+} imaging and two-photon laser uncaging were performed using two different fs-pulsed lasers attached to the microscope (Ultima, Bruker Corporation). MNI-glutamate (5 mM) was superfused in the recorded area and excited at 720 nm by the photostimulation laser (Chameleon, Coherent Laser Group). The two laser beams on sample are individually controlled by two independent sets of galvanometric scanning

mirrors. Pulses of 1 ms (~10 mW) were delivered to single spines located in the same focal plane (5–10 spines). Single-spine stimulation was calibrated to evoke a somatic excitatory postsynaptic potential of 1–2 mV for each stimulated spine. Custom-written software (WinFluor) was used to synchronize Ca^{2+} transients, electrophysiological recordings and two-photon laser stimulation.

Tolerability study in zQ175 and WT mice with behavior, MRI and body weight endpoints. All animal experiments were carried out according to the NIH guidelines for the care and use of laboratory animals and were approved by the National Animal Experiment Board.

HET zQ175 KI mice and WT littermate control mice were bred at Charles River Laboratories. Equal numbers of male and female mice were enrolled in the study. Mice with high glutamine levels at baseline magnetic resonance spectroscopy have been excluded from the results. Final numbers are reported in Extended Data Fig. 10.

The experimental groups for the main study arm were $n = 20$ control WT mice (no injection), $n = 15$ control HET zQ175 KI mice (no injection), $n = 22$ HET zQ175 KI mice treated with single bi-intrastriatal injection of PBS (4 μl per hemisphere) at 6 months of age, $n = 19$ HET zQ175 KI mice treated with single bi-intrastriatal injection of AAV1 (1 + 2)-ZFP-D (4 μl per hemisphere) at 6 months of age and $n = 21$ HET zQ175 KI mice treated with single bi-intrastriatal injection of AAV1 (1 + 2)-GFP (4 μl per hemisphere) at 6 months of age.

Husbandry and animal handling. All mice were housed in groups of up to five per cage (single sex), in a temperature- $(22 \pm 1 °C)$ and humidity- $(30–70\%)$ controlled environment with a normal light/dark cycle (07:00–20:00). All mice were housed in cages with clean bedding covering the ground that was changed as frequently as needed to provide the animals with dry bedding. This basic environment was enriched with the addition of a gumabone (BioServ, No. K3214) and shredded paper. Food (Purina Lab Diet 5001) and water were available ad libitum to the mice in their home cages.

Mice (F1 generation) were bred by Charles River by mating zQ175 het males with zQ175 het females (strain background, C57BL/6 J). Pups were weaned from their mothers and segregated to new cages by gender, not exceeding four to five mice per cage. Ear or tail snips were taken during the weaning process at 2–3 weeks for processing at Laragen Inc.—genotyping with PCR and CAG repeat number analysis. In addition, tail samples were collected at the endpoint and sent to Laragen Inc. for genotype and CAG repeat number confirmation.

Animals were monitored twice daily by laboratory personnel (08:00 and 16:00). In cases where the general health status of an animal was significantly worsened, it was euthanized by an overdose of CO_2 and decapitated. Definitions of acceptable endpoints included: no spontaneous movements and inability to drink or eat in 24-h observation period, massive bleeding, spontaneous inflammation, missing anatomy, swelling or tumors >20 mm, inability to right itself in 30 s, and previously mentioned or other severe adverse effects related to compound treatment.

Striatal viral administration. Bilateral intrastriatal administration of ZFP-D- or eGFP-expressing viruses (4 μl per hemisphere; 2.1×10^{13} GC particles ml^{-1}) or vehicle was performed using the stereotaxically guided Hamilton syringes and infusion system (Harvard Apparatus). Infusions were performed in the striatum with the following coordinates: AP = +0.8 mm; ML = ±1.8 mm; DV = −3.0 mm. Briefly, mice were anesthetized with 5% isoflurane (in 70% N_2O and 30% O_2; flow rate 300 ml min^{-1}). During surgery the concentration of anesthetic was reduced to 1.0–1.5%. The rectal temperature was maintained at $37.0 \pm 1.5 °C$ with a homeothermic blanket system. Ointment was applied to mouse eyes to prevent drying, infections or fiberoptic light damage during surgery. Following midline skin incision on the scalp, a burr hole was generated to selected coordinates using stereotaxic coordinates and a dental drill. Thereafter a small puncture in the dura was made at the epicenter of the burr hole and a 10-μl Hamilton syringe with a 28-gauge needle was lowered to a specified depth to reach the striatum. Administration volume was 4 μl and infusion rate was 1 μl min^{-1} (>4 min per hemisphere). The infusion needle was then left in place for a stabilization period of 5 min before withdrawal from the striatum. This was performed slowly, and was paused for 30 s when the needle tip was in the cortical area. Thereafter, the surgical wound was sutured and anesthesia disconnected. The mice were allowed to recover from anesthesia and were carefully monitored for possible postoperative complications. After recovery, mice were returned to their home cages with ad libitum access to food and water. The animals were closely monitored and any abnormal behavior was recorded. Supportive care was provided if necessary.

Pain management and postoperative care. Opioid partial agonist: 0.1 mg kg^{-1} administered subcutaneously postoperatively during anesthesia, together with carprofen.

All mice were also monitored for dehydration and were given 0.9% sterile saline subcutaneously following surgery, and additionally as needed.

Behavioral evaluation studies. Body weight, spontaneous locomotor activity in the open field, clasping and accelerated rotarod performance were evaluated essentially as described[39]. All motor function tests were performed before MRI and magnetic

resonance spectroscopy measurements, at approximately 5.5 (baseline), 9, 12 and 15 months of age.

MRI measurements. MRI acquisitions were performed (20 WT mice and 20 control HET zQ175 mice; 24 per group in other groups) at approximately 5.5 (baseline), 9, 12 and 15 months of age using a horizontal 11.7 T magnet with a bore size of 160 mm, equipped with a gradient set capable of maximum gradient strength 750 mT m^{-1} and interfaced to a Bruker Avance III console (Bruker Biospin, GmbH). A volume coil (Bruker Biospin, GmbH) was used for transmission and a surface-phased array coil for receiving (Rapid Biomedical, GmbH). Mice were anesthetized using isoflurane, fixed to a head holder and positioned in the magnet bore in a standard orientation relative to gradient coils. Anatomical images were acquired using a TurboRARE sequence with repetition time/echo time (TR/TE) = 2,500 36 ms^{-1}, matrix size 256 × 256, field of view (FOV) 20.0 × 20.0 mm^2, 19 contiguous 0.7 mm-thick slices and eight averages. To aid precise voxel placement, additional localizer images were acquired in the axial direction using RARE sequence with TR/TE = 1,800 36 ms^{-1}, matrix size 256 × 128, FOV 20.0 × 20.0 mm^2, 12 contiguous 0.5 mm-thick slices and two averages.

ARG and microPET studies. Heterozygous zQ175 mice (mixed gender) were injected unilaterally with AAV1/2-hSYN1-ZFP-D or AAV2/1-hSYN1-eGFP at Evotec Hamburg, at either 2 or 4 months of age.

The brains of two cohorts of zQ175 het mice were examined with ARG using the striatal markers [^{3}H]raclopride (D2 ligand), [^{3}H]MNI-659 (PDE10 ligand) and [^{3}H]NNC112 (D1 ligand).

One cohort ($n = 10$ mice per group) of animals injected at 2 months of age was sacrificed at 6 months, shipped to Karolinska Institutet and the brains were examined by in vitro ARG using the radioligands.

A second cohort was injected at 4 months of age ($n = 33–41$ mice per group). Animals were shipped to Karolinska Institutet and microPET imaging was performed with the dopamine D2/D3 receptor radioligand [^{11}C]raclopride and with [^{18}F]MNI-659, a radioligand for the PDE10A enzyme, at 6.5–7 and 10 months of age. A subset of this group ($n = 10$ animals per group) was sacrificed at the end of the 10-month imaging study and ARG carried out using [^{3}H]raclopride (D2 ligand), [^{3}H]MNI-659 (PDE10 ligand) and [^{3}H]NNC112 (D1 ligand).

At Karolinska Insititutet, animals were housed at the animal department of Karolinska University Hospital in a temperature- $(\pm 21 °C)$ and humidity- $(\pm 40\%)$ controlled environment on a 12/12 h light/dark cycle (lights on at 07:00) with access to food and water ad libitum. Animals were allowed at least 1 week to habituate to the animal department before the start of the imaging sessions. All experiments were conducted during the light phase of the cycle. All experiments were performed in accordance with the guidelines of the Swedish National Board of Laboratory Animals under protocols approved by the Animal Ethics Review Board of Northern Stockholm, Sweden (No. N558/11).

Brain removal and sectioning. Brains were quickly removed from the skull and placed for freezing in isopentane (2-methylbutane, 99% solution) at approximately −40 °C for 15–20 s. Frozen brains were wrapped in tinfoil and stored at −80 °C until use. The central part of the striatum (~1 mm) was sectioned (coronal) at 14 μm thickness on a cryostat cryomicrotome (Leica CM 1860). Three sections per slide (75 sections = 1 mm tissue = 25 slides) were thaw-mounted on microscope slides (SuperFrostPlus, Menzel-Gläser), air-dried and directly re-frozen in the cryostat. Slides were kept at −20 °C until used. Sectioning was done sequentially, meaning that there were sections from three levels on the same slide.

Radioligands. [^{3}H]NNC112 (77 Curies (Ci) mmol^{-1}) was synthesized at Karolinska Institutet, Department of Clinical Neuroscience. [^{3}H]raclopride (81 Ci mmol^{-1}) was purchased from Novandi Chemistry AB. [^{3}H]MNI-659 (57 Ci mmol^{-1}) was provided by CHDI Foundation. The radiochemical purity of all radioligands was measured before ARG experiments (>95%).

In vitro ARG. Slides were thawed at room temperature and pre-incubated for approximately 20 min in binding buffer (Tris HCl 50 mM, pH 7.4 including 120 mM NaCl, 5 mM KCl, 2 mM CaCl$_2$ and 1 mM MgCl$_2$). The slides were then incubated at 1 nM radioligand in binding buffer for 60 min at room temperature.

In a duplicate set of containers, butaclamol ([^{3}H]NNC112 and [^{3}H]raclopride) or MP-10 ([^{3}H]MNI-659) at 10 μM was added to establish non-displaceable binding. After incubation the slides were washed three times for 10 min in Tris HCl 50 mM, pH 7.4 followed by a brief wash in distilled water. The slides were dried overnight at room temperature or for ~30 min on a heated (37 °C) plate. Slides were placed following autoradiographic microscale standards (American Radiolabeled Chemicals Inc.) and exposed on tritium-sensitive phosphor imaging plates (Fujifilm Plate BAS-TR2025, Fujifilm) for 90 h.

The tissue sections used for [^{3}H]MNI-659 were subjected to fixation in 4% paraformaldehyde before exposure to the phosphor imaging plates. This resulted in a decrease in signal strength, which is essential for analysis of the signal due to the high potency of the radioligand. This technique, with post-fixation of the tissue, was previously used to enable multiple use of phosphor imaging plates for low-energy isotopes such as tritium [^{3}H]. In this context we used post-fixation

to decrease signal strength of [³H]MNI-659 in the tissue, to utilize binding at higher concentrations (for example, 1 nM) which is essential for equilibrium between bound and free fractions. Without the post-fixation step we are limited to performing binding at concentrations <0.15 nM, and that is not sufficient to reach equilibrium and hence visualization of discrepancy between WT and zQ175 [³H] MNI-659 in vitro binding cannot be carried out.

The drawback of post-fixation with [³H]MNI-659 is that the deceased signal influences the image analysis in lower quantitative values of specific binding (fmol mg⁻¹ tissue). Nevertheless, the ratio between analyzed brain regions remains the same, meaning that the difference in specific binding between groups is equivalent.

Image analysis. The phosphor imaging plates were scanned and the resulting images were processed in a Fujifilm BAS-5000 phosphor imager (Fujifilm). ROI analysis was applied by manual delineation of the injection site based on EM48 immunoreactivity as visualized by fluorescence IHC. Mean pixel values of ROIs from six sections were then transformed into radioactivity values and to binding density (fmol mg⁻¹ tissue, tissue wet weight) using the microscale standard. Quantitative analysis was performed using Multi Gauge 3.2 phosphorimager software (Fujifilm). Specific binding was calculated by subtracting the level of non-specific binding from the total binding for each section.

Radiosynthesis. Radiosynthesis of [¹¹C]raclopride was performed at Karolinska Institutet as previously described[73] by methylation of the desmethyl precursor using [¹¹C]methyltriflate. The incorporate rate was >50% and the radiochemical purity was >99%.

Radiosynthesis of [¹⁸F] MNI-659 was carried out as described in ref. [43].

In vivo imaging with [¹¹C]raclopride and [¹⁸F]MNI-659. PET measurements were performed using the Mediso nanoScan PET-MRI and the nanoScan PET-CT preclinical small animal imaging systems[74,75]. Both systems have identical PET performance[74] and were calibrated to provide consistent results. The first PET measurement was performed when the animals were 6.5–7 months of age. On the day of the experiment, animals were anesthetized by inhalation of isoflurane (4–5% isoflurane in 100% oxygen). After induction of anesthesia, the isoflurane concentration was lowered to 1.5–2% (50/50 air/oxygen) and the animals were positioned in the scanner on a designated mouse bed. A cannula was inserted into the tail vein through which the radioligand was administered. A 63-min dynamic PET scan was initiated immediately following intravenous injection of the radioligand. Following completion of the imaging sessions, the animals were returned to their cages. The animals were housed at the animal department at Karolinska Institutet until 10 months of age, when the imaging was repeated using the same radioligands. Data on the animals' weight, radioactivity levels and injected mass from the experiments are shown in Supplementary Table 20.

Image analysis. The acquired list mode data were reconstructed into 25 timeframes (63-min scan: 4×10 s, 4×20 s, 4×60 s, 7×180 s, 6×360 s). Image reconstruction was made with a fully 3-dimensional maximum-likelihood expectation maximization algorithm with 20 iterations, without scatter and attenuation correction. Reconstructed dynamic PET images were co-registered to an inbuilt mouse MRI template available in PMOD, which also incorporates volumes of interest sets (PMOD Technologies Ltd.). With the help of these sets, decay-corrected time activity curves were generated. The binding potential (BP_{ND}) was calculated in PMOD with the simplified reference tissue model using cerebellum as a reference region. The percentage difference between left and right striata was calculated according to the following equation: percentage difference = (right striatum − left striatum)/left striatum × 100. The difference between the sides of the striatum was analyzed by within-subject paired *t*-test. In addition, the percentage difference between striata between the control-treated group and the repressor-treated group was analyzed by between-subject unpaired *t*-test.

Statistical analysis. Statistical analysis in this work was performed using GraphPad Prism v.7 for Windows (GraphPad Software) except where noted. Analysis of microarray data was performed using Transcriptome Analysis Console 4.0 (Applied Biosystems). IGOR Pro 6.32 (WaveMetrics) was used for data smoothing and statistics of electrophysiology data. Behavioral data from the R6/2 mouse study were analyzed using SAS/STAT (SAS Institute Inc.). Statistical analysis of the zQ175 and WT tolerability study with behavior, MRI and body weight endpoints and was performed using IBM SPSS. The statistical tests used for each study are provided in Methods and/or Figure legends. The following standard abbreviations are used to reference *P* values: NS, not significant; # $P < 0.1$; * $P < 0.05$; ** $P < 0.01$; *** $P < 0.001$; **** $P < 0.0001$.

Reporting Summary. Further information on research design is available in the Nature Research Reporting Summary linked to this article.

Data availability

All requests for data will be reviewed by Sangamo Therapeutics, Inc. and the institutions involved to verify whether the request is subject to any intellectual property or confidentiality obligations. If deemed necessary, a material transfer agreement between requestor and Sangamo Therapeutics, Inc. and/or collaborating institutions may be required for sharing of some data. Any data that can be freely shared will be released. All microarray data that support the findings of this study have been deposited in the National Center for Biotechnology Information Gene Expression Omnibus (GEO) and are accessible through the GEO Series accession Nos. GSE127820 and GSE127821.

References

61. Urnov, F. D., Rebar, E. J., Holmes, M. C., Zhang, H. S. & Gregory, P. D. Genome editing with engineered zinc finger nucleases. *Nat. Rev. Genet.* **11**, 636–646 (2010).
62. Dull, T. et al. A third-generation lentivirus vector with a conditional packaging system. *J. Virol.* **72**, 8463–8471 (1998).
63. Trettel, F. et al. Dominant phenotypes produced by the HD mutation in STHdhQ111 striatal cells. *Hum. Mol. Genet.* **9**, 2799–2809 (2000).
64. Bradley, C. K. et al. Derivation of Huntington's disease-affected human embryonic stem cell lines. *Stem Cells Dev.* **20**, 495–502 (2011).
65. Morlan, J., Baker, J. & Sinicropi, D. Mutation detection by real-time PCR: a simple, robust and highly selective method. *PloS ONE* **4**, e4584 (2009).
66. Latorra, D., Campbell, K., Wolter, A. & Hurley, J. M. Enhanced allele-specific PCR discrimination in SNP genotyping using 3' locked nucleic acid (LNA) primers. *Hum. Mutat.* **22**, 79–85 (2003).
67. You, Y., Moreira, B. G., Behlke, M. A. & Owczarzy, R. Design of LNA probes that improve mismatch discrimination. *Nucleic Acids Res.* **34**, e60 (2006).
68. Plautz, S. A., Boanca, G., Riethoven, J. J. & Pannier, A. K. Microarray analysis of gene expression profiles in cells transfected with nonviral vectors. *Mol. Ther.* **19**, 2144–2151 (2011).
69. White, J. K. et al. Huntingtin is required for neurogenesis and is not impaired by the Huntington's disease CAG expansion. *Nat. Genet.* **17**, 404–410 (1997).
70. Mangiarini, L. et al. Exon 1 of the HD gene with an expanded CAG repeat is sufficient to cause a progressive neurological phenotype in transgenic mice. *Cell* **87**, 493–506 (1996).
71. Minderer, M. et al. Chronic imaging of cortical sensory map dynamics using a genetically encoded calcium indicator. *J. Physiol.* **590**, 99–107 (2012).
72. Zolotukhin, S. et al. Recombinant adeno-associated virus purification using novel methods improves infectious titer and yield. *Gene Ther.* **6**, 973–985 (1999).
73. Langer, O. et al. Precursor synthesis and radiolabelling of the dopamine D2 receptor ligand [11C] raclopride from [11C] methyl triflate. *Journal of Labelled Compounds and Radiopharmaceuticals: The Official Journal of the International Isotope Society* **42**, 1183–1193 (1999).
74. Nagy, K. et al. Performance evaluation of the small-animal nanoScan PET/MRI system. *J. Nucl. Med.* **54**, 1825–1832 (2013).
75. Szanda, I. et al. National Electrical Manufacturers Association NU-4 performance evaluation of the PET component of the NanoPET/CT preclinical PET/CT scanner. *J. Nucl. Med.* **52**, 1741–1747 (2011).
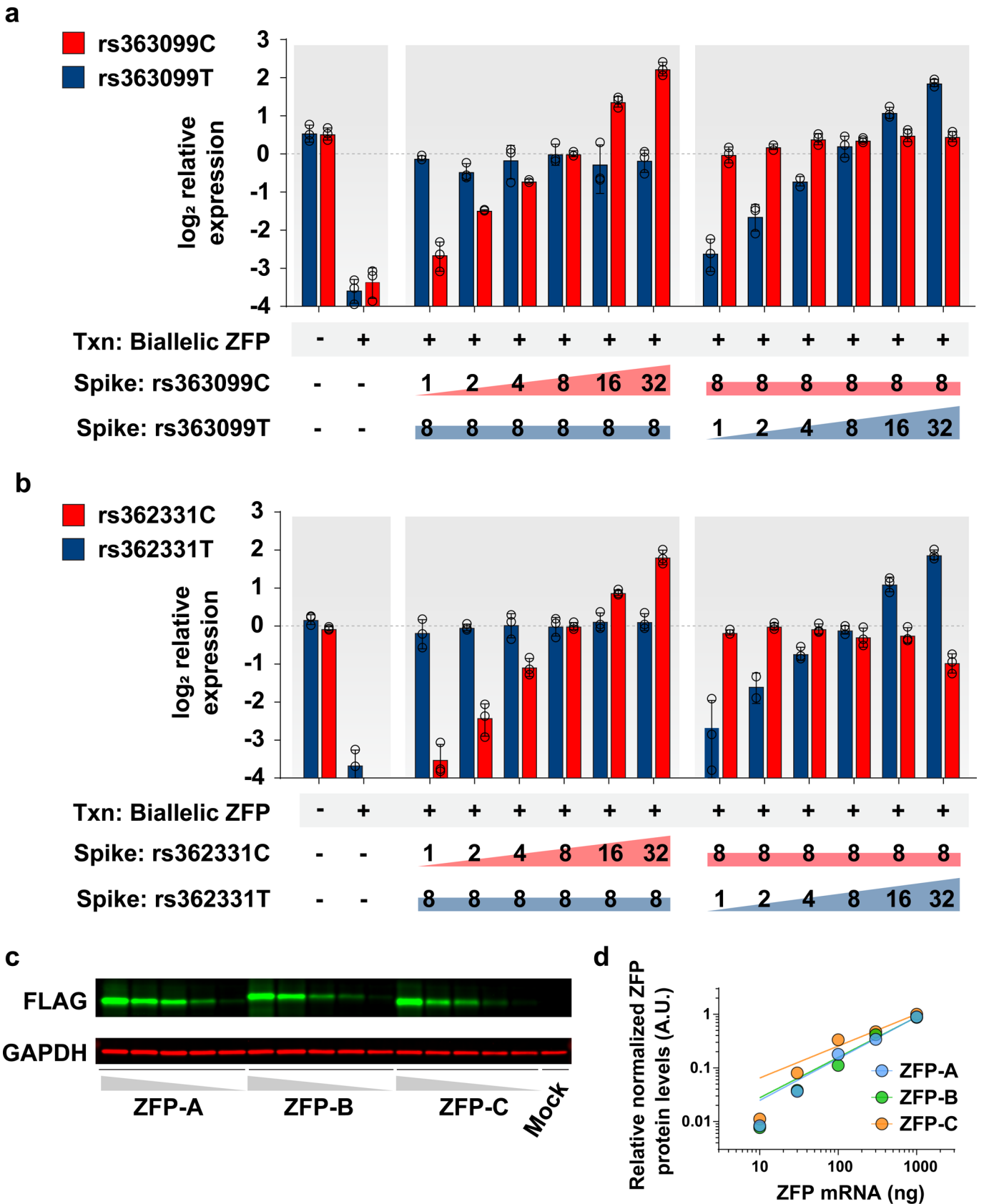
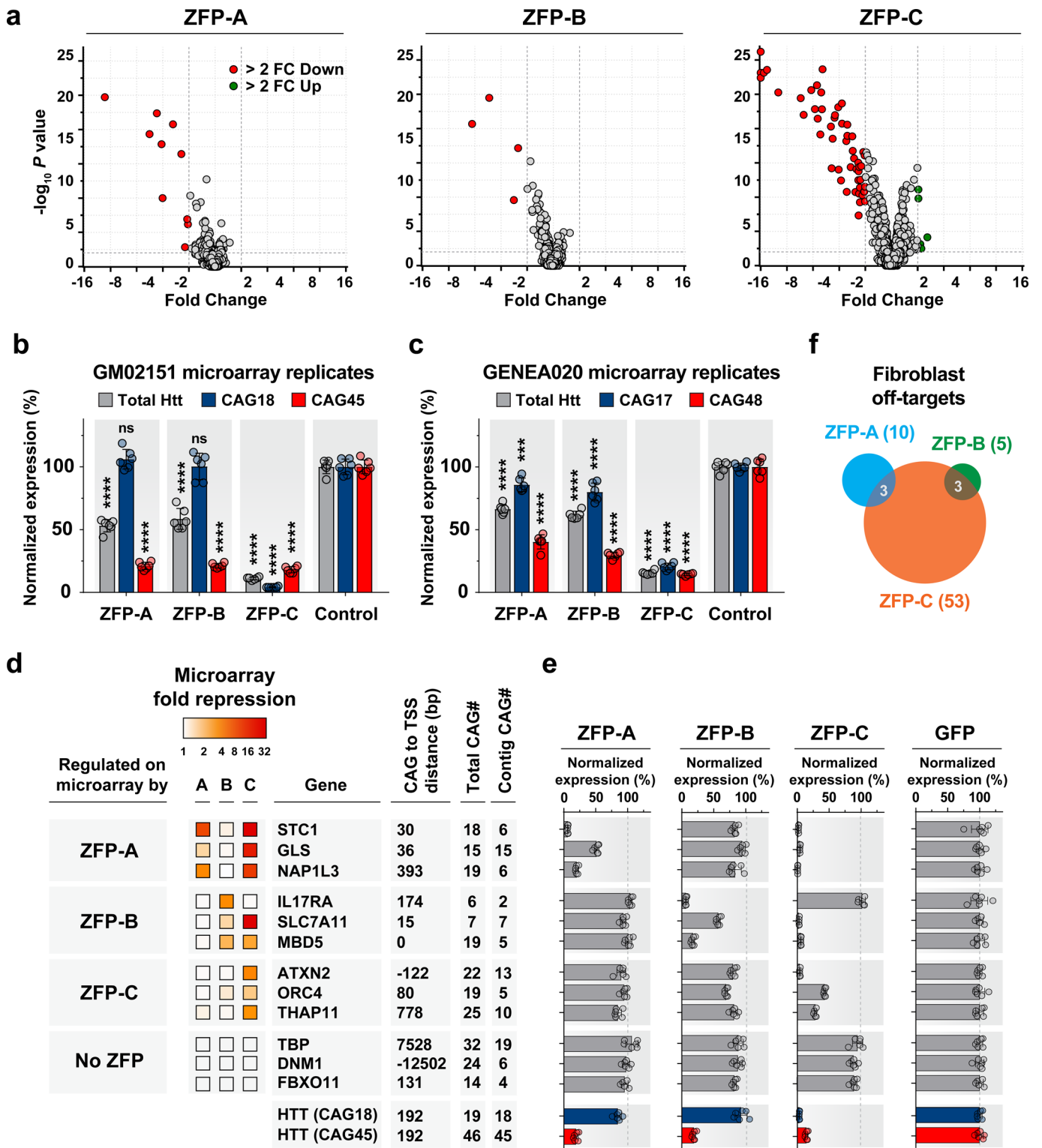**Extended Data Fig. 1 | see figure caption on next page.**

Extended Data Fig. 1 | Validation of custom allele-specific RT–qPCR assays and dose-dependent ZFP protein expression. a, Validation of the rs363099 RT–qPCR assay. GM02151 (CAG18/45) and GM04723 (CAG15/67) fibroblasts are heterozygous for the SNP rs363099T/C. In these lines, the rs363099T variant is in phase with normal *HTT* and rs363099C is in phase with m*HTT*. Separate plasmid templates harboring the rs363099C or rs363099T amplicons were generated. The rs363099C template was serially diluted twofold, from 5 to 0.156 femtograms (fg), in the presence of a fixed amount (1.25 fg) of the rs363099T template (ratio of rs363099C/rs363099T, 0.125/1–4/1; left panel). Conversely, the rs363099T template was serially diluted twofold, from 5 to 0.156 fg, in the presence of a fixed amount (1.25 fg) of the rs363099C template (ratio of rs363099T/rs363099C, 0.125/1–4/1; right panel). Plasmids were diluted into total cDNA prepared from fibroblasts for which *HTT* and m*HTT* expression had been repressed using a strong biallelic *HTT* repressor. Plasmid inputs were chosen so that the RT–qPCR signal from the 1/1 plasmid ratio gave approximately the same signal as *HTT* and m*HTT* in untreated cells. rs363099C- (red) or rs363099T-specific (blue) RT–qPCR assays (see Methods) were performed independently for each of the dilution samples. Relative quantities were scaled to the values obtained for the 1/1 ratio of the rs363099C and rs363099T templates. **b**, Validation of the rs362331 RT–qPCR assay. ND30259 (CAG21/38) fibroblasts are heterozygous for the C/T SNP rs362331. The rs362331T variant is in phase with normal *HTT* and rs362331C is in phase with m*HTT*. Separate plasmid templates harboring rs362331C or rs362331T amplicons were generated and evaluated in the same manner as in **a** using a reciprocal serial dilution range of 2–0.0625 fg in the presence of 0.5 fg of fixed template. rs362331C- (red) or rs362331T-specific (blue) RT–qPCR assays were performed independently for each of the dilution samples. Relative quantities were scaled to the values obtained for the 1/1 ratio of the rs362331C and rs362331T templates. **a,b**, $n = 3$ technical replicates; mean ± s.d. Similar results were replicated in at least one independent experiment for each assay combination. **c**, Representative cropped image of ZFP-A, -B and -C protein levels assessed by immunoblotting in GM04723 fibroblasts transfected at doses of 1,000, 300, 100, 30 and 10 ng ZFP-TF mRNA. Similar results were replicated in one independent experiment. The uncropped scans are provided as source data. **d**, Relative quantitation of protein levels from **c**. ZFP/GAPDH ratios for each sample were scaled to the signal from the 1,000-ng ZFP-C transfected sample.
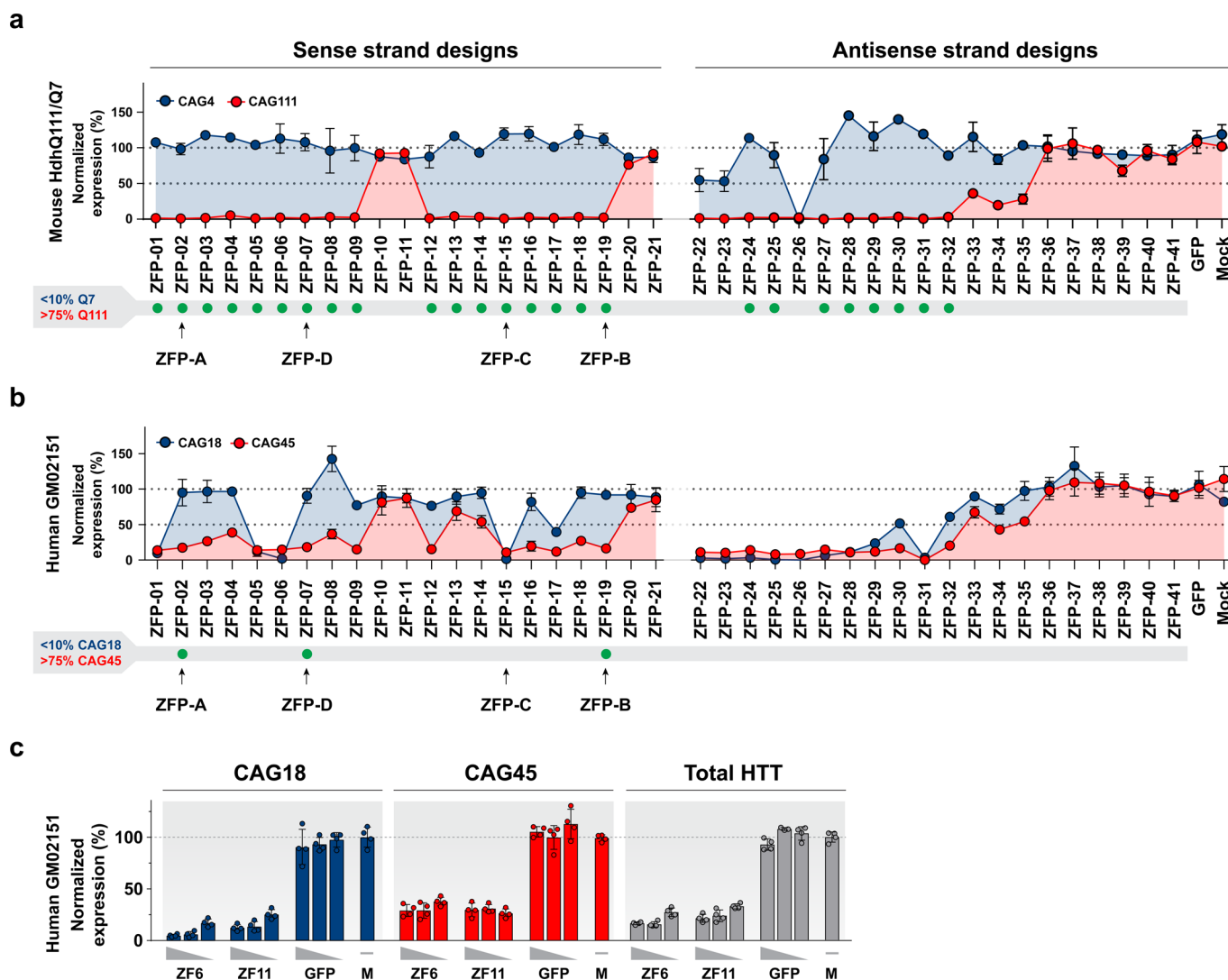
Extended Data Fig. 2 | Evaluation of candidate ZFPs in HdhQ111/HdhQ7 striatal cells and HD fibroblasts. a,b, Comparison of allele selectivity exhibited by candidate ZFP-TF designs in (**a**) the mouse cells used in a previous study[27] (striatal cells derived from the HdhQ111/HdhQ7 mouse model, CAG111/4) versus (**b**) the human HD fibroblast screening system used in the current study (GM02151, CAG18/45). Only three tested designs (ZFP-A, -B and -D) exhibit highly allele-selective repression in the human HD fibroblast system (>75% repression of the mutant allele with <10% repression of the WT allele, denoted by green circles). In contrast, 25 designs manifest such behavior in the less stringent mouse cells. *n* = 3 biologically independent samples; mean ± s.d. **c,** Evaluation of endogenous m*HTT* allele selectivity for the CAG-targeted ZF6xHunt–Kox-1 (ZF6) and ZF11xHunt–Kox-1 (ZF11) from ref. [27] in GM02151 fibroblasts. Normalized transcript levels for normal (CAG18, blue), mutant (CAG45, red) and total *HTT* (gray) in fibroblasts transfected with 1,000, 300 or 100 ng ZFP or GFP mRNA. M, mock transfection. *n* = 4 technical replicates; mean ± s.d.
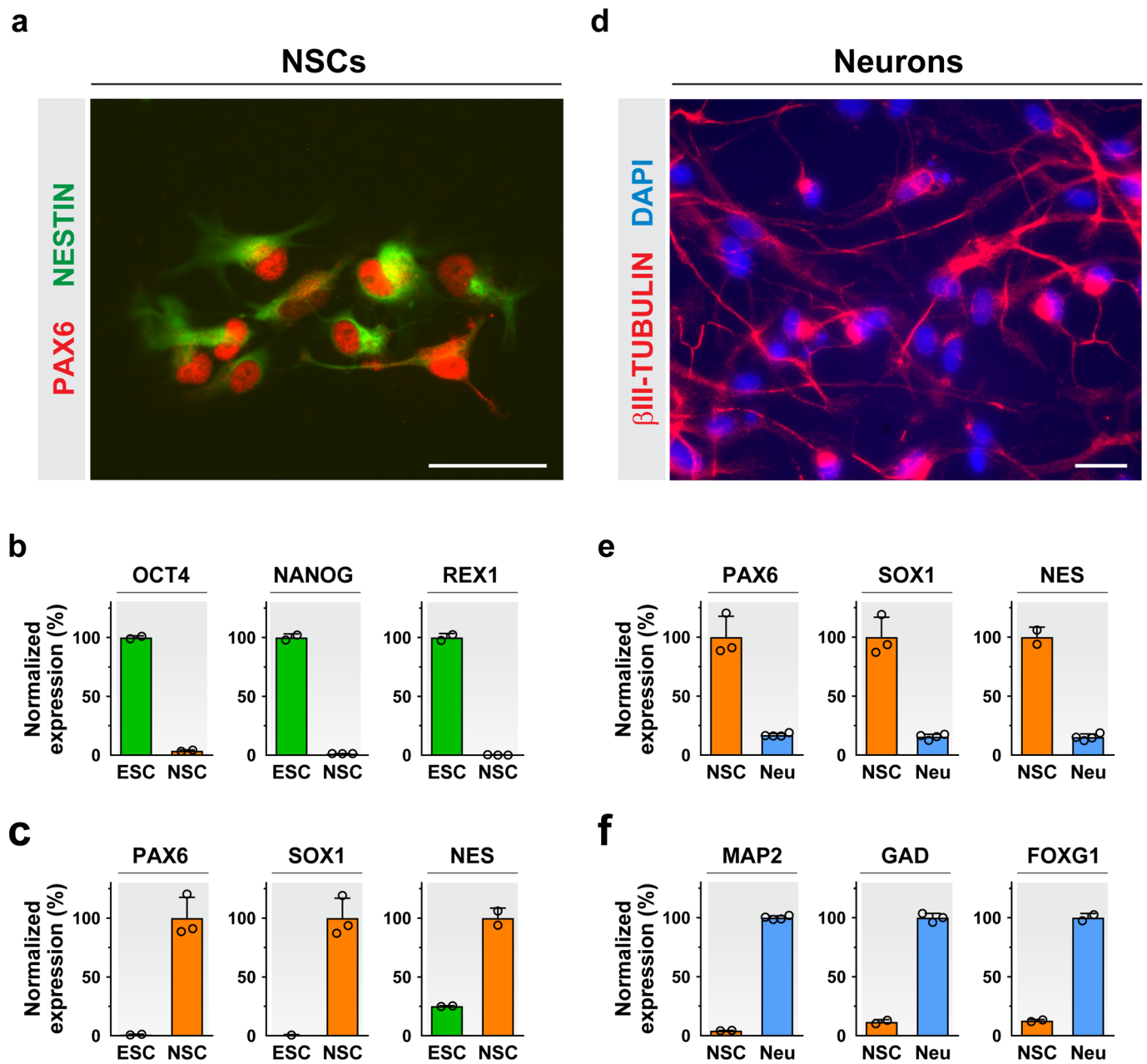
Extended Data Fig. 3 | Validation of NSC and neuronal marker expression in differentiated CAG17/48 hESCs. a,d, Immunofluorescence staining of (**a**) PAX6 (red) and NESTIN (green) expression in NSCs differentiated from GENEA020 ESCs and (**d**) βIII-TUBULIN expression (red) in differentiated neurons (DAPI, blue). Similar results were replicated in three independent experiments. Scale bar, 20 μM. **b,c**, Normalized transcript levels for a panel of (**b**) pluripotency markers (*OCT4*, *NANOG* and *REX1*) and (**c**) NSC markers (*PAX6*, *SOX1* and *NES*) in ESCs and differentiated NSCs. **e,f**, Normalized transcript levels for a panel of (**e**) NSC markers (*PAX6*, *SOX1* and *NES*) and (**f**) neuronal markers (*MAP2*, *GAD1* and *FOXG*1) in differentiated NSCs and neurons. Expression levels were normalized to GAPDH and scaled to the expression of (**b**) ESCs, (**c,e**) NSCs or (**f**) neurons. ESCs, $n = 2$ differentiated lots; NSCs, $n = 2$ differentiated lots; neurons, $n = 4$ differentiated lots; mean ± s.d.

a

ZFP-A | ZFP-B | ZFP-C

> 2 FC Down
> 2 FC Up

b GM02151 microarray replicates

Total Htt | CAG18 | CAG45

c GENEA020 microarray replicates

Total Htt | CAG17 | CAG48

f Fibroblast off-targets

ZFP-A (10) | ZFP-B (5)
ZFP-C (53)

d Microarray fold repression

1 2 4 8 16 32

Regulated on microarray by	A	B	C	Gene	CAG to TSS distance (bp)	Total CAG#	Contig CAG#
ZFP-A				STC1	30	18	6
				GLS	36	15	15
				NAP1L3	393	19	6
ZFP-B				IL17RA	174	6	2
				SLC7A11	15	7	7
				MBD5	0	19	5
ZFP-C				ATXN2	-122	22	13
				ORC4	80	19	5
				THAP11	778	25	10
No ZFP				TBP	7528	32	19
				DNM1	-12502	24	6
				FBXO11	131	14	4
				HTT (CAG18)	192	19	18
				HTT (CAG45)	192	46	45

**e**

ZFP-A | ZFP-B | ZFP-C | GFP

Normalized expression (%)

Extended Data Fig. 4 | see figure caption on next page.

Extended Data Fig. 4 | ZFP specificity assessment in vitro by microarray and RT–qPCR. a, Microarray assessment of GM02151 (CAG18/45) HD fibroblasts transfected with ZFP-A, -B or -C. Each dot represents the mean fold change compared to control-treated cells for a given gene (x value) and the associated P value (y value) determined by an eBayes ANOVA analysis. Genes with ≥ 2 FC change and P < 0.01 are colored red (downregulated) or green (upregulated). ZFP-A, -B and -C: n = 6 biologically independent samples; control: n = 5 biologically independent samples. **b,c**, RT–qPCR analysis of normal (blue), mutant (red) and total HTT for transfected (**b**) GM02151 fibroblast and (**c**) GENEA020 neuron replicates evaluted for microarray analysis. n = 6 biologically independent samples; mean ± s.d.; one-way ANOVA with Tukey's multiple comparison test; **** P < 0.0001. Allele-specific RT–qPCR was performed as in Fig. 2b (GENEA020 NSCs) and Fig. 1i (GM02151 fibroblasts). **d**, Twelve genes were selected for RT–qPCR validation of the microarray results. Three genes were chosen for each ZFP based on two criteria: (1) at least one ZFP treatment resulted in ≥ 2 FC change with P < 0.01, and (2) the gene contained ≥ 6× CAG repeats (allowing up to three mismatches per 6× CAG) within 1 kb of a TSS (see Methods and Supplementary Table 7). An additional three genes were chosen that had large CAG arrays and which were not regulated by any ZFP in the microarray study ('No ZFP' group). The distances of the CAG repeat from the TSS, total CAG count and contiguous CAG count are indicated (see Supplementary Table 7). Normal and mutant HTT CAG alleles for GM02151 fibroblasts are shown for reference. **e**, Regulation of the CAG repeat genes in **d** was confirmed by RT–qPCR. Normalized expression levels were scaled to the control treatment. n = 6 biologically independent samples; mean ± s.d. **f**, Venn diagram of regulated genes in **a**. No genes were commonly regulated (≥ 2 FC change; P < 0.01) by ZFP-A (n = 10) and ZFP-B (n = 5); there was partial overlap with genes regulated by ZFP-C (n = 53).
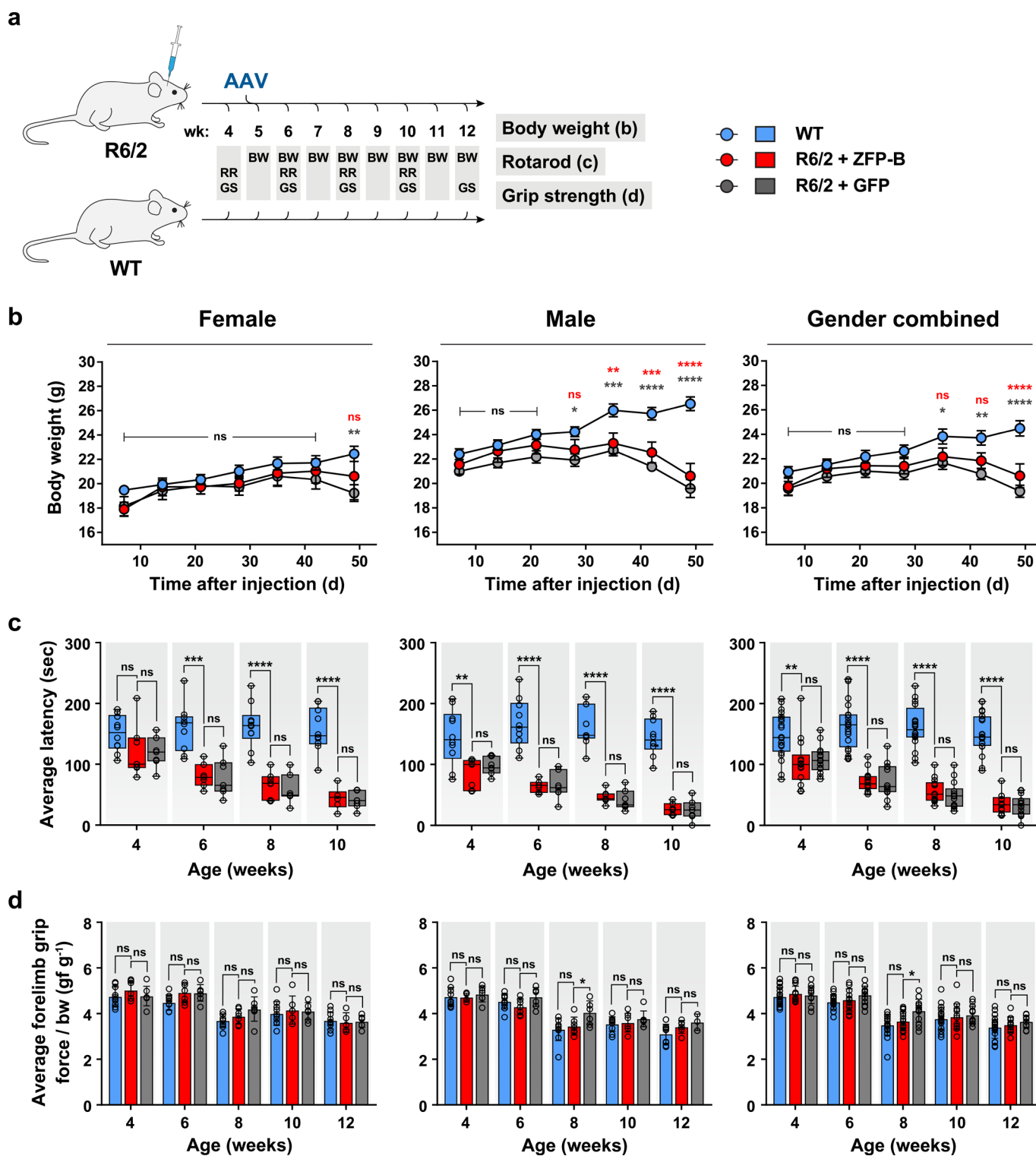
Extended Data Fig. 5 | Additional endpoints evaluated in the R6/2 mouse study. a, Timeline overview of additional endpoints assessed in WT and AAV2/6-treated R6/2 mice. **b–d**, Body weight (**b**), accelerating rotarod (**c**) and forelimb grip strength (**d**) were assessed at the indicated timepoints for untreated non-transgenic littermates (WT, blue, $n = 20$), ZFP-B-treated R6/2 (red, $n = 14$) or GFP-treated R6/2 mice (gray, $n = 14$). Data are shown for female (left), male (middle) and gender combined (right) analyses. **b**, Two-way ANOVA with Tukey's multiple comparison test; results are presented for treatment versus WT comparisons; * $P < 0.05$, ** $P < 0.01$, *** $P < 0.001$, **** $P < 0.0001$; mean ± s.d. **c**, Repeated measures with mixed-effects models; genotype main effect $P < 0.0001$, treatment effect $P = 0.898$. Center line, median; limits, 25–75th percentiles; whiskers, min–max; all points shown. **d**, Repeated measures with mixed-effects models; genotype main effect $P = 0.0025$; treatment effect $P = 0.114$; mean ± s.d. **c,d**, Unpaired two-tailed *t*-test results are shown for each timepoint: * $P < 0.05$, **** $P < 0.0001$.
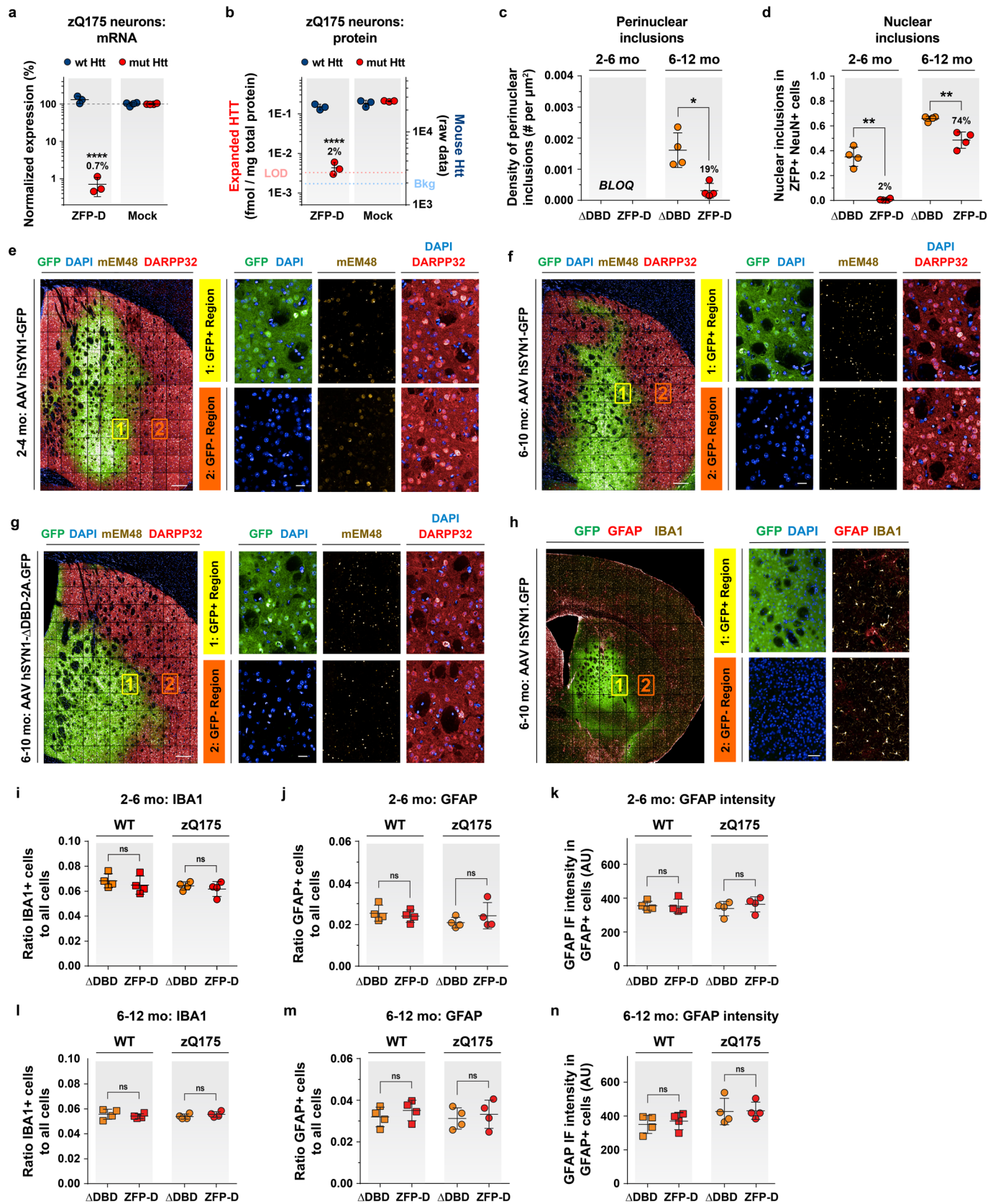
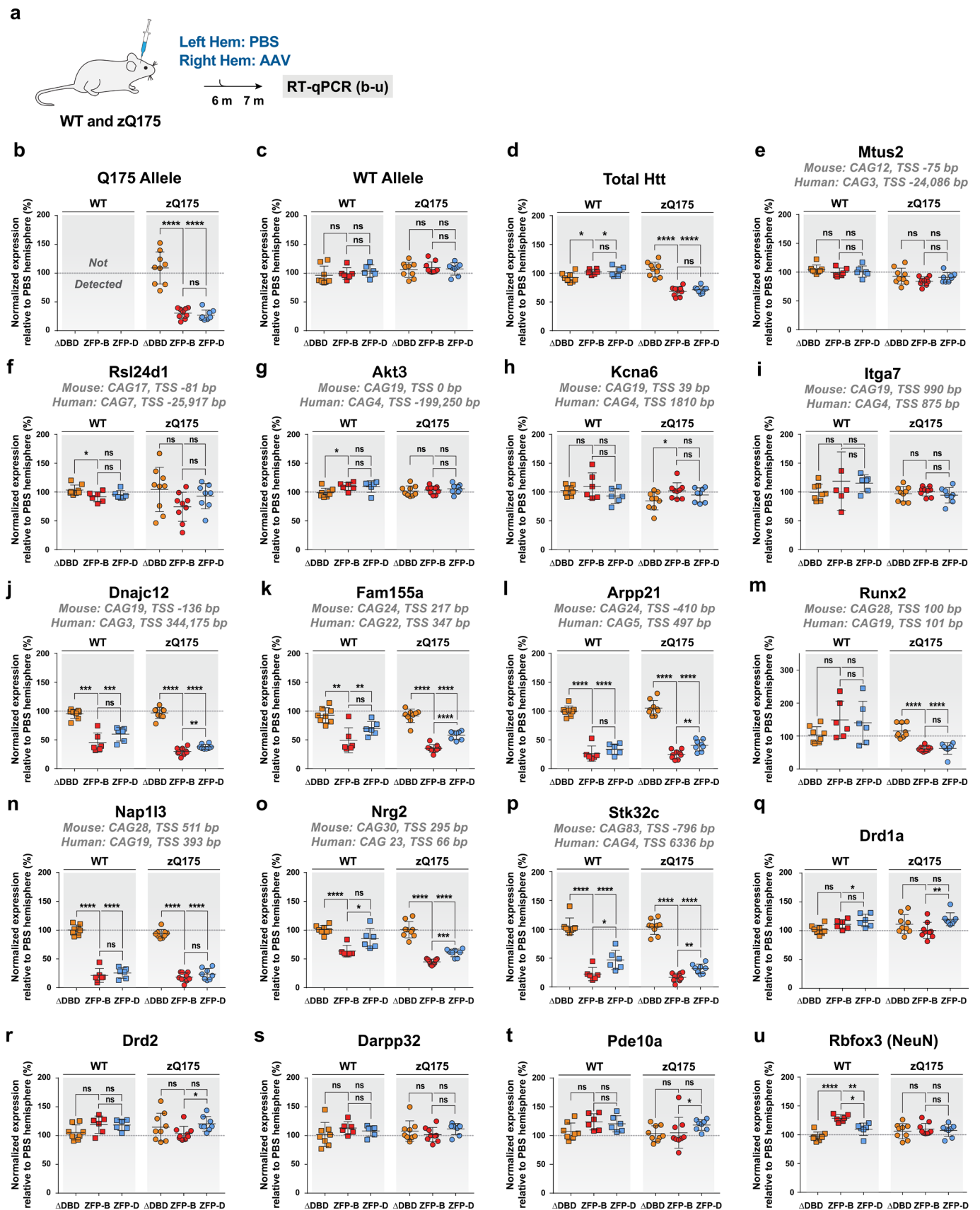Extended Data Fig. 6 | see figure caption on next page.

Extended Data Fig. 6 | zQ175 bridging data for ZFP-D and control treatments. a,b, mRNA (**a**) or soluble protein (**b**) levels of WT and m*HTT* in zQ175 het neurons 10 d after infection with AAV2/1 + 2 ZFP-D as assessed by RT–qPCR (**a**), Singulex (mouse HTT) or MSD (mHTT) (**b**). LOD, limit of detection; Bkg, background limit. $n = 3$ biologically independent samples; mean ± s.d.; one-way ANOVA with Tukey's multiple comparison test; mean ± s.d.; **** $P < 0.0001$. **c,d**, Quantitation of perinuclear (**c**) or nuclear inclusions (**d**) in ZFP+ NEUN+ cells for 2–6- (left) or 6–12- (right) month-old cohorts of zQ175 het mice treated with AAV2/1 + 2 ΔDBD or ZFP-D. BLOQ, below limit of quantitation. $n = 4$ mice; mean ± s.d.; two-tailed unpaired *t*-test with Welch's correction; * $P < 0.05$, ** $P < 0.01$. **e–g**, Representative striatal immunostaining images from 2–4- (**e**) or 6–10- (**f,g**) month-old zQ175 het cohorts injected with AAV2/1 + 2 GFP (**e,f**) or ΔDBD.T2A.GFP (**g**); scale bar, 200 μm. HTT inclusions (mEM48), yellow; GFP, green; DARPP32, red; DAPI, blue. Expanded GFP+ and GFP- regions are shown at right; scale bar, 20 μm. Similar results were replicated in at least one independent experiment. **h**, Representative striatal GFAP and IBA1 immunostaining images from 6–10-month-old zQ175 het cohorts injected with AAV2/1 + 2 GFP; scale bar, 200 μm. GFP, green; DAPI, blue; GFAP, red; IBA1, yellow. Expanded GFP+ and GFP- regions are shown at right; scale bar, 50 μm. Similar results were replicated in at least one independent experiment. **i–n**, Quantitation of IBA1+ cells (**i,l**), GFAP+ cells (**j,m**) and GFAP intensity (**k,n**) in WT (left panels) or zQ175 (right panels) striata injected with AAV2/1 + 2 ΔDBD or ZFP-D for 2–6- (**i–k**) or 6–12- (**l–n**) month cohorts. $n = 4$ mice; mean ± s.d.; two-tailed unpaired *t*-test with Welch's correction.
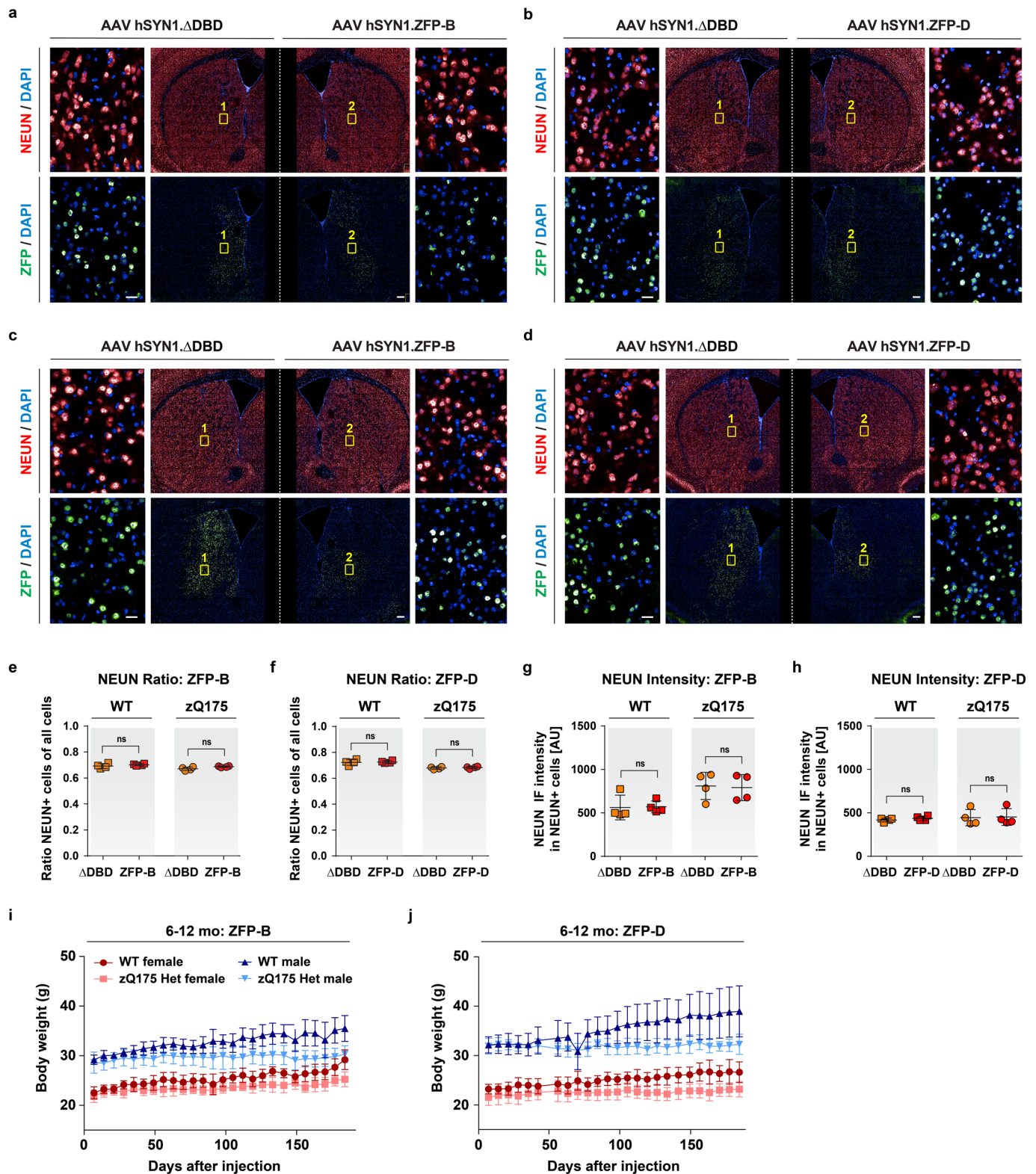
Extended Data Fig. 7 | Assessment of NEUN⁺ cells and body weight in ZFP-treated mice. a–d, Representative whole-brain NEUN and ZFP immunostaining images from 6–12-month-old WT (**a**,**b**) and zQ175 het (**c**,**d**) cohorts injected with AAV2/1+2 ΔDBD in the left hemisphere and either AAV2/1+2 ZFP-B (**a**,**c**) or ZFP-D (**b**,**d**) in the right hemisphere; scale bar, 200 μm. ZFP, green; DAPI, blue; NEUN, red. Expanded regions are shown at left (labeled 1) and right (labeled 2); scale bar, 50 μm. Similar results were replicated in at least one independent experiment. **e–h**, Quantitation of NEUN⁺ cells (**e**,**f**) and NEUN intensity (**g**,**h**) in WT (left panels) or zQ175 het (right panels) mice injected with AAV2/1+2 ZFP-B (**e**,**g**) or ZFP-D (**f**,**h**). **e–h**. n = 4 mice; mean ± s.d.; two-sided unpaired t-test with Welch's correction. **i**,**j**, Weekly body weight assessments for ZFP-B- (**i**) and ZFP-D- (**j**) treated 6-month-old WT and zQ175 het mice until 12 months of age. WT female (red circles, n = 6); WT male (navy triangles, n = 6); zQ175 het female (pink squares, n = 6); zQ175 het male (blue inverted triangles, n = 6); mean ± s.d.
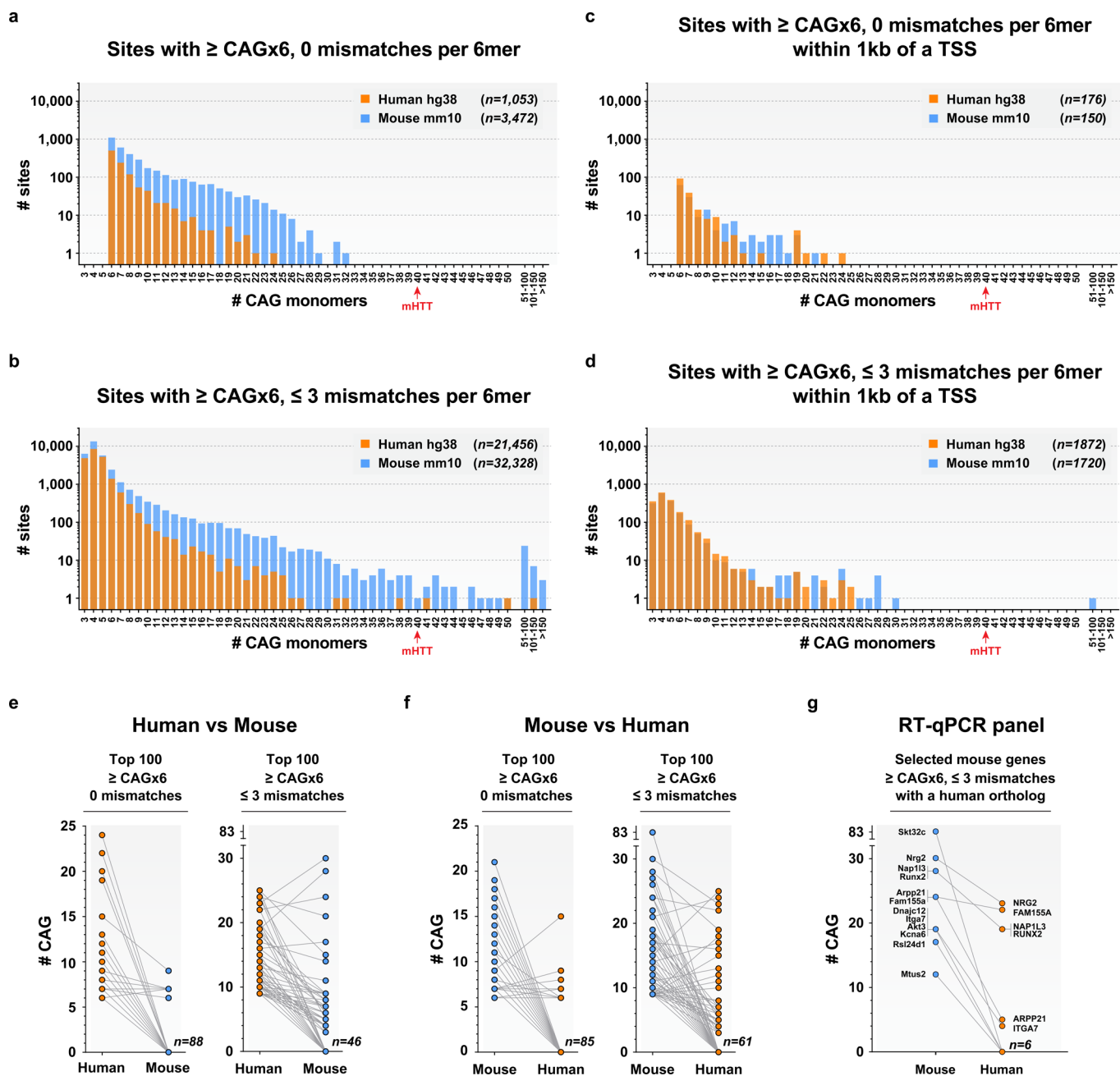
Extended Data Fig. 8 | Analysis of CAG repeat content in the human and mouse genomes. a–d, Distribution of all ≥6× CAG arrays with 0 (**a,c**) or up to three (**b,d**) mismatches per CAG hexamer subsite to capture longer, discontiguous repeat tracts (see Methods and Supplementary Tables 8–15) in the human (hg38, orange) and mouse (mm10, blue) genomes. **a,b,** All CAG arrays represented. **c,d,** CAG arrays located within 1 kb of a TSS. **e,f,** Ortholog mapping and corresponding CAG counts for the top 100 genes with the largest CAG repeats within 1 kb of a TSS in the mouse (**e**) or human (**f**) genome. A line connects the total CAG count for the mouse gene and its human ortholog (**e**), or the human gene and its mouse ortholog (**f**). Search criteria were ≥6× CAG repeats within 1 kb of the TSS with zero (left panel) or up to three (right panel) mismatches per 6× CAG subsite. The number of genes with either no CAG array in the orthologous gene or no ortholog in the other genome is shown at the bottom right of each panel. For clarity, only the top 100 genes are shown; lists were sorted on CAG length, then absolute distance from the TSS. Overlaps may be present for some entries due to multiple ortholog relationships sharing the same CAG counts. See Supplementary Tables 16–19 for complete ortholog lists. **g,** As in (**f**) except that only the 12 genes that were selected for monitoring by RT–qPCR are shown (see Extended Data Fig. 9). Only genes with a human ortholog are included.

Extended Data Fig. 9 | see figure caption on next page.

Extended Data Fig. 9 | In vivo examination of neuronal biomarker and CAG repeat gene regulation in treated WT and zQ175 het mice. a, Timeline overview for the 1-month in vivo RT–qPCR study. Six-month-old WT or zQ175 het mice were treated with unilateral injections of AAV2/1+2 encoding either ΔDBD ($n = 8$ WT, $n = 9$ zQ175), ZFP-B ($n = 6$ WT, $n = 9$ zQ175) or ZFP-D ($n = 6$ WT, $n = 8$ zQ175) in the right hemisphere. PBS was injected into the left hemisphere. **b,c**, Normalized allele-specific transcript levels for Q175 (**b**) and WT (**c**) *Htt*. **d–u**, Normalized RT–qPCR levels for total *Htt* (**d**), 12 mouse genes with TSS-adjacent CAG repeats (**e–p**) and five neuronal biomarker transcripts (**q–u**). **b–u**, The ratio of the normalized transcript level for the AAV-treated hemisphere to that of the PBS-treated hemisphere is shown for each mouse in the WT (left panel) and zQ175 het (right panel) treatment groups. Mean ± s.d.; unpaired two-tailed *t*-test with Welch's correction. * $P < 0.05$, ** $P < 0.01$, *** $P < 0.001$, **** $P < 0.0001$. **e–p**, The length of the closest CAG tract ($\leq$ three mismatches per 6× CAG site; see Extended Data Fig. 8g) and its distance to the TSS are shown for the mouse and human ortholog of each profiled gene.
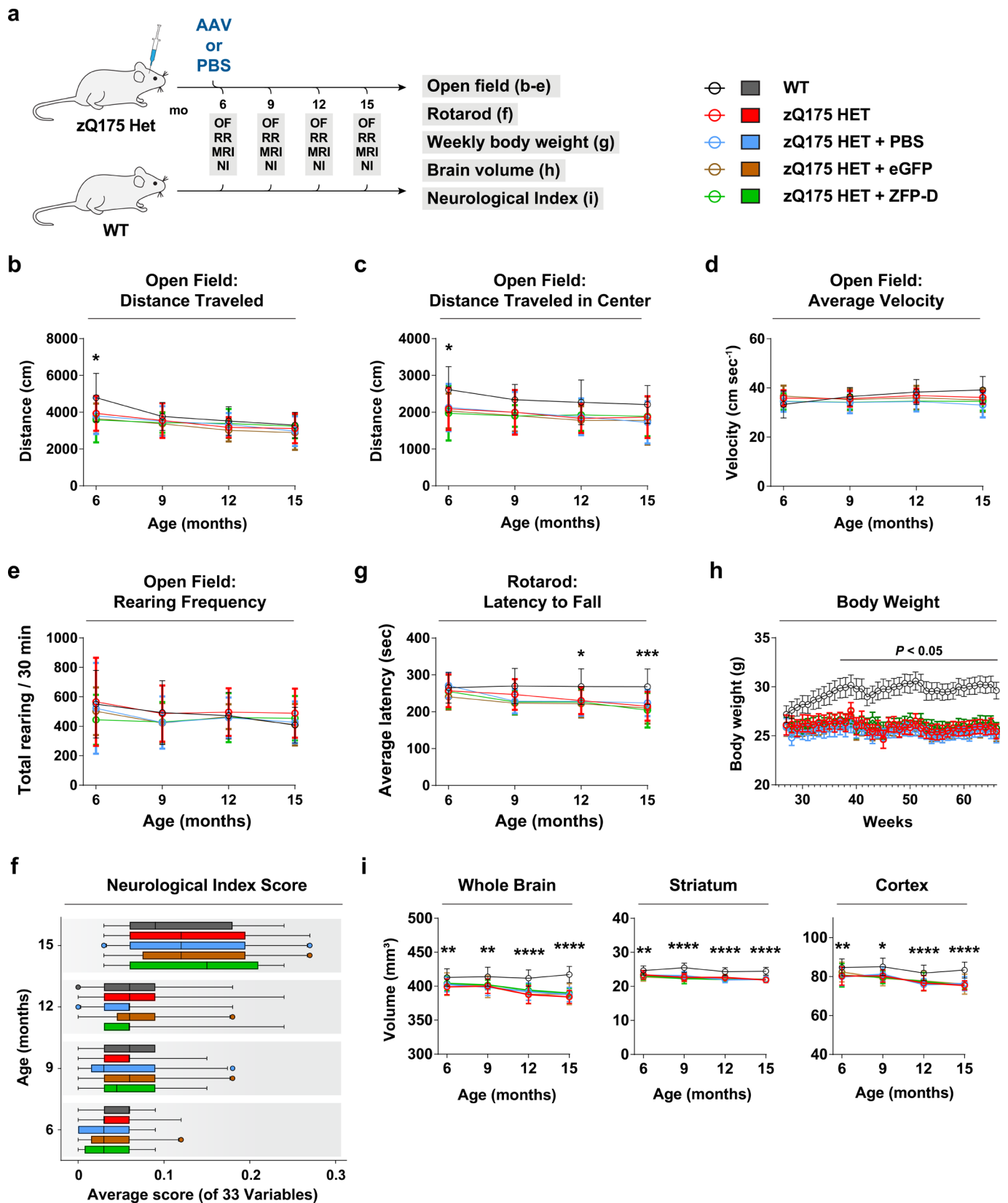
Extended Data Fig. 10 | see figure caption on next page.

Extended Data Fig. 10 | Tolerability assessment of ZFP-treated WT and zQ175 het mice. a, Six-month-old zQ175 mice were bilaterally injected with ZFP-D (green, $n=17$), eGFP (brown, $n=21$) or PBS (blue, $n=21$) and monitored for 9 months alongside age-matched WT (black, $n=19$) or non-injected zQ175 (red, $n=14$) controls. **b–e**, Open field testing of total (**b**) or center (**c**) distance traveled, average velocity (**d**) and rearing frequency (**e**). **f**, Neurological index scores represent the average of 33 metrics (see Methods). **g**, Average latency to fall using the rotarod test. **h**, Body weight measurements. **i**, MRI-based volumetric measurements of whole brain (left), striatum (middle) and cortex (right). Measurements were taken at 5–6 months (baseline, before injection), 9, 12 and 15 months of age (**b–g,i**) or weekly (**h**). Repeated measures (**b–e,g,i**) or ordinary (**f,h**) two-way ANOVA with Dunnett's multiple comparison test. **b–e,g,i**, mean ± s.d. **f**, Center line, mean; limits, 25–75th percentiles; whiskers, 5–95% confidence interval; points, outliers. **h,** mean ± s.e.m. **b–i**, P values are indicated only for comparisons achieving significance; in all cases these correspond to genotype effects. **b**, * $P=0.0146$; zQ175 het versus WT. **c**, * $P=0.0212$; zQ175 het versus WT. **g**, * $P=0.0257$, *** $P=0.0008$; zQ175 het versus WT. **h**, * $P<0.05$; zQ175 het versus WT. **i**, * $P<0.05$, ** $P<0.01$, *** $P<0.001$, **** $P<0.0001$; zQ175 het versus WT.

nature research

NMED-A85147C-Z
Bryan Zeitler

Corresponding author(s): Ignacio Munoz-Sanjuan

Last updated by author(s): Apr 23, 2019

Reporting Summary

Nature Research wishes to improve the reproducibility of the work that we publish. This form provides structure for consistency and transparency in reporting. For further information on Nature Research policies, see Authors & Referees and the Editorial Policy Checklist.

Statistics

For all statistical analyses, confirm that the following items are present in the figure legend, table legend, main text, or Methods section.

n/a	Confirmed	
☐	☒	The exact sample size (*n*) for each experimental group/condition, given as a discrete number and unit of measurement
☐	☒	A statement on whether measurements were taken from distinct samples or whether the same sample was measured repeatedly
☐	☒	The statistical test(s) used AND whether they are one- or two-sided *Only common tests should be described solely by name; describe more complex techniques in the Methods section.*
☐	☒	A description of all covariates tested
☐	☒	A description of any assumptions or corrections, such as tests of normality and adjustment for multiple comparisons
☐	☒	A full description of the statistical parameters including central tendency (e.g. means) or other basic estimates (e.g. regression coefficient) AND variation (e.g. standard deviation) or associated estimates of uncertainty (e.g. confidence intervals)
☐	☒	For null hypothesis testing, the test statistic (e.g. *F*, *t*, *r*) with confidence intervals, effect sizes, degrees of freedom and *P* value noted *Give P values as exact values whenever suitable.*
☒	☐	For Bayesian analysis, information on the choice of priors and Markov chain Monte Carlo settings
☒	☐	For hierarchical and complex designs, identification of the appropriate level for tests and full reporting of outcomes
☒	☐	Estimates of effect sizes (e.g. Cohen's *d*, Pearson's *r*), indicating how they were calculated

Our web collection on statistics for biologists contains articles on many of the points above.

Software and code

Policy information about availability of computer code

Data collection	- Mouse studies (behavior and MRI): Open Field Activity Chambers and Activity Monitor: Med Associates Inc (St Albans, VT); Rotarod: AccuScan Instruments (Columbus, OH); MRI: Bruker Biospin GmbH (Ettlingen, Germany). - Electrophysiology studies: Data were visualized and analyzed with custom image-processing shareware software (PicViewer and WinFluor - John Dempster) - zQ175 microPET studies: nanoScan Nuclein (Mediso Ltd.; Hungary; version: 2.00.021)
Data analysis	- Image analysis for Q175 studies: Automated image acquisition of tissue sections was conducted using the Opera® High Content Screening system and Opera software 2.0.1 (PerkinElmer Inc.). Image data was imported into the Columbus® image data management and analysis system version 2.4 (PerkinElmer Inc.). Image analysis was conducted using Acapella® Studio 3.1 (PerkinElmer Inc.) and the integrated Acapella® batch analysis as part of the Columbus® system. - Microarray studies: Fold-change analysis was performed using Transcriptome Analysis Console 4.0 (Applied Biosystems, Foster City, CA) with "Analysis Type – Expression (Gene)" and "Summarization – RMA" options selected. Further details in methods section. - qRT-PCR studies: BioRad CFX manager software V3.1 (BioRad Laboratories, Hercules, CA). - Electrophysiology studies: IGOR Pro 6.32 (WaveMetrics, Lake Oswego, OR) was used for data smoothing and statistics. The mean fluorescence as a function of time (F(t)) was the spatial average of 5 adjacent pixels. The basal fluorescence, Fo, was average of the first 30 time points in a line scan. The percent change in Ca2+ signal (ΔF/Fo) was defined as the maximum fluorescence change normalized by the basal fluorescence. The acquired fluorescence data was then imported to IGOR Pro where traces were smoothed with a binomial Gaussian filter. - MicroPET studies: The analyses of the microPET data were done using the commercially available software PMOD (PMOD Technologies Ltd., Zurich; version: 3.5) - Searches for hexameric CAG motifs in genomes were performed with moods_dna.py from the MOODS 1.9.3 package (https://github.com/jhkorhonen/MOODS/blob/master/python/scripts/moods_dna.py) and converted to BED format using a custom python script (moods2bed.py v0.1.0). Regions were merged and closest features detected using bedtools12 (v2.25.0). Ortholog mapping was performed using a custom python script (get_biomart_orthologs.py v0.1.0) using pybiomart (https://github.com/jrderuiter/pybiomart) v0.2.0.

For manuscripts utilizing custom algorithms or software that are central to the research but not yet described in published literature, software must be made available to editors/reviewers. We strongly encourage code deposition in a community repository (e.g. GitHub). See our Nature Research guidelines for submitting code & software for further information.

> - Statistical analysis: All other molecular, cellular and zQ175 behavioral endpoints - GraphPad Prism 7 (GraphPad Software, San Diego, CA); R6/2 behavioral data were analyzed using SAS/STAT (SAS Institute Inc, Cary, NC).

For manuscripts utilizing custom algorithms or software that are central to the research but not yet described in published literature, software must be made available to editors/reviewers. We strongly encourage code deposition in a community repository (e.g. GitHub). See the Nature Research guidelines for submitting code & software for further information.

Data

Policy information about availability of data

All manuscripts must include a data availability statement. This statement should provide the following information, where applicable:
- Accession codes, unique identifiers, or web links for publicly available datasets
- A list of figures that have associated raw data
- A description of any restrictions on data availability

> All requests for data will be reviewed by Sangamo Therapeutics, Inc. and the institutions involved to verify whether the request is subject to any intellectual property or confidentiality obligations. If deemed necessary, an MTA between requestor and Sangamo Therapeutics and/or collaborating institutions may be required for sharing of some data. Any data that can be freely shared will be released. All microarray data that support the findings of this study have been deposited in the National Center for Biotechnology Information Gene Expression Omnibus (GEO) and are accessible through the GEO Series accession numbers GSE127820 and GSE127821.

Field-specific reporting

Please select the one below that is the best fit for your research. If you are not sure, read the appropriate sections before making your selection.

☒ Life sciences ☐ Behavioural & social sciences ☐ Ecological, evolutionary & environmental sciences

For a reference copy of the document with all sections, see nature.com/documents/nr-reporting-summary-flat.pdf

Life sciences study design

All studies must disclose on these points even when the disclosure is negative.

Sample size	The sample size (n) of each experiment is provided in the corresponding main figure captions, extended data captions and/or methods section. - HD patient cell line studies: Fig. 1e-j, Fig. 2b-h, Extended Data 1-4 - Sample sizes were chosen to support meaningful conclusions, based on prior studies. - HdhQ50/Hdh+ (Q50) mouse studies: Fig. 2k,l - Sample sizes were chosen to support meaningful conclusions, based on prior studies. - R6/2 mouse studies: Fig. 3b-g, Extended Data 5b-d - Group size was chosen based on historical studies testing other agents in the same model. - zQ175 in vitro cellular and molecular endpoint studies: Fig. 4a-b, Extended Data 6a,b - Sample size was chosen based on previous in vitro experiments, no power analysis done. - zQ175 in vivo cellular and molecular endpoint studies: Fig. 4d-m,r-t, Extended Data 6c-n, Extended Data 7a-j, Extended Data 9b-u - Sample size was chosen based on previous in vivo experiments, no power analysis done. - zQ175 electrophysiology studies: Fig. 4n-q - Sample sizes were based on the results of a pilot study with five cells from two ZFP-treated animals. The effect size in this group was roughly 25%. Based upon this estimated effect size, six mice were alloted to each experimental group. Previous work suggested that this sample size should be sufficient to assess significance. No explicit power calculations were made. - zQ175 microPET and ARG studies: Fig. 5b-f - Sample sizes were chosen to support meaningful conclusions, based on prior studies and power analysis done to identify a potential effect of treatment. - zQ175 behavioral studies and MRI studies: Extended Data 10b-i - Sample sizes were chosen to support meaningful conclusions, based on prior studies and power analysis done to identify a potential effect of treatment (null hypothesis is no change of genotype differences in the various endpoints used).
Data exclusions	- zQ175 electrophysiology studies: Fig. 4p-q - The statistical significance of small, unmatched samples was determined using a non-parametric, one-tailed Mann-Whitney U test. No outliers were detected and no data were excluded. - zQ175 microPET and ARG studies: Fig 5 - Data were excluded based on radioligand specific activity levels in PET imaging where the injected mass was violating the aim of tracer level injections of product based on pre-established criteria. - Microarray data from HD fibroblasts: Extended Data 4a - One control-treated sample was excluded from the analysis based on an exploratory grouping analysis which identified it as an outlier using predetermined criteria. - zQ175 in vivo cellular and molecular endpoint studies: Extended Data 9b-u - Animals were excluded from the analysis if RNA from only one hemisphere was analyzed. Additionally, 1 animal from the wild-type cohort and 2 animals from the Het cohort were excluded due to predetermined exclusion criteria for sample quality. - zQ175 behavioral studies and MRI studies: Extended Data 10b-i - For the behavioral data repeated measures analysis, individual data were excluded for those individuals not having values from all time points based on predetermined criteria.
Replication	- For all in vitro experiments in HD patient cell lines, the results were replicated at least one additional time with the same outcome. For many ZFP-B endpoints, the experiments were replicated at least five times with the same outcome. - HdhQ50/Hdh+ (Q50) mouse study: Results were repeated one more time in a similar experiment with the same outcome. - R6/2 mouse studies: All in vivo experiments with behavioral endpoints were performed once for each age and time point. Fig3e-g, the results of a pilot experiment had a similar outcome. - zQ175 electrophysiology studies: The identical approach was subsequently tested in cohort of mice that were more advanced in age when they became even more symptomatic. This study resulted in the same finding as the study currently under consideration. - zQ175 behavioral studies and MRI studies: All in vivo experiments were performed once for each age and time point unless otherwise

indicated in the figure legends.
- zQ175 microPET and ARG studies: All in vivo experiments were performed once for each age and time point.
- zQ175 cellular and molecular endpoint studies:
Fig. 4a: the experiment was repeated at least five times with the same outcome
Fig. 4b: the exact experiment was repeated one more time with the same outcome
Fig. 4d-m,r-t, Extended Data 6c-n, Extended Data 7a-h: the same, or very similar in vivo experiment was repeated at least one more time with similar outcome
Extended Data 6a: the experiment was repeated at least three times with the same outcome
Extended Data 6b: the experiment was repeated one more time with the same outcome
Extended Data 9: some genes were tested in an pilot experiment with similar outcomes (mHtt; Mtus2; Dnajc12; Nap1l3)

| Randomization | - R6/2 mice and their WT litter-mates were randomly chosen (equal numbers male/female) from a large breeding colony comprised of multiple litters based on the appropriate age.
- HdhQ50/Hdh+ (Q50) were randomly chosen (equal numbers male/female) from a large breeding colony comprised of multiple litters based on the appropriate age.
- zQ175 electrophysiology studies: zQ175 mice and their WT litter-mates were randomly chosen from a large breeding colony comprised of multiple litters based on appropriate age.
- zQ175 behavioral studies and MRI studies: Randomization of the animals was performed based on the body weight and litter of the test animals; i.e. the pre-treatment average body weight difference between the different Q175 HET groups was ≤0.5 g, and animals from each litter were distributed in several treatment groups.
- zQ175 microPET and ARG studies: Randomization of the animals was performed based on equal Het and WT animal distribution during and between imaging days.
- zQ175 in vivo cellular and molecular endpoint studies:
Fig. 4d-m,r-t, Extended Data 6c-n, Extended Data 7a-h: All samples from one experiment were processed and analyzed together, order of samples during staining and recording was mixed to avoid any bias
Extended Data 7a-h, Extended Data 9b-u: for each injection day different genders, genotypes and AAV constructs were used (stereotactic AAV injections): complete randomization not possible
- Microarray studies in HD fibroblasts and neurons - Samples were randomized prior to processing to avoid batch effects. |

| Blinding | - HdhQ50/Hdh+ (Q50) study: Methods for group allocation, data collection and all related analyses were predetermined. Blinding was applied to in vivo procedures and all data collection.
- R6/2 studies: Methods for group allocation, data collection and all related analyses were predetermined. Blinding was applied to in vivo procedures and all data collection.
- zQ175 electrophysiology studies: All mice were ear-tagged and the injections given and recored by a technician. After recording and data analysis, the tag numbers were matched to the data sample so the data could be assigned to the appropriat test group.
- zQ175 behavioral studies and MRI studies: Methods for group allocation, data collection and all related analyses were predetermined. Blinding was applied to in vivo procedures and all data collection.
- zQ175 microPET and ARG studies: Methods for group allocation, data collection and all related analyses were predetermined. Blinding was applied to in vivo procedures and all data collection.
- zQ175 cellular and molecular endpoint studies:
Fig. 4a-b, Extended Data 6a-b: no blinding necessary, since all samples were handled together in parallel pipetting steps
Fig. 4d-m,r-t, Extended Data 6c-n, Extended Data 7a-h: automated image recording and data analysis, no blinding needed
Fig. Extended Data 7i,j, Extended Data 9b-u: no blinding |

Reporting for specific materials, systems and methods

We require information from authors about some types of materials, experimental systems and methods used in many studies. Here, indicate whether each material, system or method listed is relevant to your study. If you are not sure if a list item applies to your research, read the appropriate section before selecting a response.

Materials & experimental systems

n/a	Involved in the study
☐	☒ Antibodies
☐	☒ Eukaryotic cell lines
☒	☐ Palaeontology
☐	☒ Animals and other organisms
☒	☐ Human research participants
☒	☐ Clinical data

Methods

n/a	Involved in the study
☒	☐ ChIP-seq
☐	☒ Flow cytometry
☐	☒ MRI-based neuroimaging

Antibodies

| Antibodies used | Fig. 1g: anti-Htt; Merck-Millipore; "MAB2166";1:500. anti-Calnexin; Sigma; C4731; 1:5000
Fig. 1g: anti-Mouse IgG1; Li-Cor; IRDye 800CW #926-32350 1:5000. anti-Rabbit; LiCor; IRDye 680RD #926-68071; 1:10,000
Fig. 4/Extended Data 6: anti-mutant huntingtin; Merck-Millipore; "mEM48"; MAB5374; lot#2135055; 1:100
Fig. 4/Extended Data 6: anti-DARPP-32; Cell Signaling; "clone 19A3"; #2306; lot#2; 1:250
Fig. 4/Extended Data 6: anti-GFAP; Merck-Millipore; "GA5"; MAB3402; lot#1990686;1:500
Fig. 4/Extended Data 6: anti-Iba1; Wako Chemicals; polyclonal; #019-19741, lot#SAE6921:1:500
Fig. 4/Extended Data 6,7: Anti-Mouse IgG (H+L), CF-568; Sigma-Aldrich; #SAB4600082; 1:1000
Fig. 4/Extended Data 6: Anti-Rabbit IgG (H+L), CF-647; Sigma-Aldrich; #SAB4600184; 1:1000 |

Fig. 4b/Extended Data 6b: anti-HTT "2B7", Millipore #MAB5492, 4 μg/mL; anti-HTT "4C9" ST (sulfo-tagged), 0.1 μg/mL ; for total human huntingtin
Fig. 4b/Extended Data 6b: anti-HTT "MW8", 4 μg/mL; anti-HTT "4C9" ST (sulfo-tagged), 1 μg/mL ; for aggregated human huntingtin
Fig. 4b/Extended Data 6b: anti-Mouse IgG (H+L); MSD® SULFO-TAG; Meso Scale Discovery; #R32AC; 1:1000
Fig. 4b/Extended Data 6b: anti-HTT "CHDI-90000147", 625 ng/mL; anti-HTT "MAB2166-4C8", Millipore #MAB2166, 125 ng/mL; for Singulex mouse HTT.
Fig. Extended Data 1c: anti-FLAG; Sigma; "M2" F1804;1:250. anti-GAPDH; Sigma; G8795; 1:5000.
Fig. Extended Data 1c: anti-Mouse IgG1; Li-Cor; IRDye 800CW #926-32350 1:5000. anti-Mouse IgM; LiCor; IRDye 680RD #926-68180; 1:15,000
Fig. Extended Data 2a,b: anti-PAX6; Merck-Millipore; AB2237;1:1000. anti-Nestin-488; Merck-Millipore; MAB5326A4; 1:250. anti-β-III tubulin; R&D Systems; MAB1195; 1:500.
Fig. Extended Data 2a,b: Anti-Mouse IgG (H+L) Alexa 488; Cat. A11001; Molecular Probes; 1:500. Anti-Rabbit IgG (H+L) Alexa 555; Cat. A21428 ; Molecular Probes; 1:500.
Fig. Extended Data 7: anti-ZNF-10; Novus Biologicals; polyclonal; NBP1-81348; lot#A95371; 1:100
Fig. Extended Data 7: anti-NeuN; Merck-Millipore; polyclonal; ABN78; lot#2140086;1:500
Fig. Extended Data 7: anti-Rabbit IgG (H+L), CF-488; Sigma-Aldrich; #SAB4600042; 1:1000

Validation

-Anti-Htt "MAB2166-4C8"; mouse monoclonal; clone 1HU-4C8; raised against a fusion protein encompassing the region from amino acid (aa) 181 to 810 in the N-terminal region of the human/mouse HTT; Vendor information: No detectable cross reactivity to other proteins by Western blot. Citations (CiteAb.com): https://www.citeab.com/antibodies/226859-mab2166-anti-huntingtin-protein-antibody-a-a-181-81?des=FB2BA62DB4D2DDDE
-Anti-Calnexin; C4731
Vendor information: "Rabbit anti-calnexin antibody reacts specifically with calnexin (90 kDa) of dog, mouse, rat and human."
Citations (CiteAb.com) - https://www.citeab.com/antibodies/1492186-c4731-anti-calnexin?des=4BEF6A7A886445FC
-"mEM48"; MAB5374
Vendor information: "Reacts with human huntingtin protein (both native and recombinant protein). MAB5374 reacts with mutant huntingtin in patients and in transgenic animals that express different numbers of repeats (from 82 to 150 glutamines). Thus, it should recognize different forms of mutant huntingtin"
Citations (CiteAb.com): https://www.citeab.com/antibodies/226701-mab5374-anti-huntingtin-protein-antibody-clone-mem48?des=D4FD4230D4D8E66E"
-Anti-DARPP-32 (19A3)
Vendor information: "Rabbit mAb detects endogenous levels of totoal DARPP-32 protein. Species Reactivity: Mouse, Rat"
Citations (CiteAb.com): https://www.citeab.com/antibodies/123189-2306-darpp-32-19a3-rabbit-mab?des=96D36535EB1687C0"
-Anti-ZNF10; NBP1-81348
Vendor information: "ZNF10 antibody verified on a Protein Array containing target protein plus 383 other non-specific proteins."
Data Sheet: https://www.novusbio.com/PDFs/NBP1-81348.pdf"
-Anti-NeuN; ABN78
Vendor information: "A highly specific rabbit polyclonal antibody that targets NeuN and has been tested in Immunocytochemistry, Immunofluorescence, Immunohistochemistry, and Western Blotting."
Citations (CiteAb.com): https://www.citeab.com/antibodies/224941-abn78-anti-neun-antibody-rabbit?des=E8728D7B0A955931"
-"GA5"; MAB3402;
Vendor information: "The antibody reacts with GFAP from human, pig, chicken and rat. In tissue sections this antibody stains astrocytes and Bergman glia cells (Debus, E., 1983)."
Citations (CiteAb.com): https://www.citeab.com/antibodies/227307-mab3402-anti-glial-fibrillary-acidic-protein-antibody?des=599A45E2E526A0C4"
-Anti-Iba1; #019-19741, lot#SAE6921
Vendor information: "Specific to microglia and macrophage, but not cross-reactive with neuron and astrocyte. Reactive with human, mouse an rat Iba1."
Additional References: http://www.wako-chem.co.jp/english/labchem/product/life/Iba1/index.htm"
-Anti-Htt "2B7"; mouse monoclonal; human/mouse HTT 7-13. Vendor information (Millipore #MAB5492): Reacts with huntingtin protein, amino acids 1-82. The antibody recognizes wild type and mutant huntingtin.
Citations (CiteAb.com): https://www.citeab.com/antibodies/226766-mab5492-anti-huntingtin-antibody-a-a-1-82?des=A7439860FC0B86A5
-Anti-PolyQ "MW1"; mouse monoclonal; Vendor (DSHB) information: Appears to recognize an altered conformation of the polyQ domain generated as the polyQ domain of Htt increases in length. Time-resolved Förster resonance energy transfer (TR-FRET) assay has been developed using MW1 to assay soluble huntingtin. PMID: 22365609 23966247 23626768 23100324 22984513. RRID:AB_528290
Additional Citations (CiteAb.com): https://www.citeab.com/antibodies/150912-mw1-htt-antibody-mw1?des=C7E517B990B0F52B
-Anti-Htt "4C9"; mouse monoclonal; binding against the poly-proline domain of human HTT (amino acids 51-71) (Weiss et al., 2012; Baldo et al., 2012; Cui et al., 2014; Cariulo et al., 2017).
-Anti-Htt "MW8"; mouse monoclonal; generated using soluble human GST-tagged exon 1-Q67 boosted with exon 1-Q67 aggregates; the epitope was mapped to amino acids 83-90 (AEEPLHRP) at the C-terminus of human exon 1 HTT (Ko et al., 2001).
Citations (CiteAb.com): https://www.citeab.com/antibodies/150921-mw8-htt-antibody-mw8?des=0831B840EF6EBA45
-Anti-Htt "CHDI-90000147"; rabbit polyclonal antibody raised to a synthetic peptide corresponding to the proline rich region of HTT protein; the epitope for the antibody was derived from mouse protein sequence that is divergent from the human protein seq (Macdonald et al., 2014 PlosOne)
-Anti-FLAG "M2"; F1804
Vendor information: "The ANTI-FLAG M2 mouse, affinity purified monoclonal antibody binds to fusion proteins containing a FLAG peptide sequence
Citations (CiteAb.com): https://www.citeab.com/antibodies/2304935-f1804-monoclonal-anti-flag-m2?des=34C1D33993B14392
-Anti-GAPDH, clone GAPDH-71.1; G8795
Vendor information: "Monoclonal Anti-GAPDH recognizes human, monkey, bovine, canine, rat, mouse, hamster, mink, rabbit,

chicken, and turkey GAPDH. It does not cross-react with non-vertebrate and prokaryotic species."
Citations (CiteAb.com): https://www.citeab.com/antibodies/1230569-g8795-monoclonal-anti-gapdh?des=63F3D4D3B84304C3
-Anti-PAX6; AB2237
Vendor information: "Anti-PAX6 Antibody detects level of PAX6 & has been published & validated for use in WB & IC."
Citations (CiteAb.com): https://www.citeab.com/antibodies/224104-ab2237-anti-pax6-antibody?des=495EB2181DE7AC76
-Anti-Nestin-488; MAB5326A4 "10C2"
Vendor information: "Anti-Nestin Antibody, clone 10C2, Alexa Fluor 488 conjugate detects level of Nestin & has been published
& validated for use in ICC."
Citations (CiteAb.com): https://www.citeab.com/antibodies/1473360-mab5326a4-anti-nestin-antibody-clone-10c2-alexa-fl?
des=63C779549877BE81
-Anti-β-III tubulin; MAB1195
Vendor information: "Detects mammalian and chicken neuron-specific beta -III tubulin but not other beta -tubulin isotypes in
Western blots."
Citations (CiteAb.com): https://www.citeab.com/antibodies/697655-mab1195-neuron-specific-beta-iii-tubulin-antibody?
des=44C6887BBC8C6DED

Eukaryotic cell lines

Policy information about cell lines

Cell line source(s)	- GM02151, Source: Coriell Institute: https://www.coriell.org/0/Sections/Search/Sample_Detail.aspx?Ref=GM02151&Product=CC - GM04723, Source: Coriell Institute: https://www.coriell.org/0/Sections/Search/Sample_Detail.aspx?Ref=GM04723&Product=CC - ND30259, Source: Originally obtained from Coriell Institute, now available from https://stemcells.nindsgenetics.org - GENEA020, Source: CHDI - Non-HD ("HIP") Neural Stem Cells were obtained from Globalstem (Cat# GSC-4301) - STHdhQ111/HdhQ7 (Q111/Q7) striatal cells - Source: CHDI - HEK293T cells for Lentiviral vector production were obtained from ATCC (Cat. #CRL-3216) - HEK293 cells for AAV production were obtained from Cell Biolabs (Cat.# AAV-100)
Authentication	CAG repeat lengths were confirmed by standard Sanger sequencing or by a trinucleotide repeat sizing analysis (Laragen).
Mycoplasma contamination	Cell lines were not tested for mycoplasma contamination.
Commonly misidentified lines (See ICLAC register)	There are no commonly misidentified cell lines used in this study.

Animals and other organisms

Policy information about studies involving animals; ARRIVE guidelines recommended for reporting animal research

Laboratory animals	- The HdhQ50/Hdh+ (Q50) C57BL/6J mice were provided by CHDI. 11 week old male and female mice were used. - R6/2 transgenic mice were bred at PsychoGenics by crossing ovarian transplanted females on a CBAxC57BL/6 background (Jackson Laboratories) with C57BL/6 wild-type males. CAG repeat length was confirmed in transgenic mice to be 123±0.6. 5 week old female and male mice were used. - zQ175 molecular and histology studies - Female and male heterozygous (HET) zQ175 C57BL/6J mice (Jackson Laboratory (Bar Harbor, Maine, USA)) , age 2 or 6 months and wild-type littermates. - zQ175 electrophysiology studies - 6 month old male B6J.zQ175 KI HETs (CHDI-81003003) and their WT litter-mates were used following procedures approved by the Northwestern University Animal Care and Use Committee and guidelines of the National Institutes of Health. - zQ175 behavioral studies and MRI studies - Female and male heterozygous (HET) zQ175 mice, age 6 months and wild-type litter-mates. - Q175 microPET and ARG studies - Male heterozygous (HET) zQ175 mice were used, age 6.5-10 months.
Wild animals	No wild animals were used in this study.
Field-collected samples	No field-collected samples were used in this study.
Ethics oversight	- The HdhQ50/Hdh+ (Q50) and R6/2 mouse studies were performed at PsychoGenics Inc. (Paramus, NJ) in accordance with the United States Public Health Service Policy on Humane Care and Use of Laboratory Animals, and procedures were approved by the Institutional Animal and Use Committee at PsychoGenics. - zQ175 cellular and molecular studies - The study protocol was approved by the local Ethics committee of the Authority for Health and Consumer Protection of the city and state of Hamburg ("Behörde für Gesundheit und Verbraucherschutz" BGV, Hamburg) under the file number #V11307/591 20 00.33. - zQ175 electrophysiology studies - All animal experiments were carried out according to the Northwestern University Animal Care and Use Committee and guidelines of the National Institute of Health (NIH) guidelines for the care and use of laboratory animals. - zQ175 behavior and MRI studies - All animal experiments were carried out according to the National Institute of Health (NIH) guidelines for the care and use of laboratory animals, and approved by the National Animal Experiment Board, Finland - zQ175 microPET and ARG studies - All animal experiments were carried out according to the Karolinska Institutes guidelines for the care and use of laboratory animals, and approved by the Swedish Board of Agriculture (Jurdbruksverket).

Note that full information on the approval of the study protocol must also be provided in the manuscript.

Flow Cytometry

Plots

Confirm that:

☒ The axis labels state the marker and fluorochrome used (e.g. CD4-FITC).

☒ The axis scales are clearly visible. Include numbers along axes only for bottom left plot of group (a 'group' is an analysis of identical markers).

☐ All plots are contour plots with outliers or pseudocolor plots.

☐ A numerical value for number of cells or percentage (with statistics) is provided.

Methodology

Sample preparation	Lentiviral vectors encoding CMV.ZFP.T2A.eGFP were used to create GENE020A NSCs expressing ZFP-A or ZFP-B. Concentrated vectors were inoculated with 1E6 cells in a 6 well plate. After several passages, the resulting cells were subjected to cell sorting to enrich GFP-positive cells.
Instrument	BD Influx Cell Sorter
Software	BD FACS
Cell population abundance	Provided in Supplementary Figure 2
Gating strategy	Provided in Supplementary Figure 2

☒ Tick this box to confirm that a figure exemplifying the gating strategy is provided in the Supplementary Information.

Magnetic resonance imaging

Experimental design

Design type	No functional MRI performed
Design specifications	No functional MRI performed
Behavioral performance measures	No functional MRI performed

Acquisition

Imaging type(s)	Structural T2-weighted MRI
Field strength	11.7T
Sequence & imaging parameters	TurboRARE sequence, FOV 20x20 mm, matrix 256x256, slice thickness 0.7 mm, Effective TE 36 ms, Rare factor 8, TR 2500 ms and 8 repetitions.
Area of acquisition	Whole brain

Diffusion MRI   ☐ Used   ☒ Not used

Preprocessing

Preprocessing software	No fMRI-type preprocessing steps were used.
Normalization	No fMRI-type preprocessing steps were used.
Normalization template	No fMRI-type preprocessing steps were used.
Noise and artifact removal	No fMRI-type preprocessing steps were used.
Volume censoring	No fMRI-type preprocessing steps were used.

Statistical modeling & inference

Model type and settings	No fMRI-type statistical modeling was used.

Effect(s) tested	No fMRI-type statistical modeling was used.

Specify type of analysis: ☐ Whole brain ☒ ROI-based ☐ Both

Anatomical location(s)	Regions of interest analysis of presented results were based on Paxinos mouse atlas (4th Edition). Region of interest analysis was performed manually in MATLAB environment, observer blinded to study groups.

Statistic type for inference (See Eklund et al. 2016)	No voxel- or cluster-based methods were employed.

Correction	No fMRI-type statistical modeling was used.

Models & analysis

n/a	Involved in the study
☒	☐ Functional and/or effective connectivity
☒	☐ Graph analysis
☒	☐ Multivariate modeling or predictive analysis